

博士論文

Doctoral Dissertation

InAs/GaSb および InAs/GaAs 歪みヘテロエピタキシャル結晶の
高品質化

指導教員: 杉山正和 教授

学籍番号: 37-187269

奥村滋一

Shigekazu Okumura

Department of Advanced Interdisciplinary Studies, School of Engineering,
The University of Tokyo

Abstract

In the fields of tensile-strained hetero epitaxial growth of III-V compound semiconductor by molecular beam epitaxy method, the pits on InAs layer on GaSb formed by the tensile strain and the dislocations in GaAs cover layer on InAs quantum dots formed by the anisotropic tensile strain were studied by focusing on the similarities between the two different material systems.

Before the InAs hetero epitaxial growth on GaSb, GaSb homo epitaxial growth was investigated to prepare a highly flat underlying surface. Two-step high and low temperature growth sequence was proposed, and extremely flat surface was obtained.

Adapting the flat surface obtained by two-step growth sequence, InAs bulk hetero epitaxial growth on GaSb was investigated for obtaining flat with pit-free surface applicable to the contact layer of GaSb-based device application. Pits with high index plane were observed on the InAs surface at relatively higher As₂ pressure or lower growth temperature. Pits are not conducive to lattice relaxation, but formation of high index planes contribute to reduce surface energy. Although these pits on InAs are suppressed or reduced by reducing the As₂ pressure or increasing the growth temperature, growth method for suppressing the pits with higher tolerance is needed.

In establishing a growth method that effectively suppresses pits of InAs on GaSb, the growth sequence was focused on same as the case of GaSb homo epitaxial growth. By adapting initial low and subsequent high temperature growth sequence, extremely flat surface of InAs on GaSb was obtained. This owes to the following two factors: (1) high flatness of initial InAs layer under suppressed Sb carryover, and (2) higher (001) plane preference of InAs subsequent high temperature growth.

Focusing on the similarity with InAs growth on GaSb, InGaAs/GaAs growth on InAs QDs was investigated to obtain high optical quality from two aspects of InAs QDs growth and subsequent InGaAs/GaAs cover growth. Growth temperature dependence of InAs QDs revealed that the dislocations mainly act as a non-radiative recombination center to degrade the PL characteristics. Relatively higher height InAs QDs caused the dislocation formation at cover layer directly above QDs. To clarify the mechanism of the dislocation formation, relationship with the surface morphology after cover layer growth was investigated under the various cover layer growth condition. This reveals that pit formed directly above the QD is the starting point for dislocation formation during the subsequent high temperature GaAs growth. Same as InAs/GaSb system, ensuring the surface flatness of initial low temperature cover layer is the important factor for fabricating the high-quality GaAs/InAs QDs structure with suppressed dislocations.

Table of Contents

1 Introduction	1
1.1 InAs/GaSb related material system	1
1.1.1 InAs/GaSb related material system and type-II superlattice (T2SL) infrared photodetector application	1
1.1.2 Homo epitaxial growth of GaSb	3
1.1.3 Hetero epitaxial growth of InAs/GaSb related material	5
1.2 InAs/GaAs related material system	8
1.2.1 InAs/GaAs QD laser application	8
1.2.2 Hetero epitaxial growth of InAs/GaAs related material	10
1.3 Research outline	12
2 Experimental equipment.....	14
2.1 Solid Source Molecular Beam Epitaxy (SS-MBE)	14
2.2 Reflection High Energy Electron Diffraction (RHEED).....	16
2.3 Atomic Force Microscopy (AFM).....	18
2.4 X-Ray Diffraction (XRD).....	19
2.5 Photoluminescence (PL).....	21
3 GaSb homo epitaxial growth	23
3.1 Pit formation on GaSb epitaxial layer surface.....	23
3.1.1 Experimental procedure.....	23
3.1.2 Effect of TOD temperature on GaSb surface morphology.....	25
3.1.3 Effect of growth temperature on GaSb surface morphology.....	28
3.2 Improvement of GaSb surface morphology by two-step LT/HT	29
growth sequence	29
3.2.1 TH to LT and LT to HT growth sequence.....	29
3.2.2 RHEED observation during GaSb growth	29
3.2.3 Mechanism of the planarization of the pits on GaSb.....	32
3.3 Summary of Chapter 3.....	38
4 InAs/GaSb hetero epitaxial growth	39
4.1 Effect of As ₂ pressure on InAs hetero epitaxial growth on GaSb	39
4.1.1 Experimental procedure.....	39

4.1.2	Surface observation	40
4.1.3	Cross sectional observation	42
4.1.4	Strain analysis.....	44
4.1.5	Summary of Section 4.1	49
4.2	Effect of growth temperature on InAs hetero epitaxial growth on GaSb	50
4.2.1	Experimental procedure.....	50
4.2.2	Size variation of pit with InAs growth temperature	51
4.2.3	Pit suppression by the trace amount of Sb ₂ irradiation.....	55
4.3	Effect of growth sequence on InAs hetero epitaxial growth on GaSb	57
4.3.1	Pit suppression by two-step InAs growth.....	57
4.3.2	Mechanism of pit suppression	60
4.3.3	Summary of Section 4.2 and 4.3.....	61
4.4	Summary of Chapter 4.....	63
5	InAs/GaAs hetero epitaxial growth	64
5.1	Effects of the growth temperature of InAs QDs on their structural and optical properties	64
5.1.1	Experimental procedure.....	64
5.1.2	Structural characteristics of InAs/GaAs QD structures	66
5.1.3	Optical characteristics of InAs/GaAs QD structures	71
5.1.4	Summary of Section 5.1	76
5.2	Effects of low temperature cover layer growth of InAs QDs on their optical and structural properties.....	77
5.2.1	Experimental procedure.....	77
5.2.2	Relationship between optical and structural properties of InAs QD with various LT InGaAs/GaAs cover layer conditions	79
5.2.3	Surface observation of LT InGaAs/GaAs cover layer.....	83
5.2.4	Mechanism of the dislocation formation in InAs QD structure	86
5.2.5	Summary of Section 5.2	88
5.3	Summary of Chapter 5.....	89
6	Conclusions	90
6.1	Overview of this research	90
6.2	Conclusions	92
	Appendix	94

References	95
Publication list	103
Acknowledgements	105

1 Introduction

1.1 InAs/GaSb related material system

1.1.1 InAs/GaSb related material system and type-II superlattice (T2SL) infrared photodetector application

InAs/GaSb related material system have attracted a lot of attention especially for their application to infrared (IR) photodetectors (PDs) [1-16]. III-V binary compound semiconductors of GaSb, InAs, and AlSb are so-called “6.1 Å family” [17]. Their lattice constraints are 6.094 Å, 6.058 Å, and 6.136 Å, respectively, are to each other as shown in the relationship between bandgap and lattice constant in Fig. 1-1 [1]. A superlattice structure combining InAs/GaSb has a type-II band lineup and is called type-II superlattice (T2SL) as shown in the band diagram of Fig. 1-2 [1].

As in the case of InAs/GaSb system, the type-II band alignment results in an overlap in energy between the conduction band (CB) minimum and the valence band (VB) maximum of the two materials. This energy overlap is regarded to be in the range of 140-170 meV [18-20] and is regarded as a critical parameter for designing InAs/GaSb T2SLs. As indicated in Fig 1-2, the bandgap of the InAs/GaSb T2SL is typically defined as the energy gap between the bottom of the lowest electron mini-band (C1) and the top of the highest hole mini-band (HH1). Thus, T2SLs can achieve smaller bandgaps than those of the materials comprising the SL. T2SL related alloys can provide much flexibility when designing device parameters such as absorption wavelength of IR-PD.

Regarding the substrate material, GaSb is suitable for the substrate material in terms of strain compensation since the lattice constant of GaSb is between those of InAs and AlSb [1]. Furthermore, in recent years, high-quality GaSb substrate is commercially available [21].

Adapting the T2SLs, it will be possible to realize an IR-PD capable of detecting infrared light in a wide wavelength range from near to far infrared (SWIR to LWIR). Fig. 1-3 shows the example of the device structure of IR-PD [7]. In addition to the InAs/GaSb T2SL, InAs/InAsSb and AlAs/InAs/InAsSb T2SLs were adapted to LWIR and MWIR absorptions, respectively. By combining the materials related to the 6.1 Å family, device applications in various forms will become possible including two-wavelengths detectable IR-PD as shown in the example in Ref. [7]. In addition to the diversity in device designing, T2SL related materials possess a relatively long minority carrier lifetime compared to the AlGaAs/GaAs materials constructing technologically mature quantum well infrared photodetector (QWIP) [11]. This makes it possible to increase the responsivity of the IR-

PD. Thus, in recent years, T2SL is one of the most intensively studied materials for IR-PD application.

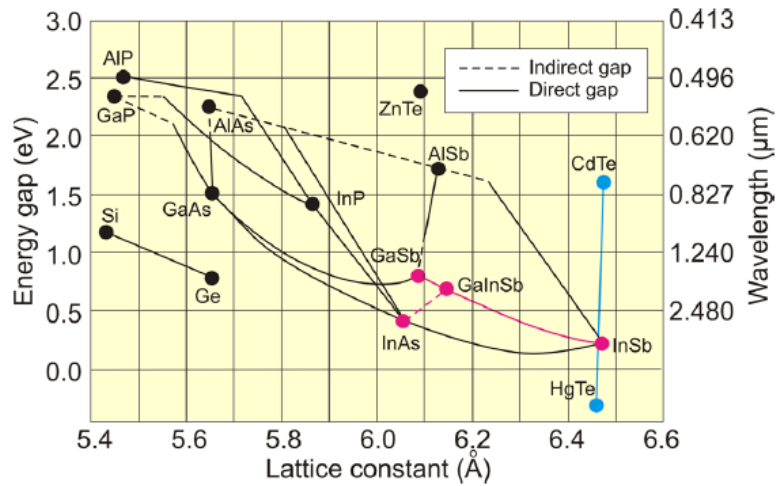


Figure 1-1 Relationship between bandgap and lattice constant of InAs/GaSb related material system so called “6.1 Å family” from Ref. [1].

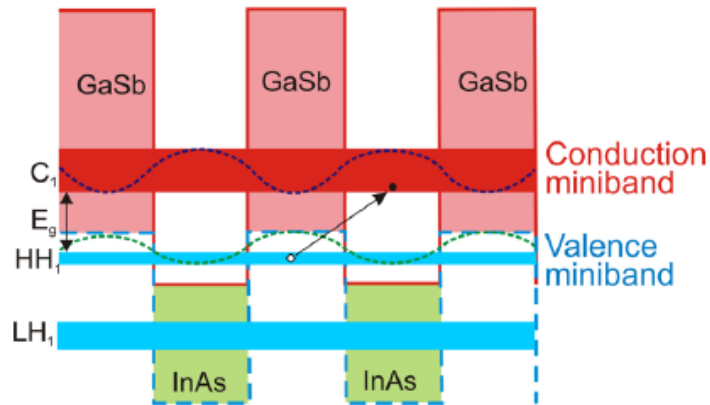


Figure 1-2 Energy band diagram of InAs/GaSb type-II superlattice from Ref. [1]. The bandgap of T2SL is typically defined as the energy difference between the top of the heavy-hole mini-band (HH1) and the bottom of the electron mini-band (C1).

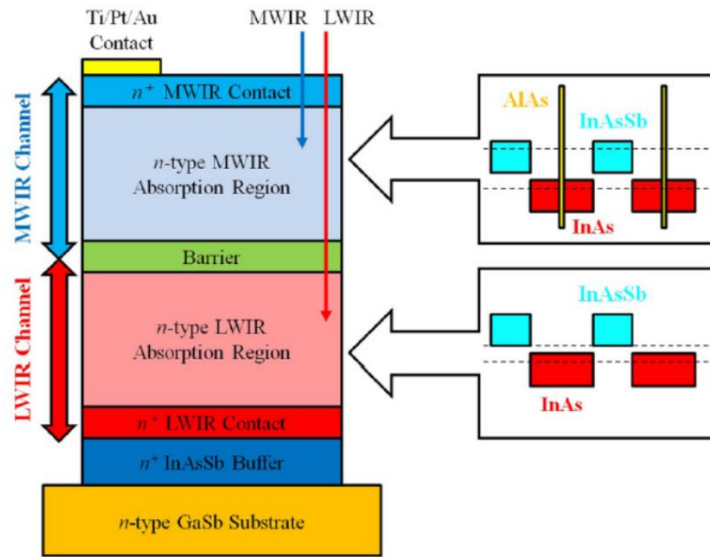


Figure 1-3 Device structure of two-wavelength detectable T2SL IR-PD from Ref. [7].

1.1.2 Homo epitaxial growth of GaSb

For the improvement of device characteristics such as responsivity in IR-PDs, a high-quality epitaxial layer is required. For that purpose, defects and dislocations in the layer should be reduced because they act as carrier traps of photocarriers. If the surface flatness of the GaSb homo epitaxial layer is not sufficient, there is a concern that this will cause defects or dislocation in epitaxial layer due to such as the strain accumulation of the composition modulation. Thus, firstly, flat surface morphology of GaSb homo epitaxial layer is one of the most crucial points for ensuring the quality of the upper active layer.

So far, GaSb homo epitaxial layer has been investigated in terms of growth parameters such as growth temperature, group-V species, and off-angle of the substrate [23]. In Noshio *et al.*'s report [23], growth temperature had a great impact on GaSb homo epitaxial layer as shown in Fig 1-4. At relatively low growth temperature around 350 °C, mound-like morphology was observed. On the other hand, a relatively smoother surface was observed on vicinal substrate at high temperature around 450 °C [23]. Moreover, since the surface before GaSb homo epitaxial growth must be rough due to its large surface oxidation [22], special treatment should be required concerning to initial surface in addition to the GaSb growth itself [23]. From this aspect, the effects of thermal oxide desorption (TOD) of GaSb surface and initial GaSb growth on a rough surface should be treated carefully.

In this study, to obtain flat with pit free GaSb surface, the influence of TOD

temperature, growth temperature, and growth step on GaSb homo epitaxial layer on the vicinal substrate were investigated systematically. An atomically flat surface was obtained at a high temperature growth, whereas pits which originated in the heavily rough substrate were observed at the same time. These pits were not observed at a low growth temperature, whereas surface roughness became greater even in the step-flow mode growth process. Combining high and low temperature with step-flow mode growth made it possible to obtain a flat, pit-free GaSb homo epitaxial layer.

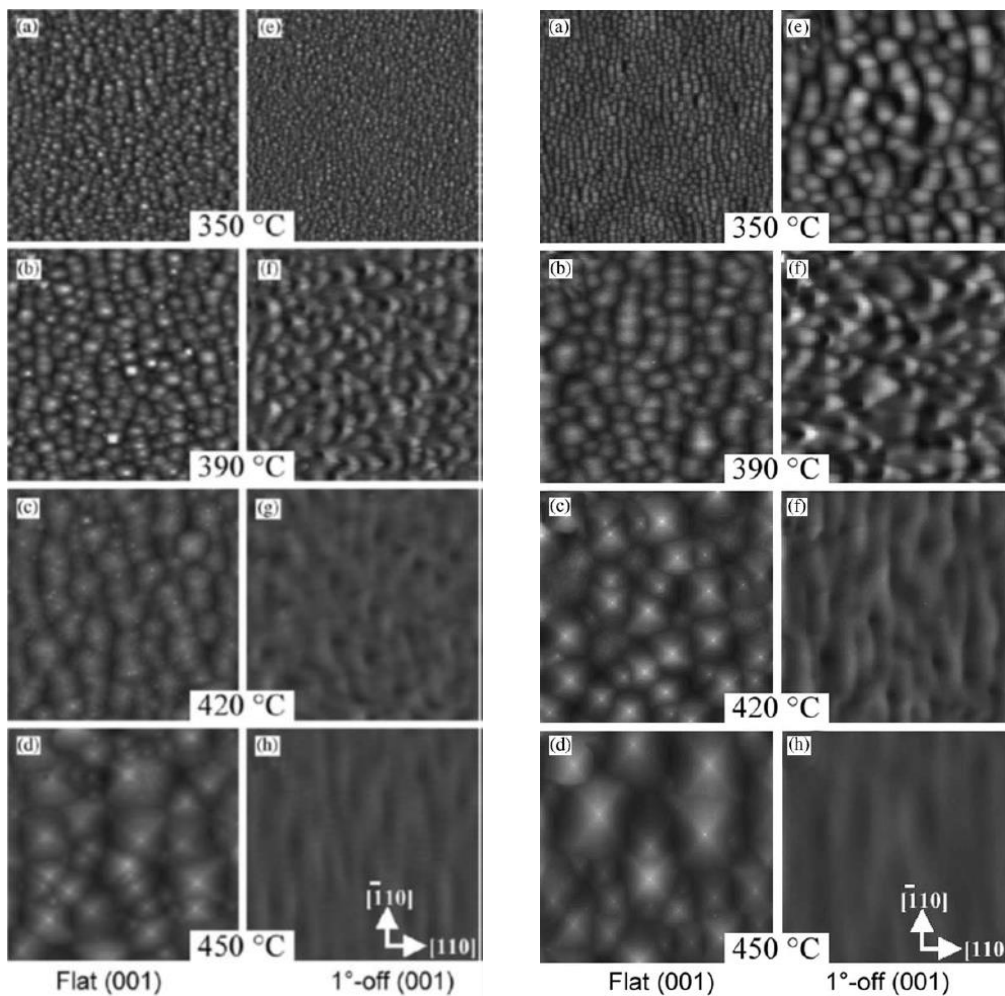


Figure 1-4 Surface morphology of GaSb homo epitaxial layer with varying the growth conditions such as growth temperature, substrate orientation, and Sb species. Left and right show in the case of using Sb_4 and Sb_2 , respectively. These figures are cited from Ref. [23].

1.1.3 Hetero epitaxial growth of InAs/GaSb related material

To improve device characteristics such as dark current and responsivity in IR-PDs, a high-quality active InAs/GaSb hetero epitaxial superlattice layer as well as high-quality InAs bulk hetero epitaxial layer for electrode contact layer is required. For these purposes, defects and dislocations in the active layer or contact layer should be reduced because they act as carrier traps. Therefore, a basic study on InAs hetero epitaxial growth on GaSb is required to improve the IR-PD characteristics.

Lattice mismatch between InAs and GaSb is relatively small of 0.7%, and it is advantageous for hetero epitaxial growth. However, As/Sb exchange such as reported in Ref. [24] and [25] occurring at the hetero interface may affect subsequent InAs growth.

Regarding As/Sb exchange, growth temperature and As_2 pressure has been reported to be two factors influencing this phenomenon [24]. As reported in Ref. [24], the influence of As_2 irradiation to GaSb surface morphology were investigated. According to this report, As/Sb exchange was enhanced in the cases of high growth temperature and As_2 pressure. This makes the GaSb surface rougher as shown in Fig. 1-5 [24]. Subsequent InAs growth are expected to be affected by this initial surface morphology.

From another perspective, in Ref. [26], growth optimization of InAs homo epitaxial growth was researched by changing the growth temperature and V/III ratio. According to this research, the growth temperature between 430 and 450 °C and an As_2 /In flux ratio of about 15:1 yielded the highest quality in terms of defect density and surface roughness as shown in Fig. 1-6 [26].

Furthermore, the initial surface state of InAs homo epitaxial growth was investigated in terms of As_2 pressure as a growth parameter. Surface states are significantly different with respect to As_2 pressure [30]. At a lower As_2 pressure close to stoichiometry, a high density of InAs compact islands on terraces is obtained as shown in Fig 1-7 (a) [30]. On the other hand, at a relatively higher As_2 pressure, the islands are large, and the step and island edges are much rougher as shown in Fig. 1-7 (b) [30]. These differences observed at the initial stage of InAs growth would affect the subsequent InAs growth especially under the existence of tensile strain. Thus, for InAs hetero epitaxial growth on GaSb, both the effect of the interface caused by the As/Sb exchange and the subsequent InAs growth under tensile strain should be considered in terms of As_2 pressure dependence.

In this study, to obtain a high-quality of flat with pit-free InAs layer on GaSb, the effects of As_2 pressure on InAs hetero epitaxial growth was investigated. It was revealed that InAs quality largely depended on As_2 pressure. A high-quality InAs hetero growth was achieved under low As_2 pressure. On the other hand, dislocations and pits were observed in InAs layer under high As_2 pressure. Strain analysis revealed that dislocations

were found to originate at the InAs/GaSb interface layer with small lattice constants due to As/Sb exchange. Pits were seemed to be a formation of high index plane as a part of strain energy relaxation between InAs and GaSb to ease the surface energy.

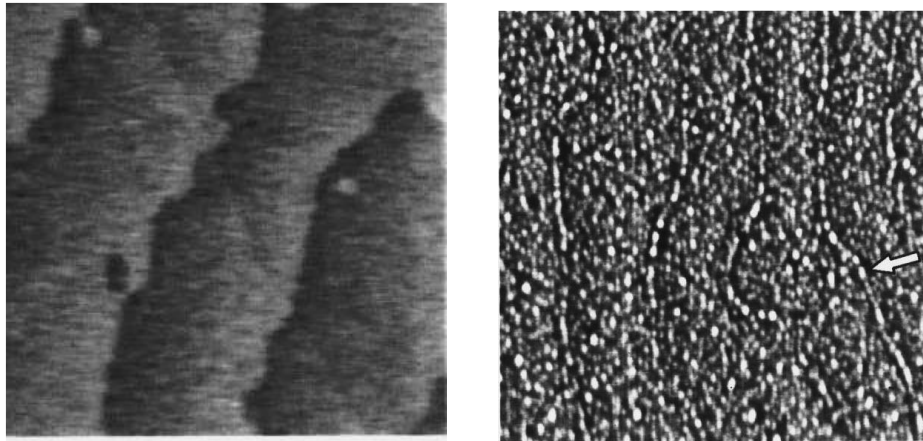


Figure 1-5 Surface morphology of GaSb after As_2 irradiation at two conditions of low As_2 pressure/low growth temperature (left), and high As_2 pressure/high growth temperature (right) reported in Ref. [24].

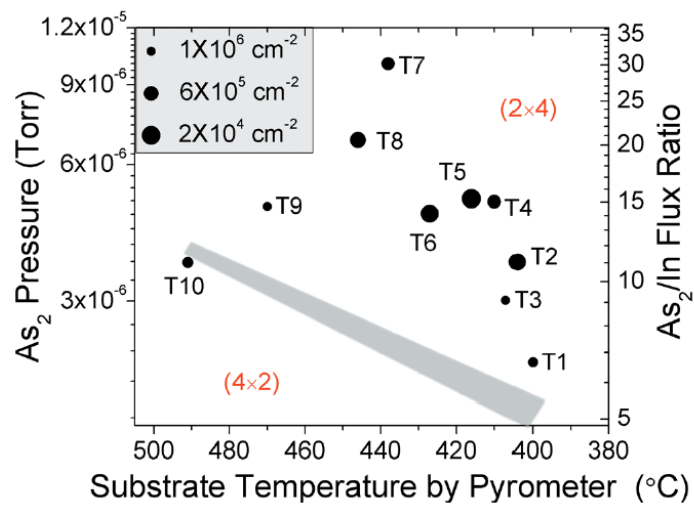


Figure 1-6 Relation between the surface defect density and growth conditions of InAs homoepitaxial layers reported in Ref. [26]. Growth temperature between 430 °C and 450 °C and an As_2/In flux ratio of about 15:1 yielded the highest quality in terms of defect density and surface roughness [26].

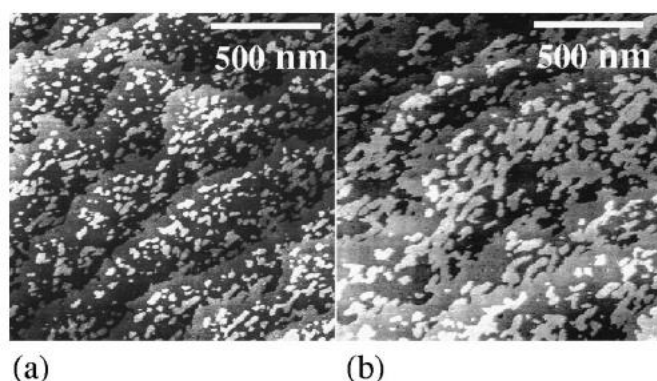


Figure 1-7 Scanning tunneling microscopy (STM) images of InAs homo epitaxial growth quenched after the growth of 10.25 ML at different V/III ratios. The substrate temperature was 450 °C, with a growth rate of 0.25 ML/s, and the V/III ratios were (a) 2:1 and (b) 6:1, respectively [30].

From the As₂ pressure dependence of InAs hetero growth on GaSb, a pit-free surface was eventually obtained at a relatively low As₂ pressure of 2.2×10^{-7} Torr. However, the growth window for obtaining good crystalline InAs was quite narrow since the As₂ pressure is extremely so low that it is difficult to control even with a valved cell. Thus, there is a concern that run-to-run wafer productivity will be affected.

In the next step, other growth parameters which affect growth kinetics of InAs such as growth temperature and Sb as a surfactant were noted. Especially InAs hetero growth on GaSb, there is a possibility that suitable growth temperature is different between at initial layer and subsequent layer.

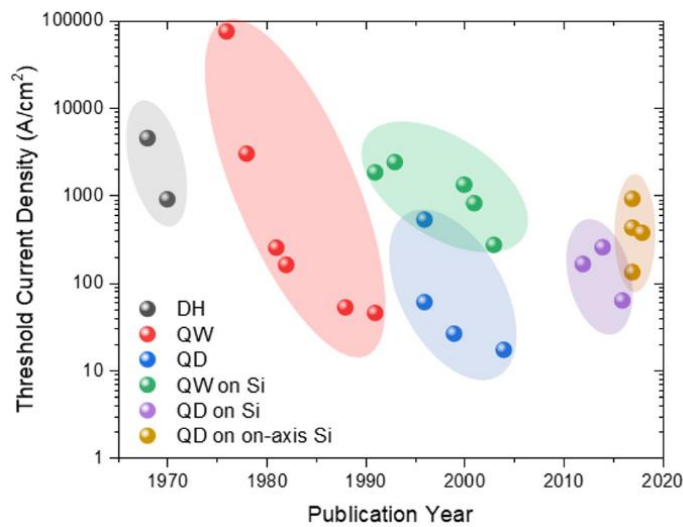
In this study, to secure greater tolerance in pit-free InAs on GaSb growth, the influence of Sb irradiation during InAs growth and the growth sequence especially in relation to the growth temperature without Sb irradiation were investigated. It was found that the formation of pits in the InAs layer was suppressed by irradiating trace amounts of Sb due to its surfactant effect. Sizes of the pits tended to become smaller as the growth temperature increased. Moreover, it was found that a two-step growth sequence that initial growth was performed at 400 °C and subsequent bulk growth was done at 520 °C can completely suppress the pits, moreover, yield an extremely flat surface at the same time. This owes to the initial flatness of the InAs layer at low growth temperatures and the higher (001) crystal plane orientation at high growth temperatures.

1.2 InAs/GaAs related material system

1.2.1 InAs/GaAs QD laser application

Self-assembled InAs/GaAs quantum dots (QDs) attract much attention especially as a laser application. Since the first proposal of Arakawa and Sakaki [31], the growth of InAs QDs using self-assembling technique has been intensively studied to improve their optical quality for applying to the active medium of the laser device [32-49]. One of the most notable features of QD laser is its low threshold current density owing to its three-dimensional carrier confinement effect compared to quantum well (QW) laser [50] as shown in Fig. 1-8. Moreover, for example, QD lasers have excellent high temperature operating characteristics shown in Fig. 1-9 [51], lower linewidth enhancement factor and reduced linewidth [52], reduced reflection sensitivity [53].

Now, due to these excellent characteristics, QD lasers shown in Fig. 1-10 [54] for 1.3 μm optical fiber communication is commercially available in the market [55].



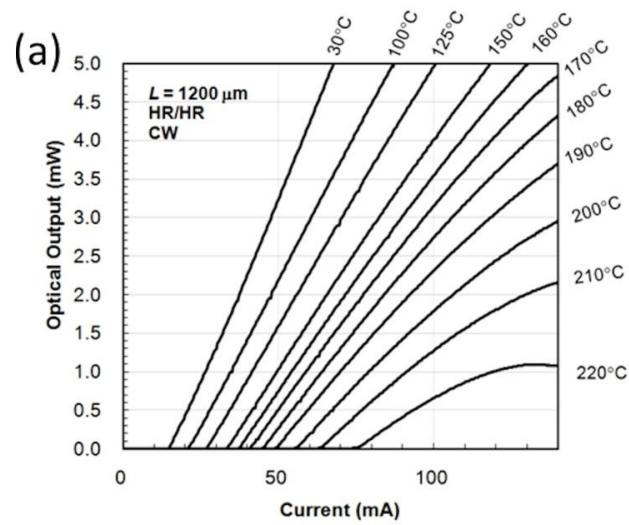


Figure 1-9 Record-setting high temperature continuous wave power output vs bias current curves for quantum dot lasers that reaches 220 °C [51].

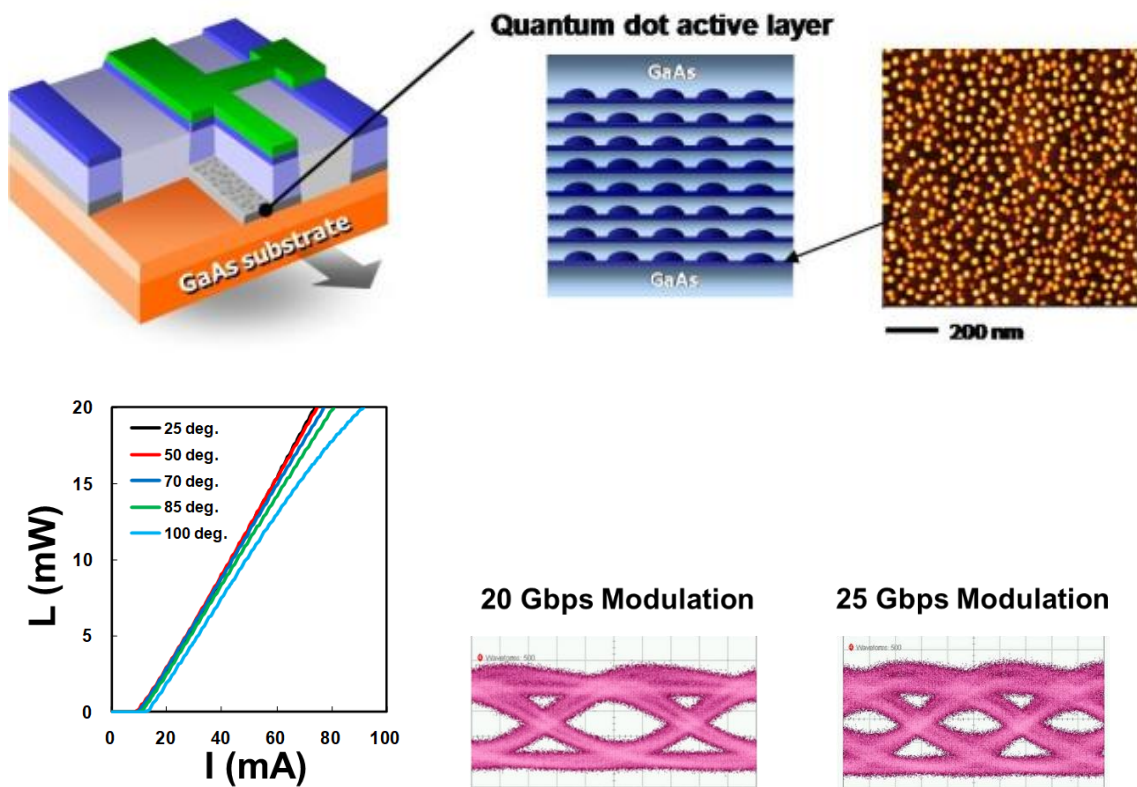


Figure 1-10 Schematic device structure of QD laser with its I - L and modulation characteristics [54].

1.2.2 Hetero epitaxial growth of InAs/GaAs related material

Regarding the epitaxial growth technique, InAs QDs capped with InGaAs strain reducing layer (SRL) has been intensively studied [56-58]. Applying InGaAs capping layer can reduce compressive strain to InAs QDs smaller compared to GaAs one. Owing to this technique, InAs QDs emission wavelength becomes longer to reach the commercially important wavelength of 1.3 μm for optical fiber communication. So far, In out-diffusion of from QDs was suppressed by optimizing the growth sequence of InGaAs SRL and the maximum ground-state optical gain of 54 cm^{-1} at 25 $^{\circ}\text{C}$ near 1.3 μm emission was obtained in 8-stacked QD structure. For more temperature stabilization of QD laser, higher optical gain should be required. In order to further increase the optical gain of InAs QDs, it is important to examine the factors that inhibit radiative recombination at especially InAs QDs including their surrounding cover layer.

As for the growth of InAs QDs including their cover layer, it has been reported that pits appear in the region where the GaAs cover layer is difficult to be grown due to the strain directly above the InAs QD [59]. Figure 1-11 shows the surface and schematic image of the pits described in Ref. [59]. The growth temperature of the cover layer plays a role in whether pits form or not. In the case that the cover layer was grown at a low temperature same as InAs QDs, pit size increased and crystallinity of QD structure deteriorated significantly as shown in Fig. 1-12 (a). By annealing at high temperature during the cover layer growth, the pits disappeared and a QD structure with good crystallinity is formed as shown in Fig. 1-12 (b). Although large pits as shown in Fig. 1-11 that significantly impair crystallinity can be suppressed by high-temperature annealing or high-temperature growth of the cover layer, dislocations caused by the pits may degrade the optical properties, and a detailed study is needed to further improve the optical gain of the QD structure.

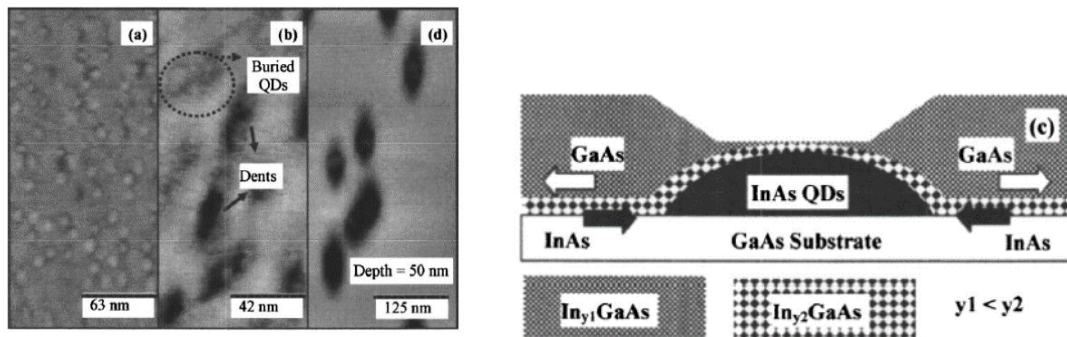


Figure 1-11 Surface (left) and cross-sectional schematic figure (right) of GaAs cover layer grown on InAs QDs from Ref. [59].

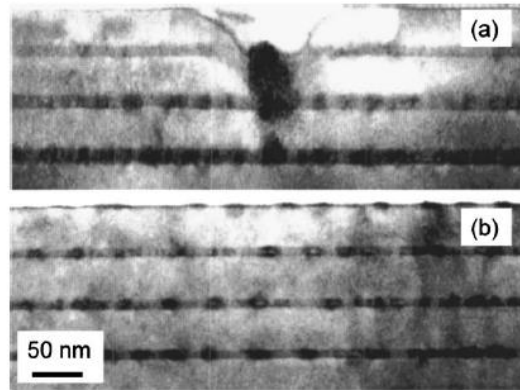


Figure 1-12 Cross-sectional TEM images of QD structure where (a) GaAs cover layer was grown at same temperature of QDs and (b) high-temperature annealing was introduced during the GaAs cover layer growth from Ref. [59].

In this study, firstly, focusing on the effect of the underlying InAs QD, the growth temperature dependence of InAs QDs to understand the relationship between their structural and optical properties of InAs QDs structure. Photoluminescence (PL) intensity and dislocation density of QD structure changed a lot with QD growth temperature. Large PL intensity with small temperature dependence was observed in the sample with low dislocation density. Time-resolved PL measurement revealed that PL lifetime became longer as the dislocation density of the sample became lower. This means that dislocations in QD structure act as nonradiative centers degrading the PL intensity characteristics.

Following the results of the study of the underlying InAs QDs effect, secondly, the effect of InGaAs/GaAs cover layer growth on the optical properties of InAs QDs structures was investigated by changing the growth temperature and thickness of the cover layer. PL intensity decreased as the dislocation density observed around InAs QD increased. This indicates that the dislocations mainly act as a nonradiative recombination center same as confirmed in the case of InAs QDs with their temperature dependence. With surface observation of the cover layer, it was revealed that dislocations are formed during HT GaAs growth, originating from pits that remain on the surface after LT cover layer growth and subsequent annealing.

1.3 Research outline

The purpose of this study is to obtain a high-quality hetero epitaxial layer in the tensile-strained III-V compound semiconductor system. In this study, two different tensile-strained hetero epitaxial growth: InAs on GaSb and GaAs on InAs were investigated to obtain high-quality crystals in each material system.

The purpose of InAs growth on GaSb is to obtain flat with pit-free surface suitable for the GaSb-based device application such as electrode contact layer of photodetector. Prior to the investigation of InAs/GaSb hetero growth, GaSb homo epitaxial growth was investigated for obtaining highly flat underlying GaSb layer suitable for InAs hetero epitaxial growth. Next, adapting the flat GaSb underlying layer, InAs hetero epitaxial growth was investigated by changing such as As₂ pressure, growth temperature, growth sequence. The generation and suppression mechanisms of the pits were also discussed.

The purpose of GaAs growth on InAs is to obtain optically high-quality QDs structure for improving the laser characteristics such as wall plug efficiency. The effects of growth condition of both underlying InAs QDs and InGaAs/GaAs cover layer on the optical properties of QDs structure were investigated. The mechanism of dislocation formation and its suppression method were also discussed.

The outline of this study is summarized in Fig. 1-13.

In the main context, experimental equipment used in this study and their principles are introduced in Chapter 2.

In chapter 3, GaSb homo epitaxial growth concerning to the pit formation on its surface and their suppression method are discussed. A part of content of this chapter is based on Ref. [1] in publication list of regular paper.

In Chapter 4, adapting the flat underlying GaSb layer obtained in Chapter 3, InAs hetero epitaxial growth with respect to the pit formation and its suppression method are discussed. A part of content of this chapter is based on Ref. [2] and [3] in publication list of regular paper.

In Chapter 5, GaAs hetero epitaxial growth on InAs QDs concerning to the relationship between dislocations and pits formed after initial cover layer is discussed and growth method for suppressing the dislocations is proposed. A part of content of this chapter is based on Ref. [4] in publication list of regular paper.

The research will be concluded in Chapter 6.

Purpose: To obtain a high-quality epitaxial layer in the tensile-strained III-V compound semiconductor system

Chapter 1) Introduction

- InAs/GaSb T2SL structure
- InAs/GaAs QD structure
- Research outline

Chapter 2) Experimental equipment

- SS-MBE
- AFM
- CWPL/TRPL
- XRD/RSM

Chapter 3) GaSb homo epitaxial growth

- Pit formation on GaSb
- Improvement of GaSb by two-step growth

Chapter 4) InAs/GaSb hetero epitaxial growth

- As₂ pressure dependence
- Growth temperature dependence
- Pit suppression by LT/HT growth

Chapter 5) InAs/GaAs hetero epitaxial growth

- Effect of InAs underlying InAs QDs
- Effect of initial LT cover layer
- Relationship between dislocations and pits

Chapter 6) Conclusion

- Adapting the flat underlying GaSb surface
- Common features of two-step growth
- Common features of tensile-strained hetero growth
 - Pit formation
 - Importance of the flatness at initial LT growth

Figure 1-13 The outline of this study.

2 Experimental equipment

2.1 Solid Source Molecular Beam Epitaxy (SS-MBE)

MBE is one of the sophisticated epitaxial growth techniques enabling precise control of material purity, interface formation, alloy compositions, and doping concentrations. These qualities owe to the extremely clean ultrahigh-vacuum (UHV) environment in the material growth system. UHV conditions typically are controlled to a very low partial pressures of background impurity gases under 10^{-14} Torr. This leads to extremely low background impurity levels in the resultant epitaxial layer. In MBE, noninteracting molecular beams of constituent materials are evaporated or sublimed from effusion cells and allowed to chemically interact only on a heated substrate. The use of pure solid-source material enables not only very pure epitaxial growth but also much simplified chemical reaction when the source material reaches the substrate. MBE is suitable for extremely producing very sharp interfaces. The effusion cells that produce the molecular beams of source materials are typically paired with a mechanical shutter that can quickly start or stop the beams in much less time than it takes to grow an atomic layer of material. The temperature of the source in the crucible, which is very reproducible and stable, controls the flux generated from the effusion cells. This makes the generation of specific fluxes of constituent materials simple to control for accurate alloy compositions and doping concentrations. The UHV environment also makes it possible to incorporate various in situ monitoring techniques that can be used during growth, including reflection high-energy electron diffraction (RHEED), and mass spectrometry.

Figure 2-1 shows an example of an MBE reactor for research. The growth chamber is attached to a buffer chamber containing a heater stage for outgassing substrates, and then to a load-lock for the introduction of substrates into the vacuum environment. Figure 2-2 shows a schematic of a typical MBE growth system. Effusion cells, pointed at the heated substrate, provide a flux of material that can be started and stopped with mechanical shutters. Various pumping technologies are used to maintain the vacuum, including cryopumps, ion pumps, turbomolecular pumps, and the liquid nitrogen-filled cryopanel. This helps keep background contamination of epitaxial layer as low as possible.

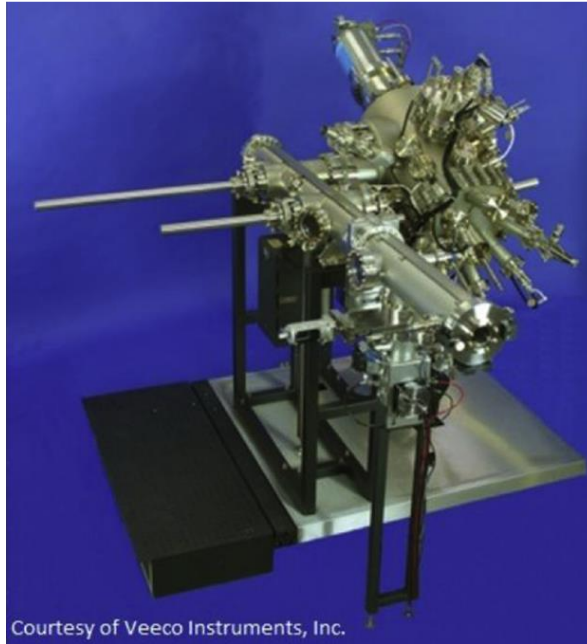


Figure 2-1 The photograph of MBE chamber. The photo shows the loadlock (front), the buffer chamber, and the growth chamber [60].

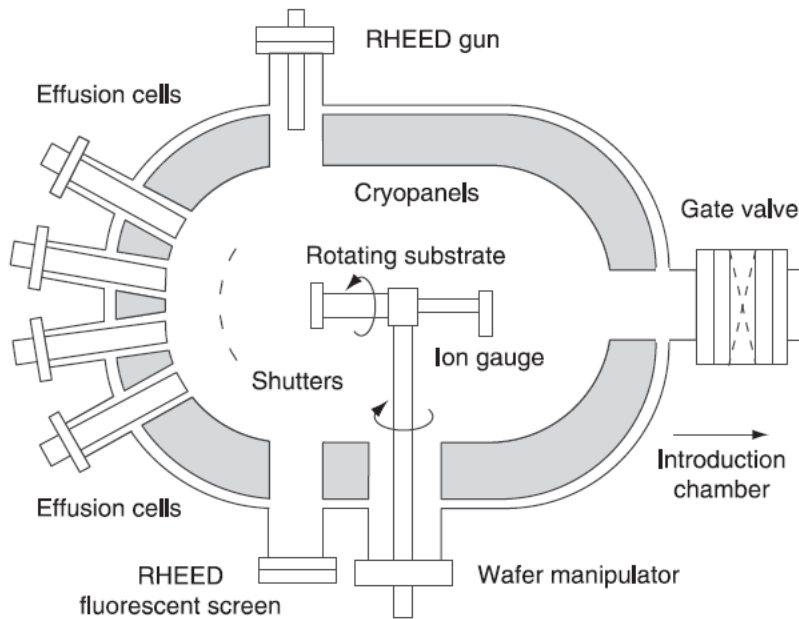


Figure 2-2 Schematic of an MBE system [60].

2.2 Reflection High Energy Electron Diffraction (RHEED)

RHEED is a powerful observation tool for the semiconductor surface structures analysis. In the RHEED technique, electrons from an electron source reflect off and diffract from a surface at a very low angle of $1^\circ - 3^\circ$ as can be seen from the position of the RHEED equipment in Fig. 2-2. Due to the shallow angle, the energy transfer normal to the semiconductor surface is minimal, and predominantly elastically scattered electrons escape from a few monolayers of material, causing this to be a rather surface-sensitive technique. The high energy electrons of typically 10 - 20 keV applied to RHEED can locally affect surface reconstructions, growth kinetics, and doping [61–63]. The reflected and diffracted beams create a pattern on a phosphor-coated screen on the opposite side of the system from the electron gun shown in Fig. 2-2. This pattern can be recorded using a CCD camera for real-time qualitative analysis.

Briefly, the Ewald sphere construction denotes that a sphere with its center positioned at the origin in reciprocal space, with a radius equal to the incident electron k-vector ($2\pi/\lambda$), will produce diffracted intensity when it intersects a crystal reciprocal lattice point. The Ewald sphere construction is shown in Fig. 2-3 [64]. For III-V materials and typical electron RHEED energies, the Ewald sphere is much larger than the spacing between reciprocal lattice points. For a perfectly flat, surface/vacuum interface, the constraint of the dimension normal to the semiconductor surface forces the reciprocal lattice points to extend into rods. A perfectly flat surface with a completely monochromatic electron source would produce “spots” where the Ewald sphere intersects the reciprocal lattice rods. However, due to the inevitable spread in electron energies, the vibration of atoms, and the much larger size of the Ewald sphere with respect to the spacing between the rods, the Ewald sphere is actually a thin shell and the reciprocal lattice rods are very thin cylinders. These effects make the diffraction pattern take the form of elongated “streaks” for smooth surfaces. When spots are observed, this is characteristic of atomic scale roughening, with the spots created by a transmission electron diffraction condition. RHEED is valuable for determining the surface structure of crystalline materials.

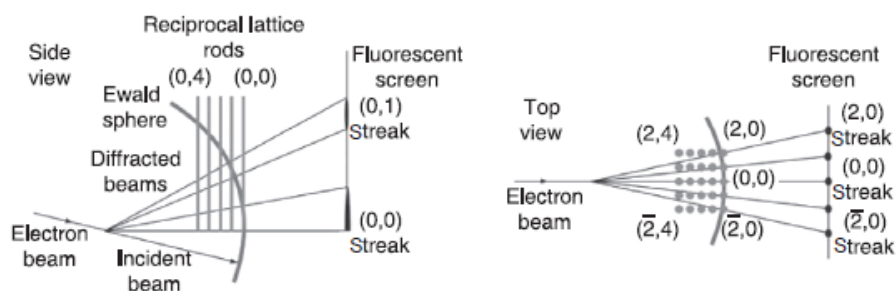


Figure 2-3 Schematic relationship between the Ewald sphere construction and the

RHEED diffraction in both side view (left) and top view (right) from Ref. [64].

In addition, for the analysis of MBE growth, RHEED intensity oscillations are an important technique. First observed in the early 1980s [65–69], the intensity of the electron beam specular reflection, and other diffraction features, oscillate during growth under specific conditions. The oscillation period is equal to the time it takes to grow just one monolayer (ML) of material. Therefore, RHEED oscillations are generally used for the determination of growth rate.

The simple schematic picture of RHEED oscillations is shown in Fig. 2-4. An initial smooth surface before growth starts yields a certain diffraction intensity. Once growth starts under conditions that yield an island growth mode, islands begin to nucleate on the formerly smooth surface. It causes an increase in disorder and providing additional scattering sites, that is step edges, for the incoming electrons. The intensity decreases due to the decrease in long-range order and the increased scattering. The intensity continues to decrease until a 1/2 ML of material is deposited. This represents the maximum disorder during layer-by-layer growth. Subsequent growth leads to coalescence of the nucleated islands and completion of an ML of growth.

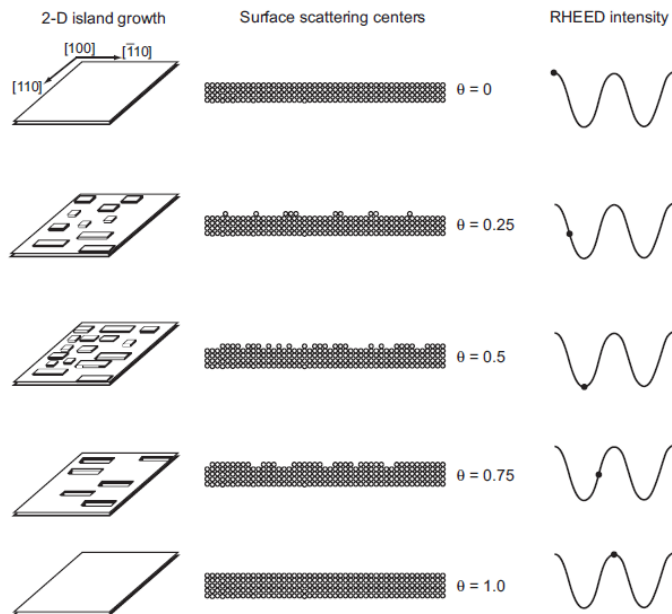


Figure 2-4 Schematic explanation of the origin of RHEED oscillations from Ref. [70].

2.3 Atomic Force Microscopy (AFM)

AFM is based on a relatively simple principle that it involves raster scanning of a sharp and hard probe which is located at the free end of a flexible cantilever. As shown in Fig. 2-5, the tip is scanned over the surface of a sample and senses the interaction forces between the tip and sample. The sample is normally mounted on a piezoelectric scanner, and it enables three-dimensional positioning with sub-nm accuracy. Interaction between the tip and the surface of the sample makes cantilever to be bended, and it is measured by laser light reflected from the cantilever to a position-sensitive photodetector. As changes in cantilever deflection result in variation of the distance between the tip and sample, a constant distance is re-established with a feedback loop between the sample-tip positioning system and a computer-controlled piezoelectric scanner. Registered values of cantilever deflection are electronically converted into a pseudo-3-dimensional image of the sample. As a result, AFM gives real 3-dimensional images of the sample with a vertical resolution of 0.1 nm and lateral resolution of 1 nm.

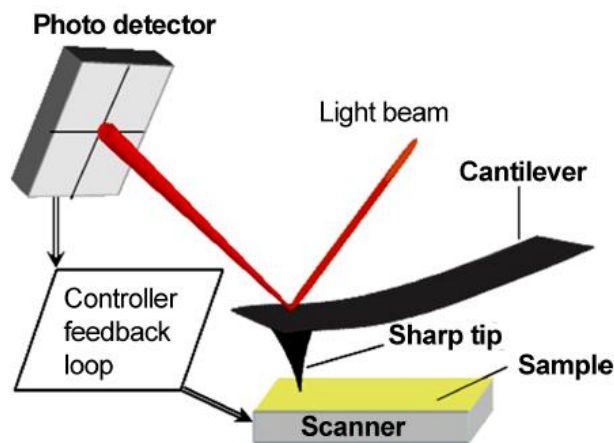


Figure 2-5 Schematic illustration of the basic principles of AFM [71].

2.4 X-Ray Diffraction (XRD)

X-ray diffraction (XRD) is a characterization tool for analyzing crystals. The characterization is conducted by irradiating the sample with X-ray and measuring the diffracted beam intensity.

The vibration of the electrons in the component atoms of the crystal occurs by the irradiation of incident X-ray. Then, this generates spherical wave of the X-ray from the atoms with the same wavelength of the incident beam. The generated X-ray is called scattered X-ray.

Figure 2-6 (a) shows the basic mechanism for the X-ray diffraction. When X-ray is irradiated on the sample at an incident angle of θ , interference of the scattered X-ray toward the same angle of θ occurs if the following formula is satisfied.

$$2d_{hkl} \sin(\theta) = n\lambda \quad (2-1)$$

where d_{hkl} is the spacing between the (hkl) planes of the atomic lattice, n is an integer, λ is the wavelength of the incident X-ray. This condition is well known as Bragg's law.

Based on this principle, the detailed structure of the samples such as thickness and composition of the epitaxial layers, and the quality of grown crystals such as lattice relaxation and mosaicity, can be examined by measuring the diffracted beam intensity at various angles for the incident beam and the detector. Figure 2-6 (b) shows a schematic of diffractometer for such a measurement, in which the two arms, one for the X-ray source and the other for the detector, can be independently rotated to determine the incident and detection angles.

Regarding X-ray sources, Cu tube is one of the most widely used. In an X-ray tube, electrons accelerated from the cathode filament by applying a high voltage of 40 to 60 kV are bombarded onto the target Cu. When the K-shell electrons of Cu is struck by the incident electron and ejected from the atomic orbit, outer-shell electrons subsequently fall into the vacant K-shell. At the same time, emission of a characteristic X-ray with an energy equivalent to the energy difference between the two atomic orbits. For XRD measurement, the emission associated with the transition from the L-shell to the K-shell, called Cu-K α X-ray, is typically adapted.

The X-ray emitted from the Cu tube firstly passes through the divergence slit (DS). It suppresses the horizontal dispersion of the incident beam. Then, X-ray is purified in terms of the wavelength in the monochromator consisted of Ge single crystals and parabolic mirrors. Then, the incident beam is irradiated on the sample after passing through the soller slit (SS) to reduce the vertical dispersion. The diffracted beam is finally detected

by the X-ray counter, where receiving slit (RS) is often inserted in front in order to enhance the measurement resolution.

At the measurement, the sample is located at the center of the diffractometer. The angles between the incident beam and the sample stage, and between the incident beam and the detector are defined as ω and 2θ , respectively. Scanning with rotation of ω axis is called rocking curve measurement for evaluation of mosaicity of the crystal. Scanning with $\Delta\omega : \Delta 2\theta = 1 : 2$ around the diffraction point is used for the evaluation of the crystal quality in a vertical direction to the corresponding crystal plane. For GaAs based epitaxial layer grown on (001) substrates, ω - 2θ scan is often performed around the (004) diffraction ($\omega = 33.0239^\circ$, $2\theta = 66.0479^\circ$). The layer structure in the growth direction can be characterized by this scanning.

If the (001) plane is completely parallel to the sample stage, the enhanced interference of the scattered X-ray takes place when $\omega = \theta$. In practice, however, offset between the ω and θ is generally non-negligible due to manual sample setting. Therefore, alignment of the each axis is typically carried out to make the diffraction intensity highest prior to the main scan.

The Bragg's law described in the eq. (2-1) is synonymous with the Laue's condition:

$$\vec{H} = \frac{\vec{s}_0 - \vec{s}}{\lambda} \quad (2-2)$$

where \vec{H} is reciprocal lattice vector, \vec{s}_0 and \vec{s} are the unit vectors for the incident and the diffracted X-ray, meaning that the constructive interference occurs when the scattering vector of the X-ray is equal to H of the corresponding plane. Therefore, mapping of the diffracted X-ray intensity by sweeping the ω and 2θ within a particular angle range gives us more detailed information regarding the epitaxial films such as lattice constant and strain. This is called reciprocal space mapping (RSM).

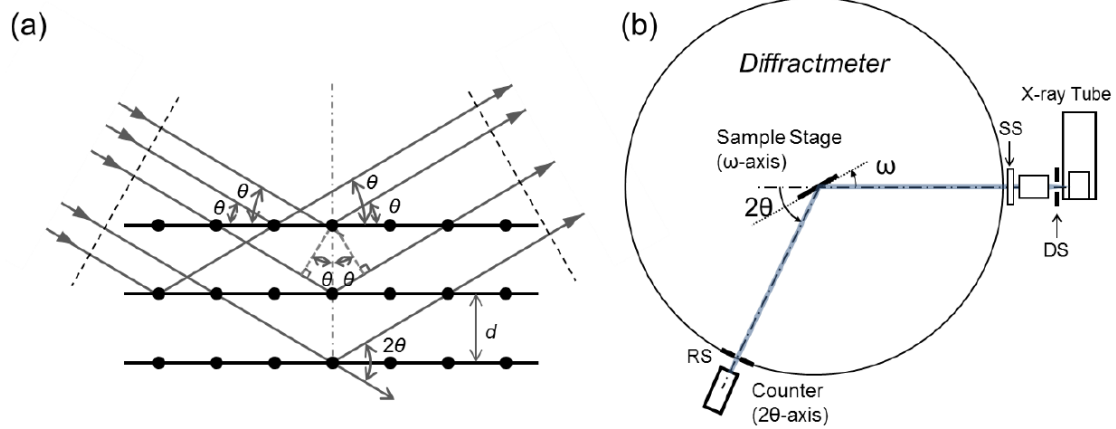


Figure 2-6 (a) Principle of X-ray diffraction (XRD) by crystal with plane spacing of d , and (b) schematic of typical diffractometer for XRD measurement.

2.5 Photoluminescence (PL)

PL spectroscopy measurement is used for a characterization of the luminescence from radiative recombination of carriers in a material generated by incident light. It is commonly used as an evaluation of crystalline quality especially in compound semiconductor. In this study, two PL measurements, continuous wave PL (CWPL) and time resolved PL (TRPL) measurements, are performed. In the case of CWPL, the luminescence spectrum from the sample is measured under continuous excitation by a laser. In the case of TRPL, the time transient of the luminescence due to carrier recombination excited by a short pulse illumination is measured. It is suitable for measuring the dynamics of carriers in a material.

Fig. 2-7 shows the experimental setup for PL measurement used in this study. In CWPL, 532 nm DPSS laser (Nd:YVO₄) or 1064 nm YAG laser are used for excitation light sources. The luminescent light from the sample passes through a long pass filter to cut the excitation light and is led to a spectrometer. The dispersed light was then detected by InGaAs sensor suitable for detection of near infrared light.

In TRPL setup, 780 nm semiconductor pulse laser whose period of 88 ps is used for excitation, which is repetitively triggered by the measurement unit at a repetition rate of 10 MHz. The time interval between triggers should be sufficiently longer than the time required for the emission by excitation to decay completely. The luminescence light from the sample is led to a monochromator. Then, only the chosen wavelength light can come out to be detected by the photomultiplier. The measurement unit integrates the electrical

signals from the photon counting unit versus the time after sending the trigger to the laser and plots them as the time transient of the PL decay.

Since the response time of the system is finite, the measured and plotted PL intensity as a function of the time TRPL(t) is the result of the convolution integral between the actual luminescence decay PL(t) and the instrument response function IRF(t) as

$$\text{TRPL}(t) = \text{PL}(t) * \text{IRF}(t) \quad (2-3)$$

Note that the instrument response time for the TRPL equipment was approximately 0.5ns, and thus the carrier dynamics faster than time scale cannot be accurately evaluated.

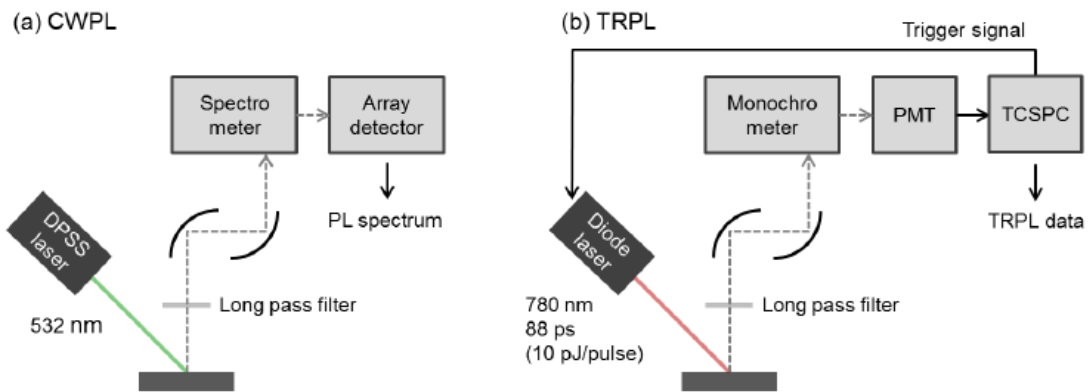


Figure 2-7 Schematic images of measurement setups for (a) CWPL and (b) TRPL

3 GaSb homo epitaxial growth

For the high-quality T2SL epitaxial growth, as a matter of course, primarily, flat surface of GaSb buffer layer should be required. However, GaSb itself is easily oxidized to form such as Sb_2O_3 , therefore, the surface of GaSb after the removal of surface oxide in MBE chamber is expected to be rough. Thus, special care should be required for GaSb homo epitaxial growth including thermal oxide desorption (TOD) before GaSb growth. In this chapter, for the purpose of obtaining the flat with pit-free surface, the surface morphology of GaSb homo epitaxial layer was investigated by changing the growth condition. The mechanism of suppressing the pits was also discussed.

3.1 Pit formation on GaSb epitaxial layer surface

3.1.1 Experimental procedure

(1) Growth condition

- SS-MBE equipped with standard effusion cells was used.
- Substrate: N-doped 0.35° off GaSb (001)
- GaSb growth rate: $0.33 \mu\text{m/h}$
- Beam equivalent pressure (Sb_4/Ga) ratio: 10
- Chemical bonding of Sb was regarded as tetramers Sb_4 because it was not cracked [72].

(2) Two types of growth sequences adapted in this study

- One-step GaSb homo epitaxial layer where the growth temperature was fixed during the GaSb growth. The thickness of the one-step GaSb homo epitaxial layer was fixed at 500 nm.
- Two-step GaSb homo epitaxial layer which was grown at two different temperatures during the GaSb growth. The thickness of two-step GaSb homo epitaxial layer were 100 nm (first layer) and 400 nm (second layer).

(3) One-step GaSb homo epitaxial layer

Thermal oxide desorption (TOD) temperature dependence was investigated under the same growth temperature of 520°C . This growth temperature is known as an appropriate

temperature for obtaining good electrical properties [73].

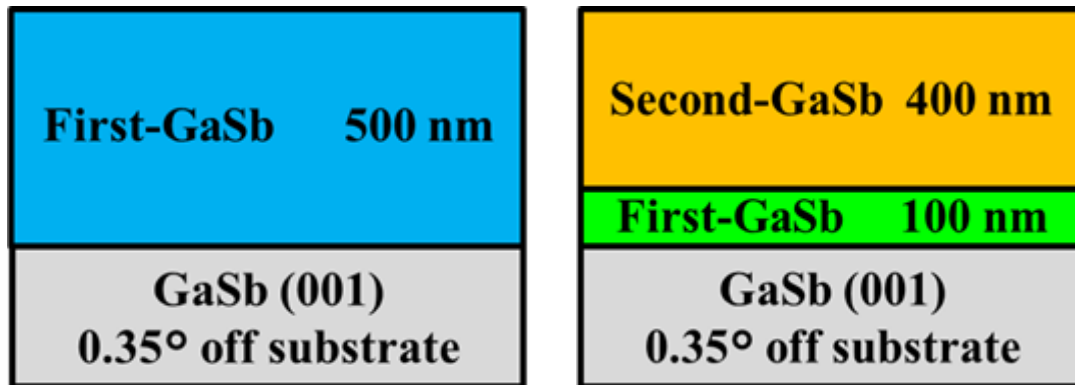
- TOD temperature: 520 °C to 580 °C under the same TOD time of 20 minutes.
- Growth temperature: 520 °C and 440 °C under the same TOD temperature of 550 °C.

(4) Two-step GaSb homo epitaxial layer

- The growth temperature of first- and second-step layer was varied between 520 °C and 440 °C, and between 440 °C and 380 °C, respectively, under the same TOD temperature of 550 °C.
- The growth temperature was changed under Sb₄ irradiation during the interruption of Ga irradiation.
- During the GaSb growth and growth interruption under Sb₄ irradiation, the RHEED pattern maintained (1×3) pattern which is in the Sb stabilization condition [74].

(5) Sample evaluation

- AFM in tapping mode was used for the evaluation of surface morphology of GaSb.
- Cross-sectional transmission electron microscopy (TEM) was used for the evaluation of structural property of GaSb homo epitaxial layer.
- RHEED was observed during GaSb homo epitaxial layer growth in MBE chamber to evaluate the growth mechanism.



(a) One-step grown GaSb

(b) Two-step grown GaSb

Figure 3-1 Schematic structures of (a) One-step grown GaSb and (b) Two-step grown GaSb.

3.1.2 Effect of TOD temperature on GaSb surface morphology

At first, the GaSb surface morphology as a function of TOD temperature was examined. Figure 3-2 (a) to (c) shows the AFM images of one-step 500-nm-thick GaSb homo epitaxial layer surfaces under TOD temperatures of (a) 520 °C, (b) 550 °C, and (c) 580 °C each for 20 minutes. In the case of TOD temperature of 550 °C, the AFM image of one-step 100-nm-thick GaSb homo epitaxial layer grown at the same condition is also shown in Fig. 3-2 (d). For comparison, Fig. 3-2 (e) shows the AFM image of the GaSb substrate immediately after TOD was performed in the MBE chamber at 550 °C for 20 minutes. The surface morphology before GaSb homo epitaxial growth in Fig. 3-2 (e) is very rough with a large root-mean-square (RMS) of 3.10 nm. This is because GaSb surfaces tend to be easily oxidized [22].

The surface of the GaSb homo epitaxial layer was atomically flattened. RMS of 500-nm-thick GaSb is relatively small of 0.10 nm, 0.13 nm and 0.19 nm at TOD temperature of 520 °C, 550 °C and 580 °C, respectively. That of 100-nm-thick GaSb is also small of 0.15 nm at TOD temperature of 550 °C. The height of the atomic steps of each sample is approximately 0.3 nm. This corresponds to 1 ML of GaSb in [001] direction. The terrace width between atomic steps along [1-10] direction is approximately 50 nm. This corresponds to the value estimated by the GaSb lattice constant of 0.61 nm and vicinal angle of 0.35°.

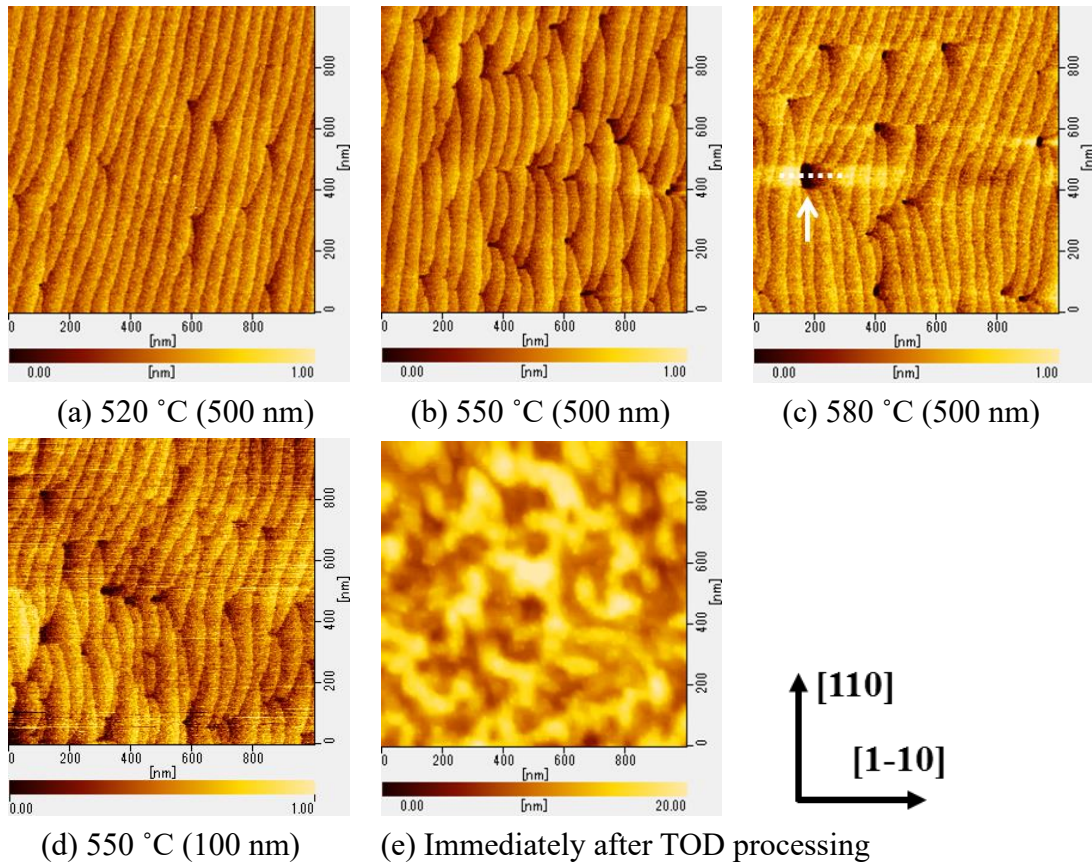


Figure 3-2 AFM images of one-step 500-nm-thick GaSb homo epitaxial layer with TOD temperatures of (a) 520 °C, (b) 550 °C, (c) 580 °C, and (d) that of 100-nm-thick with TOD temperature of 550 °C, and (e) GaSb substrate immediately after TOD processing at 550 °C. Image shows $1 \mu\text{m} \times 1 \mu\text{m}$ area. Color scale of (a)-(d) is 1 nm, and that of (e) is 20 nm.

As can be seen from Fig. 3-2 (a)-(d), the pits which interrupt the terrace could be observed at the surface. At any TOD temperature, the density of the pits on GaSb homo epitaxial layer in Fig. 3-2 was within $2 \times 10^9 \text{ cm}^{-2}$ to $3 \times 10^9 \text{ cm}^{-2}$. There is no temperature dependence of TOD. On the other hand, as shown in Fig. 3-3, the higher the temperature of TOD, the deeper the pit depth becomes. The squares and error bars in Fig. 3-3 show the mean and standard deviation of the pit depths, respectively. The number of the pits on 500-nm-thick GaSb at TOD temperature of (a) 520 °C, (b) 550 °C, and (c) 580 °C is (a) 8, (b) 14, and (c) 15, respectively in $1 \mu\text{m} \times 1 \mu\text{m}$.

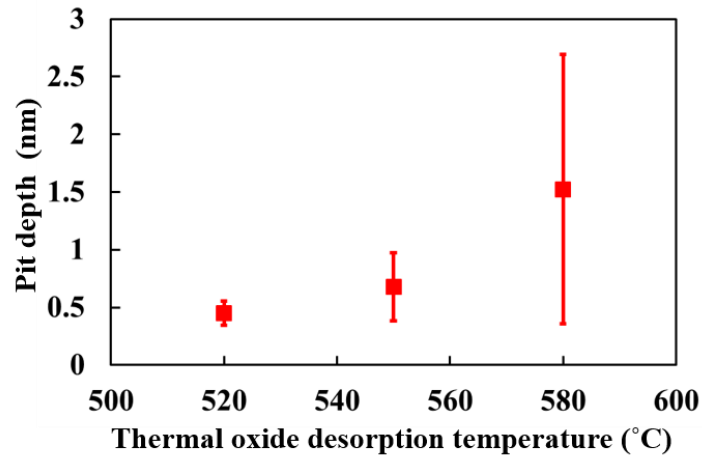


Figure 3-3 Dependence of pit depth on TOD temperature for one-step growth of a 500-nm-thick GaSb homo epitaxial layer surface at the same growth temperature of 520°C.

In order to observe the crystal structure of the pits in detail, cross-sectional TEM measurements were performed. The sample with a TOD temperature of 580 °C was tinny sliced by focused ion beam (FIB) at the pit area indicated by the dotted line in Fig. 3-2 (c). Figure 3-4 is a cross-sectional TEM image of the GaSb homo epitaxial layer observed from the [110] direction indicated by the arrow in Figure 3-2(c). As can be seen from Fig. 3-4, the pit exists only on the surface with a depth of a few nm. It does not penetrate the GaSb homo epitaxial layer. Thus, it can be concluded that the pits do not originate from defects or dislocations in the GaSb homo epitaxial layer. Based on the results of the temperature dependence of TOD, it can be assumed that the pits originate from the initial state of the GaSb surface after TOD treatment. It is also thought that the pits existed on the surface of the GaSb homo epitaxial layer without being flattened from the early stage of its growth, and that the desorption of Sb from the substrate progressed as the TOD temperature increased, resulting in larger pits. In addition, from the comparison with 500 nm and 100 nm thick GaSb in Fig. 3-2 (b) and (d), respectively, there is no significant difference in pit shape and size with typical depth of 0.5 nm to 1.0 nm. Therefore, it can be said that in this thickness range, GaSb growth proceeds while the size and shape of the pits are maintained.

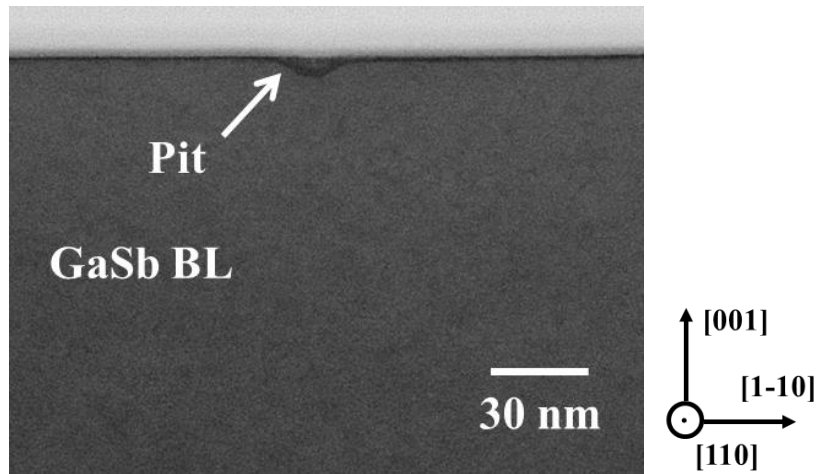


Figure 3-4 Cross-sectional TEM image of a one-step GaSb homo epitaxial layer grown at 520 °C with TOD temperature of 580 °C. The sample was sliced by FIB at the pit position indicated in Fig. 3-2 (c) and observed from [110] direction.

3.1.3 Effect of growth temperature on GaSb surface morphology

GaSb surface morphology is affected by surface migration of Ga atoms. Moreover, Ga migration length largely depends on the growth temperature [75], the growth temperature dependence of the GaSb homo epitaxial layer was investigated. The growth temperature of the GaSb homo epitaxial layer was lowered under a TOD temperature of 550 °C. Figure 3-5 shows an AFM image of the one-step GaSb homo epitaxial layer grown at 440 °C. In the case of 440 °C growth, the straightness of the steps became worse, and the flatness of the surface also became worse with an RMS of 0.16 nm, accompanying mounds and valleys compared to the growth at 520 °C (shown in Fig. 3-2 (b)) with RMS of 0.13 nm. The initial significant roughness of the GaSb substrate shown in Fig. 2 (e) could not be fully flattened due to the decrease in the surface migration length of Ga atoms. On the other hand, the pits on the surface disappeared at 440 °C growth.

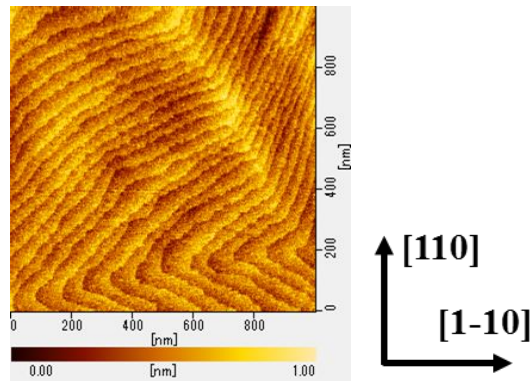


Figure 3-5 AFM image of one-step GaSb homo epitaxial growth grown at 440 °C under TOD temperature of 550 °C. Image shows 1 μm × 1 μm area. Color scale is 1 nm.

3.2 Improvement of GaSb surface morphology by two-step LT/HT growth sequence

3.2.1 TH to LT and LT to HT growth sequence

When heterostructures such as superlattices are grown on top of this GaSb homo epitaxial layer, these pits and roughness can cause defects and dislocations, which can degrade device characteristics such as IR-PD. From the results of the growth temperature dependence described in Section 3.1, it is expected that a good surface morphology can be obtained by combining low and high temperature growth. Thus, a two-step GaSb homo epitaxial growth sequence was investigated. AFM image of two-step GaSb homo epitaxial layers where the first/second layers are grown at (a) 440 °C/520 °C and (b) 520 °C/440 °C, respectively is shown in Fig. 3-6. Just as expected, by adapting two-step growth, a flat with pit-free surface of RMS 0.10 nm was obtained in both cases. a superior flat surface morphology was obtained in both two-step growth cases. However, (a) 440 °C/520 °C is better in terms of the straightness of the step. These changes in surface morphology will be discussed in the next section.

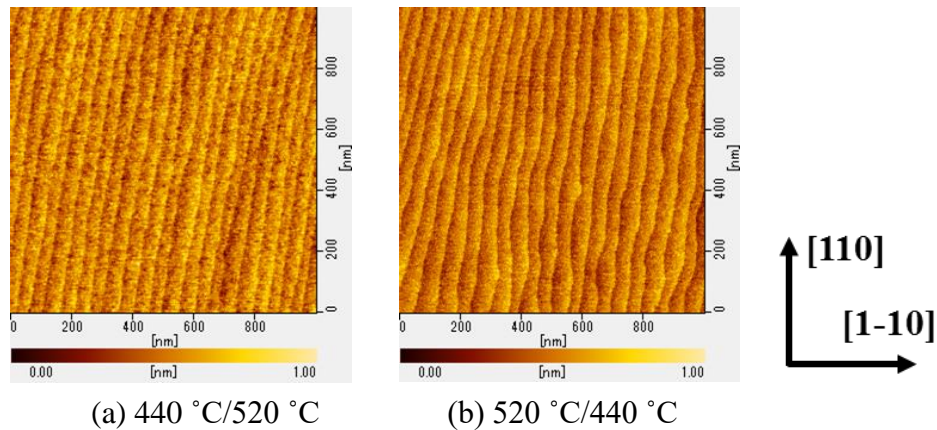


Figure 3-6 AFM image of two-step GaSb homo epitaxial layer where the first/second layers were grown at (a) 440 °C/520 °C and (b) 520 °C/440 °C, respectively. Image shows 1 μm × 1 μm area. Color scale is 1 nm.

3.2.2 RHEED observation during GaSb growth

From the perspective of fundamental crystal growth, it is important to consider the reason for the change in the shape of the atomic steps shown in Fig. 3-6. For this reason, the epitaxial growth of GaSb at an even lower temperature were performed to observe the change in surface morphology with RHEED observation during GaSb growth. Figure 3-7 shows an AFM image of the two-step GaSb homo epitaxial layer whose second layer was grown at (a) 410 °C and (b) 380 °C, under the fixed growth temperature of 520 °C at

first layer. RHEED intensity variations of a specular spot observed from [1-10] azimuth during GaSb homo epitaxial growth at 520 °C, 440 °C, 410 °C, and 380 °C, respectively, are shown in Figure 3-8.

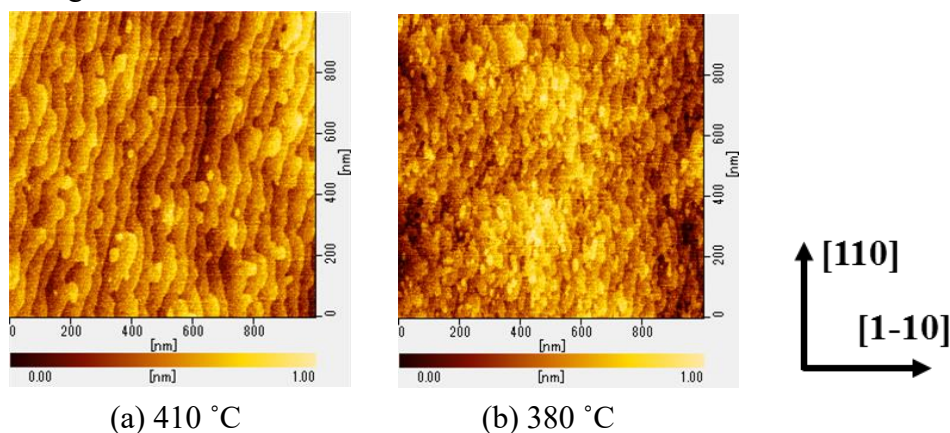


Figure 3-7 AFM image of two-step GaSb homo epitaxial layer whose second layers were grown at (a) 410 °C and (b) 380 °C. The first layers were grown at 520 °C in both cases. Image shows 1 μm × 1 μm area. Color scale is 1 nm.

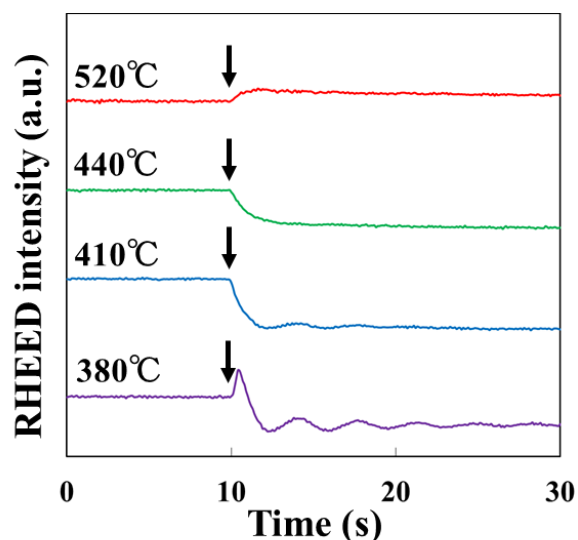


Figure 3-8 RHEED intensity variations of a specular spot observed from [1-10] azimuth during the GaSb growth at 520 °C, 440 °C, 410 °C, and 380 °C. The arrows in the figure indicate the time of Ga shutter opening.

Focusing on the growth temperatures of 520 °C and 440 °C, where the atomic steps could be clearly seen in Fig. 3-2 (b) and Fig. 3-6 (b), respectively, no RHEED intensity oscillation was observed after the GaSb growth started with Ga shutter opening. On the other hand, the surface morphology with a mixture of the atomic steps and two-

dimensional islands was observed at a growth temperature of 410 °C. When the growth temperature was further reduced to 380°C, the atomic steps were not observed, and only two-dimensional islands were observed. In this condition, RHEED intensity oscillation with relatively large amplitude was observed. Based on the relationship between surface morphology and RHEED properties with respect to the growth temperature, it is considered that the growth mode gradually transfers from step-flow mode to two-dimensional nucleation mode as the growth temperature decreased. As for surface roughness, it was kept low with an RMS of 0.10 nm between 520 °C and 440 °C, which was suitable for device structure growth. However, below 410 °C, it became larger with an RMS of 0.10 nm to 0.14 nm as shown in Table 1. This is because the Ga migration length decreases with lowering the growth temperature same as in the case of one-step GaSb homo epitaxial layers discussed in Section 3.1. Regardless of the growth mode, no pits were observed on the surface below the growth temperature of 440 °C. As a result, flat with pit-free surfaces could be obtained by two-step growth, where both growths proceed with step-flow mode.

Table 3-1 Summary of the RMS values of GaSb homo epitaxial layer with different TOD and growth temperatures.

TOD temperature (°C)	520	550	580	550				
Growth temperature (°C)	520			440	520/440	440/520	520/410	520/380
RMS (nm)	0.10	0.13	0.19	0.16	0.10	0.10	0.13	0.14

3.2.3 Mechanism of the planarization of the pits on GaSb

As discussed in the TOD temperature dependence experiment in Section 3.1, the pits already existed at the GaSb substrate surface after TOD was performed in the MBE chamber, that is, before GaSb growth started. As the TOD temperature increased, Sb desorption from the surface becomes large. This makes pits size larger as discussed in Fig. 3-2 in Section 3.1.

As already discussed in Section 3.1, pits on the GaSb surface are planarized at relatively low growth temperatures of 440 °C, 410 °C, and 380 °C. On the other hand, they are not planarized and remain on the surface at relatively high growth temperature of 520 °C.

Moreover, as inferred from the cross-sectional TEM in Fig. 3-4, the pit is estimated to consist of a number of steps and narrow terraces. Figure 3-9 shows the schematic image of the pits which exist inside wide terrace about 50 nm by vicinal substrate. Typical pit is several nm in depth and several tens of nm in width, however, here shows a pit of small size as a simplified example. Figure 3-9 also shows the image of the Ga adatom irradiated on the surface. In the case of normal MBE growth, the beam flux of element material is irradiated at a uniform density at any position on the substrate. Therefore, the growth rate of GaSb should be the same in the pit and the wide terrace regions. In this case, if there is no transfer of adatoms between terraces across the steps, the pits should remain and not be planarized as growth proceeds. Therefore, in the case of low growth temperature of 440 °C, there should be a lateral flow of Ga adatoms from the upper to the lower terrace as shown by the blue arrow in Fig. 3-9. On the other hand, in the case of high growth temperature of 520 °C, as discussed in Section 3.1, the pits remain on the GaSb surface, and their sizes are almost unchanged during the growth. Therefore, the growth rate of GaSb should be same at pit and terrace regions. Considering the Ga adatom migration properties with respect to the growth temperature, a lateral flow of Ga adatoms from the lower to the upper terraces indicated by the red arrow might exist and cancel with the flow in the opposite direction indicated by the blue arrow.

The above-mentioned difference in the behavior of these Ga adatoms at low and high temperatures can be explained by the potential barrier that occurs at the step edges. Figure 3-10 shows the schematic image of the cross section of vicinal plane and surface potential around step edge. Ga adatom which arrives at the GaSb surface hops the potential energy E_m formed by the bonding with surface Sb atoms and walks randomly at the surface. Ga adatoms diffuse two-dimensionally across the surface, but in order to move to the lower from upper terrace, they must overcome an energy barrier called the Schwoebel-Ehrlich barrier E_s [76, 77]. At the adsorption position on the valley side of the step edge, the

presence of dangling bonds from the atoms at the step edge in addition to the dangling bonds from the Sb atoms at terrace makes potential energy larger by E_i . As a result, the energies of the Ga adatoms required to move from the upper to the lower terrace and from the lower to the upper terrace are $E_m + E_s$ and $E_m + E_s + E_i$, respectively. The relationship with the energy of the Ga adatom E_{ad} determines the lateral flow of the Ga adatoms.

For example, as reported in Ref. [23, 78], at a low temperature growth of GaSb, in the case of the energy of the Ga adatom is too low to overcome $E_m + E_s$ at step edge, a pyramidal structure is formed since Ga adatom cannot move to lower from upper terrace and growth proceeds only upward inside of the terrace. In the precise GaSb growth experiments regarding to growth temperature using vicinal substrate, the growth temperature below 390 °C causes the pyramidal shape due to the existence of the Schwoebel-Ehrlich barrier at the step edge [23]. Thus, in the case of GaSb homo epitaxial growth, the barrier height of $E_m + E_s$ is roughly estimated to be equal to the thermal energy $k_B T$ at 390 °C (57.1 meV).

In the case of the low growth temperature of 440 °C in this study, whose $k_B T$ is 61.5 meV, since no pyramidal structure is observed, it can be assumed that there is a lateral move of Ga adatoms from the upper to the lower terrace as indicated by the blue arrow in Fig. 3-9. On the other hand, at this low temperature, it is not considered to have enough energy to generate the lateral move of Ga adatoms from the lower to the upper terrace. In other words, the energy relationship is $E_m + E_s < E_{ad} < E_m + E_s + E_i$. Figure 3-11 shows the schematic image of the growth process in the case of low growth temperature of 440 °C. Although the example of the growth process is shown in a one-dimensional schematic, if there is a lateral migration of 10 Ga adatoms from the terrace of the vicinal substrate to the pit area during 1 ML growth, the pit will be flattened at 5 ML growth in this example. In general, if there is even a small amount of lateral Ga adatom move from the upper terrace to the pit, the pit will be eventually planarized.

Next, the case of high temperature growth at 520 °C will be discussed. In this high growth temperature, $k_B T$ of Ga adatom (E_{ad}) is 68.3 meV. The difference in E_{ad} between 440 °C and 520 °C seems to be relatively small. This seems to be difficult to form the energy relationship of $E_{ad} > E_m + E_s + E_i$ to enable the lateral move of Ga adatoms from lower to upper terrace. However, a high temperature might induce the shrinkage of each energy barrier heights E_m , E_s , and E_i . Especially, E_i might be largely influenced by the temperature since the related number of dangling bonds is more than the others. These shrinkages of energy barriers make the energy relationship of $E_{ad} > E_m + E_s + E_i$ at 520 °C. Thus, the lateral move of Ga adatoms from the lower to the upper terrace occurs to the same extent as that in the opposite direction, and in effect, the growth proceeds at the

same rate in the pit and terrace of the vicinal substrate regions. As a result, the pits do not planarized and remain on the surface as the growth proceeds as shown in Fig. 3-12.

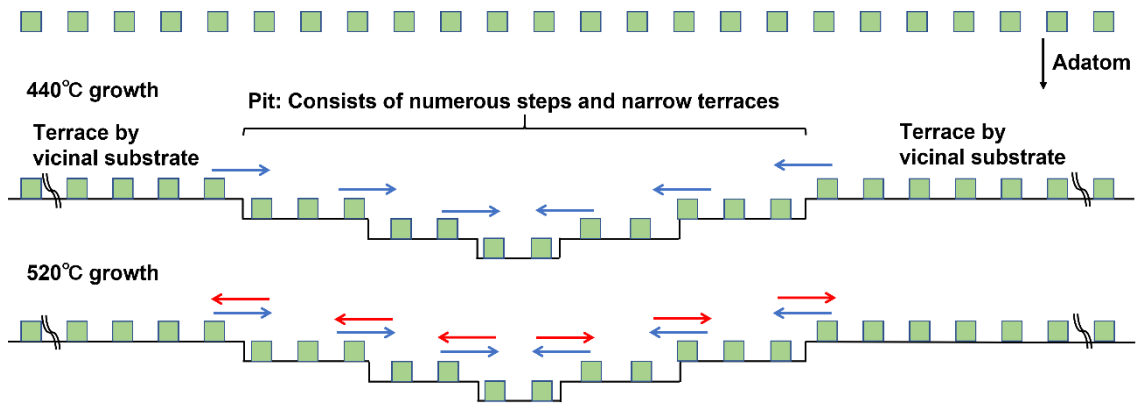


Figure 3-9 Schematic image of a pit exists in the wide terrace by the vicinal substrate. The image of the Ga adatom irradiated on the GaSb substrate with a constant flux is also shown. Blue and red arrows indicate the lateral flow direction of Ga adatom at the step of GaSb surface.

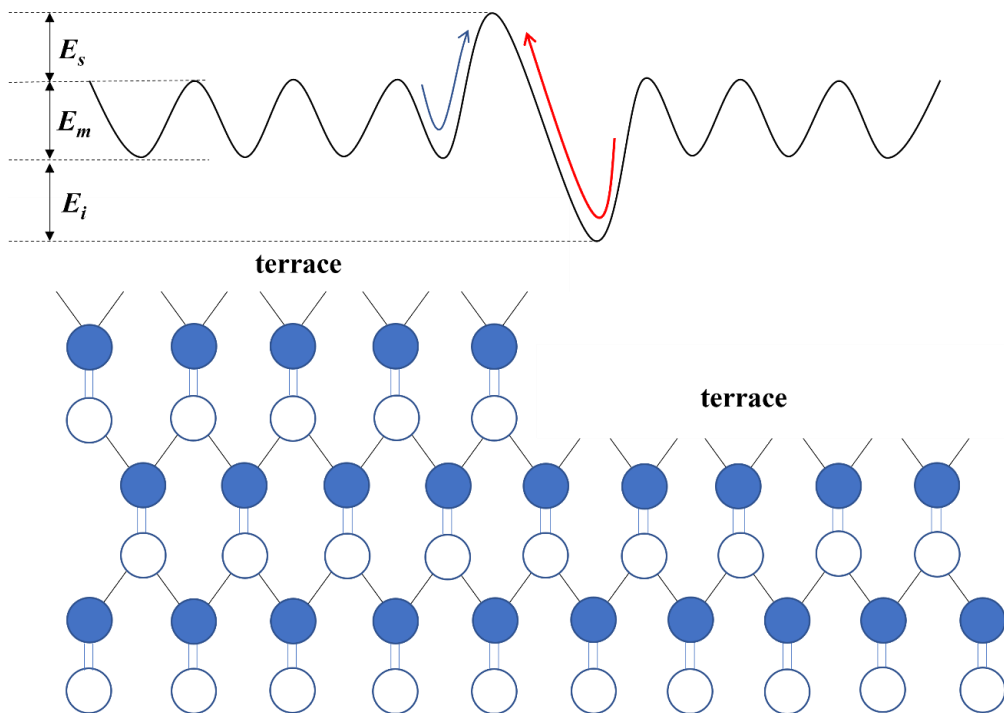


Figure 3-10 Schematic image of the cross section of vicinal plane (lower) and surface potential around step edge (upper). Filled and open circles in lower image denote Sb and Ga atoms, respectively. E_m , E_s , and E_i in upper image indicates the potential energy formed by the bonding between Ga adatoms with surface Sb atoms, the Schwoebel-Ehrlich energy specially formed at the step edge, the potential energy formed at the adsorption position on the valley side of the step edge.

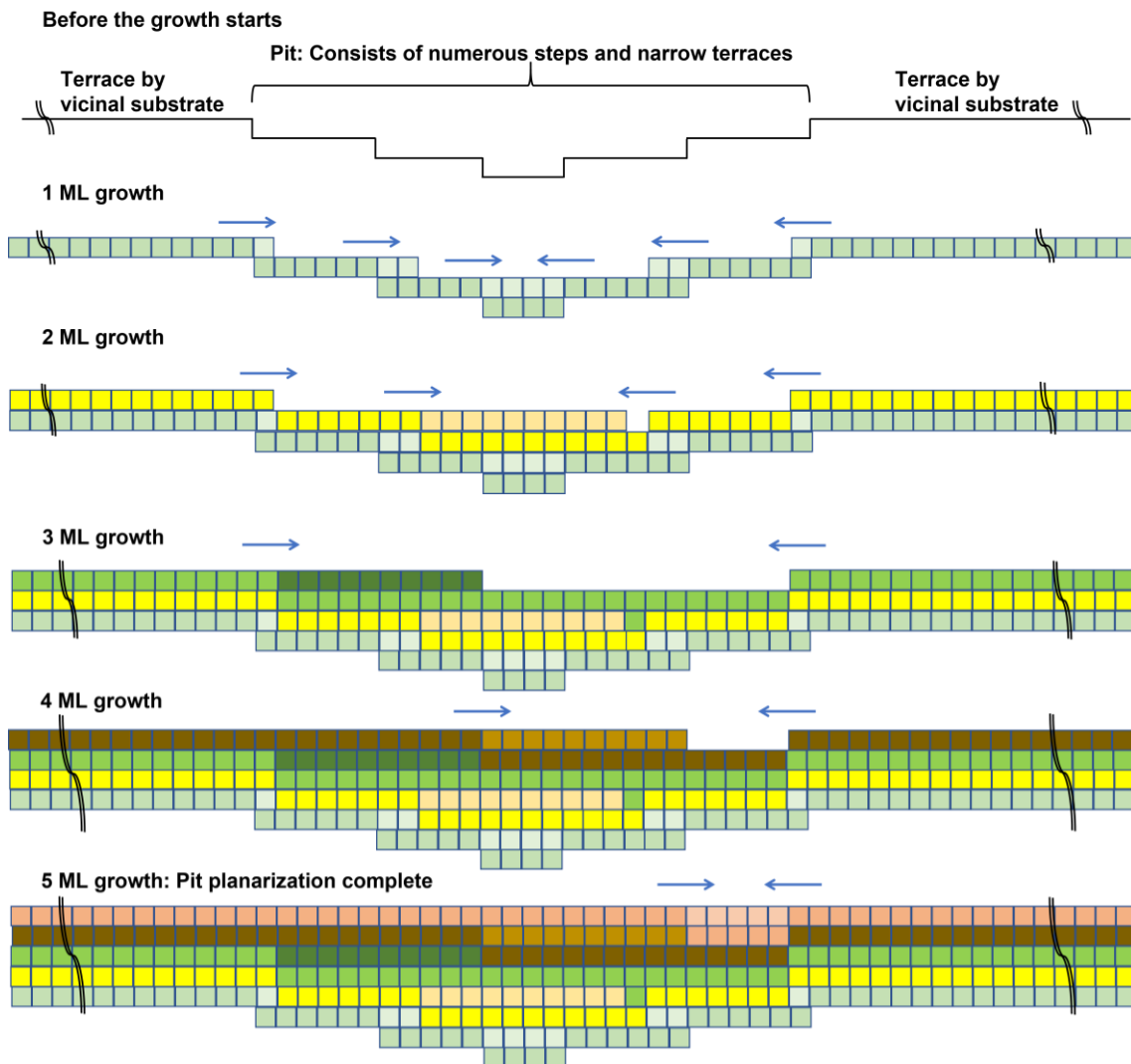


Figure 3-11 Schematic image of the GaSb growth process at pit region in the case of low growth temperature of 440 °C. The case is shown assuming that 10 Ga adatoms flow into the pit from the terrace by vicinal substrate during 1 ML growth. In this case, pit planarization completes by 5 ML growth of GaSb.

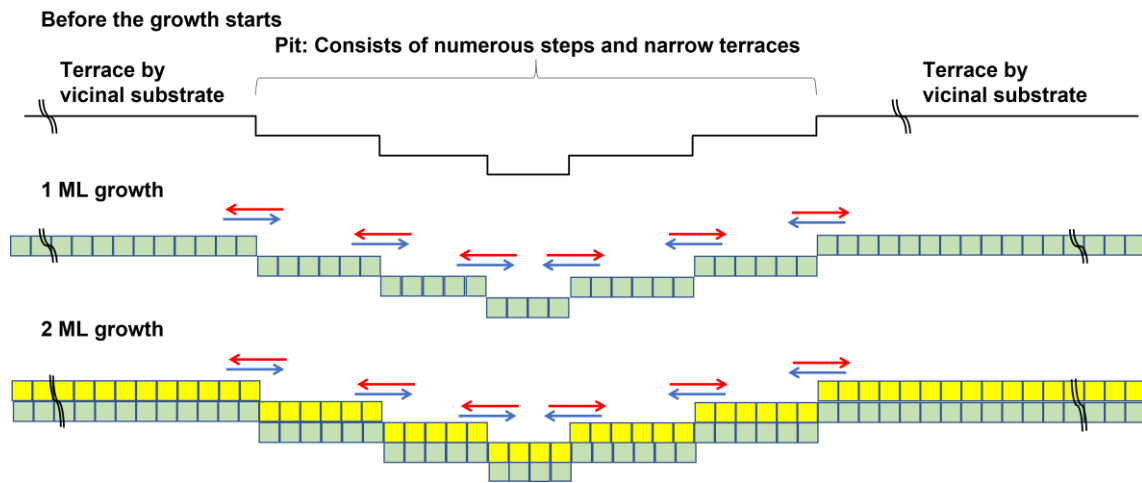


Figure 3-12 Schematic image of the GaSb growth process at pit region in the case of high growth temperature of 520 °C. The image shows in the case of 1 ML and 2 ML growth of GaSb. In this case, pit is not planarized and remains on the surface because the growth rate of GaSb is same at pit and terrace by vicinal substrate.

3.3 Summary of Chapter 3

The surface morphology of GaSb homo epitaxial layer by changing the TOD and growth temperature, and growth steps was investigated. TOD temperature dependence revealed that pits on the surface were found to originate from the initial surface state after TOD processing at a growth temperature of 520 °C. TEM observation also revealed that the pits only existed on the surface from the beginning of the growth without being planarized, and do not originate from defects or dislocations in GaSb homo epitaxial layer. These pits on the surface disappeared when the growth temperature was lowered to 440 °C, whereas the roughness of the surface becomes greater. By combining high and low growth temperatures, a flat with pit-free surface was obtained under step-flow mode in both growth steps, revealed by the relationship between AFM and RHEED observation. While a superior surface morphology was obtained in both two-step growth cases, 440 °C/520 °C is better than 520 °C/440 °C in terms of the straightness of the step. The phenomenon that the planarization of pits differs depending on the growth temperature can be explained by the relationship between the energy of Ga adatoms and the potential barrier specially formed at the step edges. At low growth temperature with low energy of Ga adatom, only unidirectional flow of Ga adatom from the upper terrace to the lower terrace is generated, advancing the planarization of the pits. On the other hand, at high growth temperature with high energy of Ga adatom, the lateral movement of Ga adatoms in both the upper and lower ways is generated and eliminates the inflow of Ga adatoms into the pits. As a result, the pits are not planarized and remains on the surface.

4 InAs/GaSb hetero epitaxial growth

From the investigation in Chapter 3, GaSb homo epitaxial layer with flat and pit free was obtained. Next step is to grow InAs hetero structure on this flat GaSb layer. The aim of this chapter is to obtain a flat and pit-free thick InAs layer on GaSb suitable for the contact layer of GaSb-based IR-PD devices. To achieve this, growth parameters that may contribute significantly to InAs growth such as As₂ pressure, growth temperature, and growth sequence of InAs were examined.

4.1 Effect of As₂ pressure on InAs hetero epitaxial growth on GaSb

4.1.1 Experimental procedure

(1) Growth condition

- SS-MBE equipped with standard effusion cells was used.
- Substrate: N-doped GaSb 0.35° off (001) in the direction of (111)
- Chemical bonding of As: dimers As₂ (Cracking temperature is 900 °C)
- The sample structure grown in this experiment is shown in Fig. 4-1.
- The sample was heated to 530 °C under Sb₄ irradiation for oxide desorption.
- 100-nm-thick-GaSb buffer layer was grown by two-step high- and low-temperature growth discussed in Chapter 3.
- The growth was switched to InAs. To observe the effects of As₂ pressure on InAs hetero growth on GaSb.
- The other growth parameters such as the In pressure and growth temperature were fixed at 4.4×10^{-8} Torr (the growth rate at 0.20 μm/h) and 440 °C, respectively.
- As₂ pressures: 2.6×10^{-6} , 1.3×10^{-6} , 6.6×10^{-7} , and 2.2×10^{-7} Torr corresponding to V/III ratios of 60, 30, 15, and 5, respectively.
- Figure 4-2 shows the shutter sequence at the InAs/GaSb interface. To observe the effects of As/Sb exchange on InAs hetero growth, the irradiation period of Sb after GaSb growth and that of As before InAs growth were set at relatively longer of 5 s, enhancing the As/Sb exchange.

(2) Sample evaluation

- AFM in the tapping mode was performed for surface observation.

- Cross-sectional TEM was performed in the [110] direction for the evaluation of structural properties.
- Fast Fourier transform mapping (FFT_M) of high-resolution TEM images and X-ray RSM were performed for strain analysis of the sample.

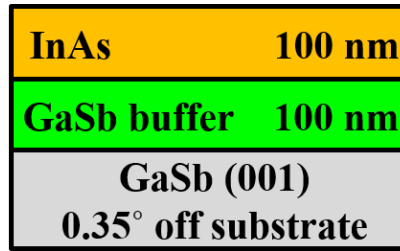


Figure 4-1 Schematic sample structure of InAs on GaSb substrate fabricated in this experiment

	GaSb	Sb irradiation 5 sec	Interruption 5 sec	As irradiation 5 sec	InAs
Ga					
Sb					
In					
As					

Figure 4-2 Shutter sequence of MBE growth at the InAs/GaSb interface adopted in this experiment.

4.1.2 Surface observation

The AFM images of InAs on GaSb substrate with four As₂ pressures under the fixed growth temperature of 440 °C are shown in Fig. 4-3. The AFM images of the GaSb homo epitaxial layer are also shown in Fig. 4-4 for comparing with InAs. Summary of the root-mean-square (RMS) of InAs epitaxial layer surface is shown in Table 4-1. Noteworthy, at a high As₂ pressure, pits were observed on the InAs surface. As the As₂ pressure decreased, the pit size decreased and finally the pits disappeared at the As₂ pressure of 2.2×10^{-7} Torr. The RMS of the sample surface also decreased as the pits disappeared. As a result, an atomically smooth surface without pits comparable to the GaSb surface was obtained at the lowest As₂ pressure condition of 2.2×10^{-7} Torr in this experiment as shown in Fig. 4-3 (h).

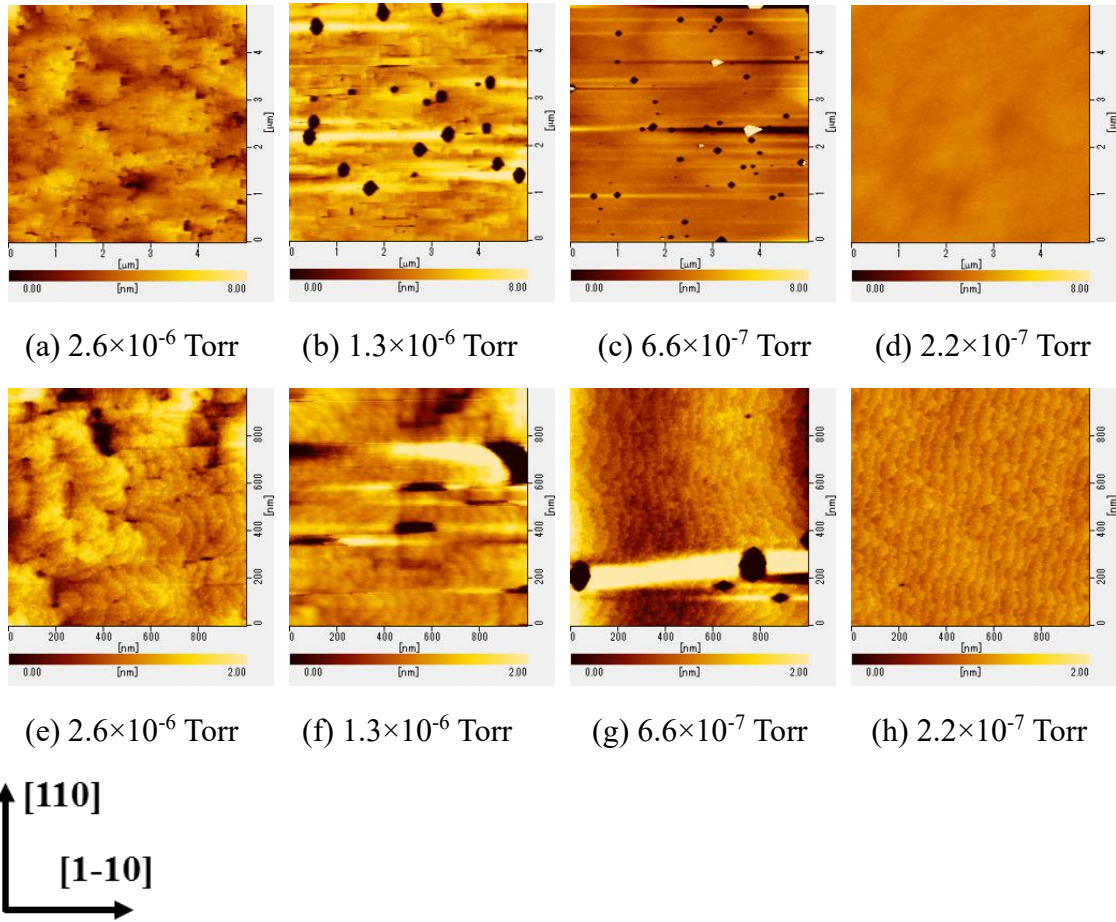


Figure 4-3 AFM images of InAs epitaxial layer on GaSb grown at different As_2 pressures. As_2 pressure is shown in each image. Images show (a) to (d) $5 \mu\text{m} \times 5 \mu\text{m}$, and (e) to (h) $1 \mu\text{m} \times 1 \mu\text{m}$ area, respectively. Color scales are (a) to (d) 8 nm, and (e) to (h) 2 nm, respectively.

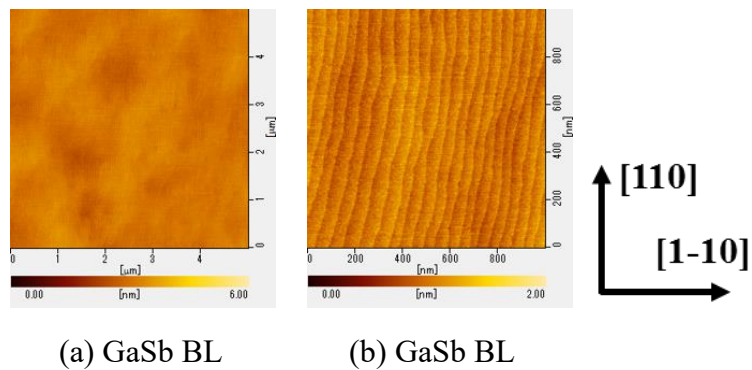


Figure 4-4 AFM images of the GaSb buffer layer. Images show (a) $5 \mu\text{m} \times 5 \mu\text{m}$ and (b) $1 \mu\text{m} \times 1 \mu\text{m}$ areas, respectively. Color scales are (a) 8 nm, and (b) 2 nm, respectively.

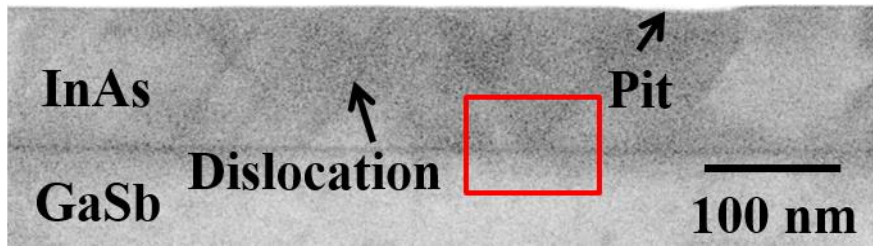
Table 4-1 The summary of the RMS roughness within AFM images of Fig. 4-3. The upper and lower rows indicate the RMS of roughness within FOV of 5 μm and 1 μm , respectively.

As ₂ pressure (Torr)		2.6 $\times 10^{-6}$	1.3 $\times 10^{-6}$	6.6 $\times 10^{-7}$	2.2 $\times 10^{-7}$	GaSb buf.
RMS (nm)	FOV 5 μm	0.91	3.66	3.08	0.18	0.18
	FOV 1 μm	0.34	0.57	1.70	0.10	0.11

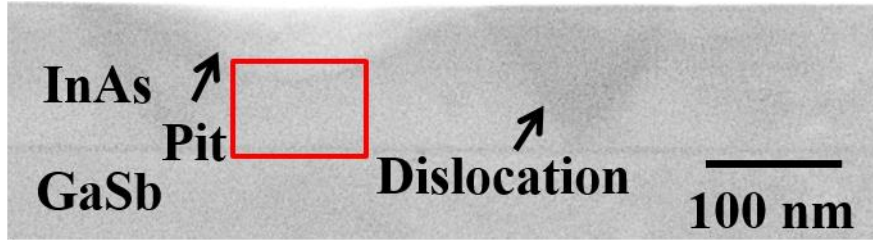
Regarding the surface morphology, the step edge of InAs hetero epitaxial layer on GaSb grown at the As₂ pressure of 2.2 $\times 10^{-7}$ Torr is rougher than that of the GaSb homo epitaxial layer. The GaSb homo epitaxial layer growth proceeds with a step-flow mode since RHEED oscillation was not observed during the growth discussed in Chapter 3. On the other hand, RHEED oscillation was observed during InAs growth at the As₂ pressure of 2.2 $\times 10^{-7}$ Torr. As discussed in Ref. [30], InAs growth proceeds with a two-dimensional (2D) nucleation mode at the terrace, at the same time, with a step-flow mode at the step edge. This causes the coalescence of a 2D island at the terrace with the step edge, consequently, rougher step edges would be observed.

4.1.3 Cross sectional observation

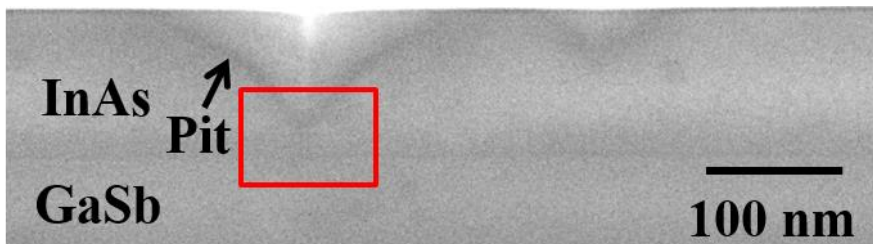
To understand the differences in surface morphology shown in Fig. 4-3 from another aspect, cross-sectional TEM measurements were performed for the four samples with different As₂ pressures. The cross-sectional TEM images of InAs on GaSb with different As₂ pressures are shown in Fig. 4-5. A relatively small pits are observed, on the other hand, the dislocation density is significantly high at the highest As₂ pressure condition of 2.6 $\times 10^{-6}$ Torr. The dislocation density monotonically decreases as the As₂ pressure decreases. Below 6.6 $\times 10^{-7}$ Torr, it disappears within the 3 μm range of the cross-sectional TEM image. Regarding the pit size, once the pits become the largest at 1.3 $\times 10^{-6}$ Torr, they become smaller as the As₂ pressure decreases. At 6.6 $\times 10^{-7}$ Torr, only pits without dislocations exist. By further lowering to 2.2 $\times 10^{-7}$ Torr, pits completely disappeared. As a result, the sample free from pits and dislocations was obtained.



(a) 2.6×10^{-6} Torr



(b) 1.3×10^{-6} Torr



(c) 6.6×10^{-7} Torr



(d) 2.2×10^{-7} Torr

Figure 4-5 Cross-sectional TEM images of InAs on GaSb grown at different As_2 pressures of (a) 2.6×10^{-6} Torr, (b) 1.3×10^{-6} Torr, (c) 6.6×10^{-7} Torr, and (d) 2.2×10^{-7} Torr.

In order to understand the origin of the dislocation and pits, high resolution TEM measurements were performed at the areas indicated with red rectangular boxes in Fig. 4-5. Figure 4-6 shows the obtained images. As can be seen from Fig. 4-6 (a), the dislocations originate at the interface between InAs and GaSb and extend in the (111) direction. However, regarding the pits, as shown in Fig. 4-6 (b) and (c), they do not originate at the InAs/GaSb interface. They appear to be formed spontaneously during the

growth.

Prior to the investigation of InAs hetero growth on GaSb, InAs homo epitaxial growth were investigated in a wide range of growth condition by changing growth temperature and As pressure in Ref. [26]. This paper reports that pit and pyramidal structure tend to be formed at relatively low and high growth temperature, respectively [26]. Regarding the pit formation, they are caused by the contamination, residual oxide, and In cluster of the substrate [26]. On the other hand, pyramidal structures at relatively high growth temperature are explained that the surface reconstruction in the In stabilization condition is the cause of them [27]. Thus, it can be said that InAs growth is easily affected by the surface condition and the stability of the (001) plane growth is easily broken compared to the other materials such as GaAs or GaSb. Therefore, the pit formation in the hetero epitaxial growth of this study is also considered to reflect this instability of InAs growth. However, since there exists no voids or particles at the bottom of the pits in Fig. 4-6 as reported in Ref. [26], it is speculated that other factors specific to hetero epitaxial growth also contribute to the formation of the pits in this study. The detail will be discussed in Section 4.1.4.

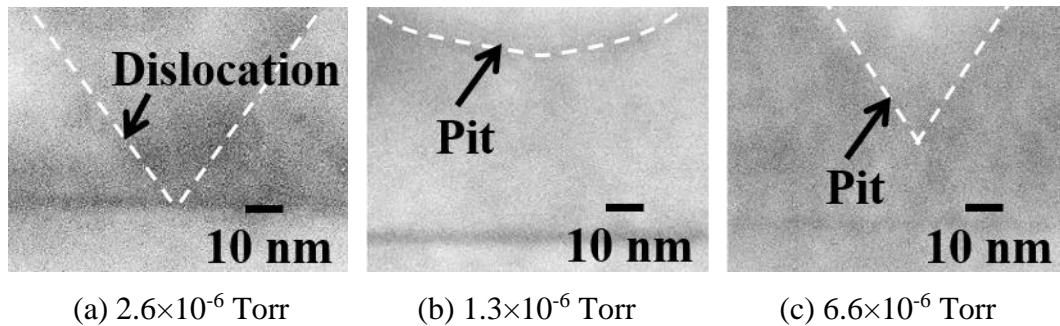


Figure 4-6 High resolution cross-sectional TEM images of InAs on GaSb indicated by the red frames in Fig. 4-5. The As_2 pressures are (a) 2.6×10^{-6} Torr, (b) 1.3×10^{-6} Torr, and (c) 6.6×10^{-7} Torr, respectively. The white dotted lines are visual guides.

4.1.4 Strain analysis

To consider the dislocations and pits of the InAs layers indicated in Fig. 4-5 and 4-6, FFTM analyses of high-resolution TEM images are performed. FFTM mapping images of the [002] lattice plane distance of InAs on GaSb with different As_2 pressures are shown in Fig. 4-7. Histograms of the lattice distance with color scales are also shown in Fig. 4-7. The blue and purple arrows in each histogram indicate the [002] lattice plane distances of free-standing and strained InAs layers which are derived from Poisson's ratio of 0.33, respectively.

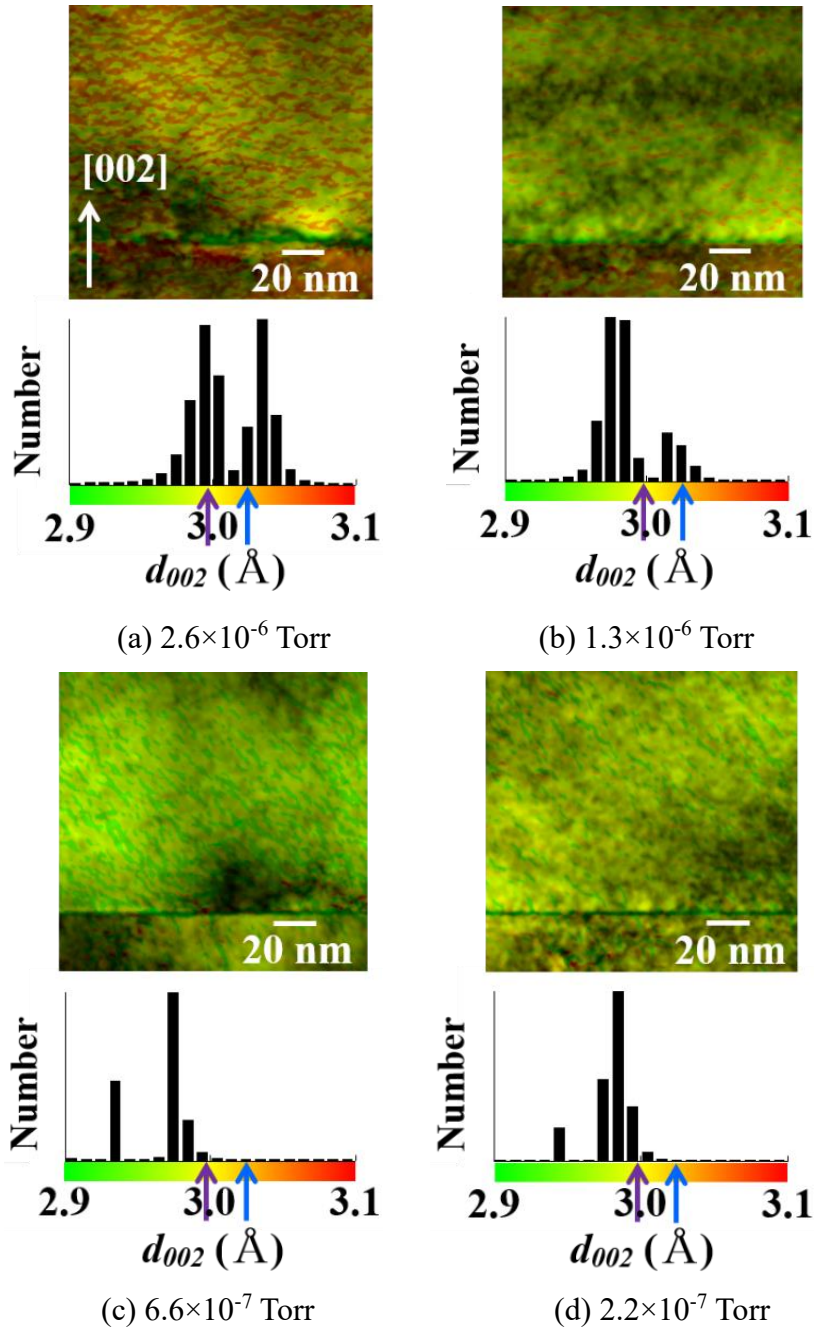


Figure 4-7 FFTM mapping images of the [002] lattice plane distance derived by high resolution TEM images of the sample grown at As_2 pressures of (a) 2.6×10^{-6} Torr, (b) 1.3×10^{-6} Torr, (c) 6.6×10^{-7} Torr, and (d) 2.2×10^{-7} Torr. Histograms of each FFTM image with a color scale of the [002] lattice plane distance are also shown.

Transition layer with a relatively small lattice distance compared with GaSb or InAs can be confirmed in each FFTM mapping image. The thickness of the transition layer decreases from approximately 5 to 1 nm as the As_2 pressure decrease.

The dark layers at the interfaces of InAs and GaSb in Fig. 4-5 are found to be transition layers with small lattice constants by comparing TEM images in Fig. 4-5 with FFTM images in Fig. 4-7. The transition layer can be considered to be formed by the As/Sb exchange during the As₂ soaking before InAs growth because InAs layer thicknesses from the upper end of the transition layers are the same at 110 nm for each sample. They are seemed to consist of a ternary material such as GaAsSb.

The ratio of relaxed InAs of As₂ pressure of 2.6×10^{-6} Torr is the largest among the four samples. As the As₂ pressure decreases, the ratio of relaxed InAs decreases. On the other hand, the ratio of the strained InAs layer increases. As a result, the dislocations observed at higher As₂ pressures are attributed to the tensile strain of transition layer at the interface. Therefore, this could be regarded as misfit dislocations caused by the tensile strain of transition layer such as GaAsSb at the interface.

To consider the strain of InAs on GaSb macroscopically, X-ray RSM of InAs on GaSb with different As₂ pressures were performed. Figure 4-8 shows the X-ray RSM images of InAs/GaSb with various As₂ pressures. The lower and upper peaks in each image correspond to (224) lattice plane diffractions of GaSb and InAs, respectively. Moreover, the summary of the InAs lattice relaxation ratios and full-widths at half-maximum (FWHMs) of GaSb diffraction intensity along an in-plane (220) direction is shown in Table 4-2. The FWHM indicates the mosaicity of the crystalline InAs. In addition, Table 4-2 indicates whether dislocations and pits were observed or not.

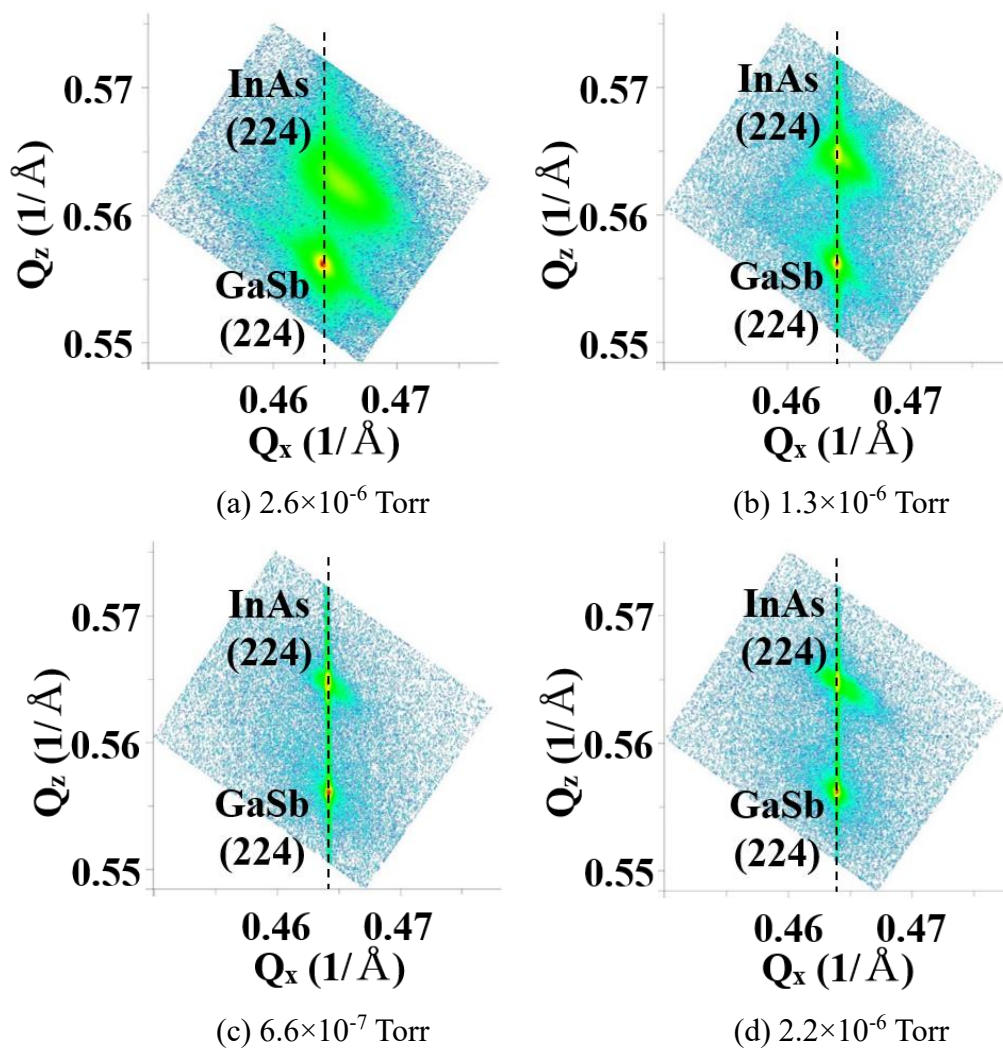


Figure 4-8 X-ray RSM images of InAs on GaSb with different As_2 pressures of (a) 2.6×10^{-6} Torr, (b) 1.3×10^{-6} Torr, (c) 6.6×10^{-7} Torr, and (d) 2.2×10^{-6} Torr. The lower and upper peaks in each image indicate the (224) plane diffraction of GaSb and InAs, respectively. Q_x and Q_z denote the absolute values of in-plane and vertical reciprocal lattice vectors, respectively.

Table 4-2 The summary of the InAs lattice relaxation ratio and FWHM of the InAs diffraction peak of the sample grown at As₂ pressures of (a) 2.6×10^{-6} Torr, (b) 1.3×10^{-6} Torr, (c) 6.6×10^{-7} Torr, and (d) 2.2×10^{-7} Torr. The presence or absence of the dislocations and pits are also indicated. The area of the measurements for the dislocation and pits are $3 \mu\text{m}$ in the cross-sectional TEM image and $5 \mu\text{m} \times 5 \mu\text{m}$ in the AFM image, respectively.

As ₂ pressure (Torr)	2.6×10^{-6}	1.3×10^{-6}	6.6×10^{-7}	2.2×10^{-7}
InAs lattice relaxation ratio	56%	1%	1%	0%
InAs Q _x FWHM (1/Å)	201	24	19	13
Dislocation	Observed	Observed	Not observed	Not observed
Pit	Observed	Observed	Observed	Not observed

At the highest As₂ pressure of 2.6×10^{-6} Torr, the InAs lattice relaxation ratio is extremely high at 56%. Moreover, its mosaicity is also large compared with those of the other samples. However, the other samples are not relaxed and their mosaicity are small. These results correlate with the FFTM analysis results in Fig. 4-7.

Regarding the sample with an As₂ pressure of 6.6×10^{-7} Torr, where only pits but no dislocations exist, InAs is not relaxed macroscopically from X-ray RSM. From the results of the comparison with the sample of the lowest As₂ pressure of 2.2×10^{-7} Torr, this implies that the pits were not formed by lattice relaxation of strained InAs layer.

The surface morphologies of InAs homoepitaxy at different As₂ pressures were investigated by scanning tunneling microscopy in Ref. [30]. Surface morphologies are significantly different with As₂ pressure. At lower As₂ pressures close to the stoichiometry, corresponding to the case of 2.2×10^{-7} Torr in this study, there is a high density of compact islands on terraces. This indicates a 2D nucleation mode, with little step-flow mode growth [30]. On the other hand, at higher As₂ pressures corresponding to 6.6×10^{-7} Torr in this study, the islands are larger, and the step and island edges are much rougher. This indicates the occurrence of step-flow mode growth [30]. In the latter case, the steps convolute with each other, thus step bunching or multistep formation seems to easily occur. Combined with the effects of tensile strain applied to the InAs layer, this may cause three-dimensional growth in localized areas, and lead to the formation of the observed pits with higher index planes as a part of strain energy relaxation to reduce the surface energy. Pits can be regarded to be formed self-assembly such as InAs QDs on GaAs case. However, in the case of InAs growth on GaSb, “reversed QD” is formed because InAs

layer undergoes the tensile strain contrary to the compressive strain in case of InAs/GaAs QDs. Once the high index planes are formed, the InAs growth proceeds with keeping the high index planes due to the instability of the (001) plane growth of the InAs layer at this low growth temperature range discussed in Section 4.1.3 [26].

On the other hand, at low As_2 pressure, where the two different growth modes are mixed, step bunching and multistep formation are suppressed. This makes it possible to suppress pit formation even under the existence of tensile strain. As a result, high-quality pseudomorphic InAs growth on GaSb was obtained.

4.1.5 Summary of Section 4.1

The effects of As_2 pressure on InAs hetero epitaxial growth on GaSb were investigated to obtain high-quality InAs with flat and pit-free for contact electrode layer. The transition layers with small lattice constants were formed at the interface by As/Sb exchange with As_2 soaking before InAs growth. Their thickness decreased as the As_2 pressure decreased. A lot of misfit dislocations were formed at the transition layer at higher As_2 pressures. These lead to a large lattice relaxation of strained InAs layer. As the As_2 pressure decreased, the misfit dislocation density decreased, whereas pits were formed on the surface. X-ray RSM measurement revealed that pits did not contribute to the lattice relaxation of strained InAs layer. It appears that instability of (001) plane at low growth temperature and special surface condition at high As_2 pressure caused by step-flow mode growth promotes the pits formation with high index plane to ease the strain energy. By further lowering the As_2 pressure, accompanying the growth mode change on the surface, pits formation to ease the strain energy was suppressed. As a result, high-quality pseudomorphic strained InAs layer on GaSb was obtained.

Although a flat with pit-free InAs surface was obtained under a low As_2 pressure of 2.2×10^{-7} Torr, it is difficult to precisely control such a low As_2 pressure even by using valved cracker cell. In order to improve run to run productivity, a stable growth method for producing flat with pit-free InAs is needed even in the case of higher As_2 pressure condition. This will be discussed in the next section.

4.2 Effect of growth temperature on InAs hetero epitaxial growth on GaSb

4.2.1 Experimental procedure

(1) Growth condition

- SS-MBE equipped with standard effusion cells was used.
- Substrate: N-doped GaSb 0.35° off (001) in the direction of (111)
- Chemical bonding of As: dimers As₂ (Cracking temperature is 900 °C)
- Chemical bonding of Sb: dimers Sb₂ (Cracking temperature is 900 °C)
- The sample structure grown in this experiment is shown in Fig. 4-9.
- The sample was heated to 570 °C under Sb₂ irradiation for oxide desorption.
- Growth rate of GaSb: 0.4 μm/h (fixed)
- Beam equivalent pressure (BEP) of Ga: 1.08×10^{-7} Torr
- BEP of Sb: 5.40×10^{-7} Torr (V/III ratio is 5)
- For GaSb buffer layer growth, two-step growth sequence discussed in Chapter 3 was adapted. After GaSb layer was grown at 560 °C, the growth temperature was lowered to 400 °C, 460 °C, and 520 °C under Sb₂ irradiation of 5.40×10^{-7} Torr. Then, GaSb was grown at each temperature [See Fig. A-1 in Appendix].
- Total GaSb homo epitaxial layer is 100 nm. Then, 85-nm-thick-InAs or -InAsSb layer was grown.
- Growth rate of InAs or InAsSb: 0.2 μm/h
- BEP of In: 7.97×10^{-8} Torr
- BEP of Sb 1.20×10^{-6} Torr (V/III ratio is 15)
- Six samples fabricated in this study are shown in Table 4-3. In sample A, B, and C, InAs layer was grown by one-step at constant temperature of 400 °C, 460 °C, and 520 °C, respectively. In sample D, in order to study the effect of Sb as a surfactant, a trace amount of Sb₂, BEP of 5.0×10^{-9} Torr, was irradiated during the one-step growth of InAs layer at 400 °C.
- Since the optimal growth temperature might be different between initial InAs growth and succeeding one in hetero epitaxial growth, the two-step low and high temperature growth in sample E and F. In sample E and F, initial 5-nm-thick-InAs was grown at 400 °C/520 °C, and growth temperature was changed to 520 °C/400 °C under As₂ irradiation of 1.20×10^{-6} Torr. Then, 80-nm-thick-InAs was grown at 520 °C/400 °C, respectively.

(2) Sample evaluation

- AFM in the tapping mode was performed for surface observation.
- Cross-sectional TEM was performed in the [110] direction for structural observation.
- Secondary ion mass spectroscopy (SIMS) was performed for composition evaluation.
- X-ray reciprocal space mapping (RSM) were performed for strain analysis.

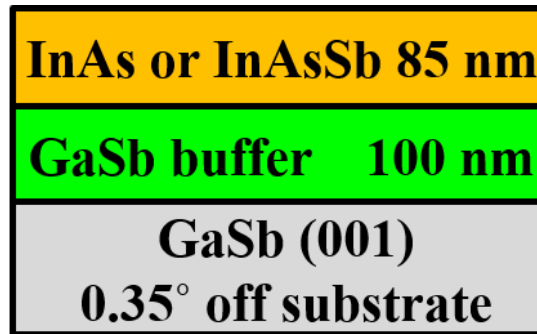


Figure 4-9 Schematic structure of InAs or InAsSb on GaSb substrate fabricated in this experiment.

Table 4-3 Summary of samples grown in this experiment.

Sample	Growth step	Layer	Thickness (nm)		Growth temperature (°C)	
			First	Second	First	Second
A	One	InAs	85		400	
B	One	InAs	85		460	
C	One	InAs	85		520	
D	One	InAs _{0.9965} Sb _{0.0035}	85		400	
E	Two	InAs	5	80	400	520
F	Two	InAs	5	80	520	400

4.2.2 Size variation of pit with InAs growth temperature

The AFM images of the one-step InAs on GaSb grown at three different temperature 400 °C, 460 °C, and 520 °C in Fig. 4-10. These are corresponding to the sample A, B, and C, respectively. There can be seen pits on the surface of each sample. Relatively large pits with the depths of approximately 50 nm can be seen in sample A. As the growth temperature increases, the RMS of the InAs surface becomes smaller from 0.98 nm to 0.25 nm due to the size reduction of the pits. In sample C, the depths of the pits are approximately 10 nm.

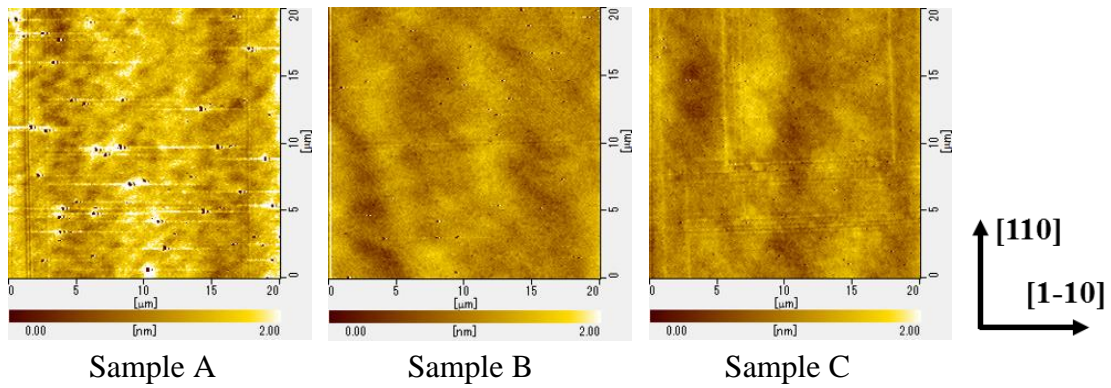


Figure 4-10 AFM images of one-step 85-nm-thick InAs on GaSb grown at constant temperature of 400 °C, 460 °C, and 520 °C (samples A, B, and C). The images are 20×20 μm². The color scales are 2 nm in height.

For structural evaluation of the pits, cross-sectional TEM measurements from [1-10] direction was performed. Figure 4-11 shows the cross-sectional TEM images of InAs on GaSb. Same tendency in the sizes of the pits as can be seen from AFM images. Both vertical and lateral sizes of the pits become smaller as the growth temperature increases. In addition, the pits are formed by the specific higher index crystal plane such as (111), (311), and (411) same as Fig. 4-5 in Section 4.1.3.

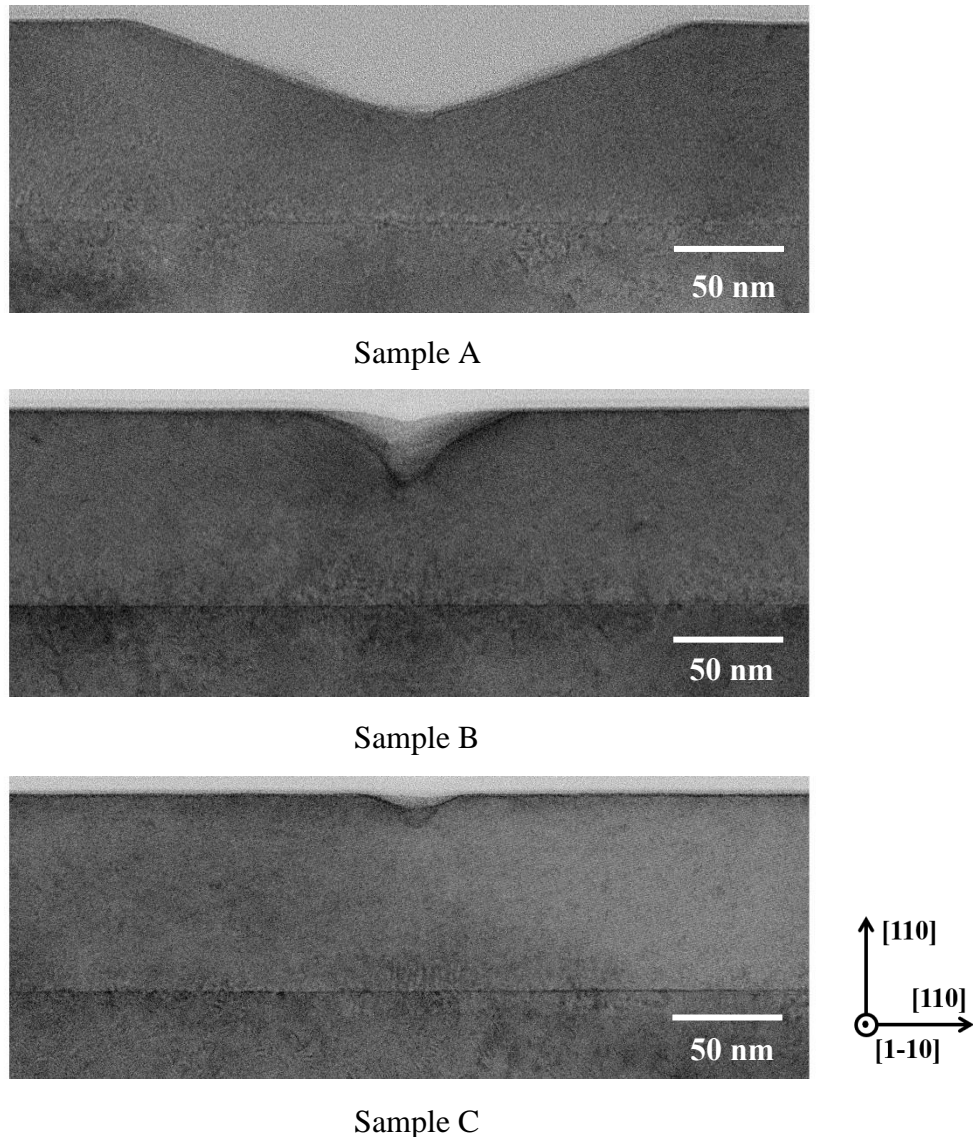


Figure 4-11 Bright field cross-sectional TEM images of InAs on GaSb grown at constant temperature of 400 °C, 460 °C, and 520 °C (samples A, B, and C). The observation was performed from the [1-10] direction.

To examine strain condition of InAs layer on GaSb, X-ray RSM was performed for sample A, B, and C. Figure 4-12 shows the X-ray RSM images of sample A, B, and C. Pseudomorphically grown InAs layers on GaSb were observed in all three samples. There exists no difference among them as for the strain state. Thus, the pits of each sample have no contribution to the lattice relaxation same as As_2 pressure dependence discussed in Section 4.1.

In the case of InAs homo epitaxial growth previously reported in Ref. [26] and [27], the pits due to surface condition of the substrate and pyramidal structure due to surface

reconstruction phase were tended to be formed at relatively low and high growth temperature, respectively. Decrease in pit size with increase in growth temperature in this study may mean that the stability of the (001) plane increases during the transition from pit to pyramid structure formation. The change in the growth mode with respect to the growth temperature is considered to be largely due to the surface state, including the surface reconstruction phase.

Regarding the InAs growth stability of (001) plane growth, the InAs growth on InAs nonplanar substrate consisting of (001) and (111)A planes was investigated with changing growth temperature and As pressure in the previous study in Ref. [28]. The growth rate of (001) plane adjacent to (111) A plane was evaluated by μ -RHEED [28]. This study revealed that the lateral flow of Ga adatoms occurs from (111)A to (001) and from (001) to (111)A planes at relatively high growth temperature/low As₂ pressure and low growth temperature/high As₂ pressure, respectively [28]. What is particularly characteristic of InAs growth is the occurrence of In adatom migration from the (001) plane to (111)A at low growth temperature/high As₂ pressure condition. Migration of the adatoms in this direction has not been observed for GaAs in similar experiments [29]. Although the tendency of growth plane preference in Ref. [28] is opposite and further study is needed, this implies that the stable plane orientation of InAs growth varies greatly depending on the growth conditions.

Since there still exist small pits on the surface even in the high temperature growth at sample C, the growth method which completely suppresses the pits formation is required from the viewpoint of applying thick InAs layer to the contact layer of the IR-PD devices. It will be discussed in the latter section.

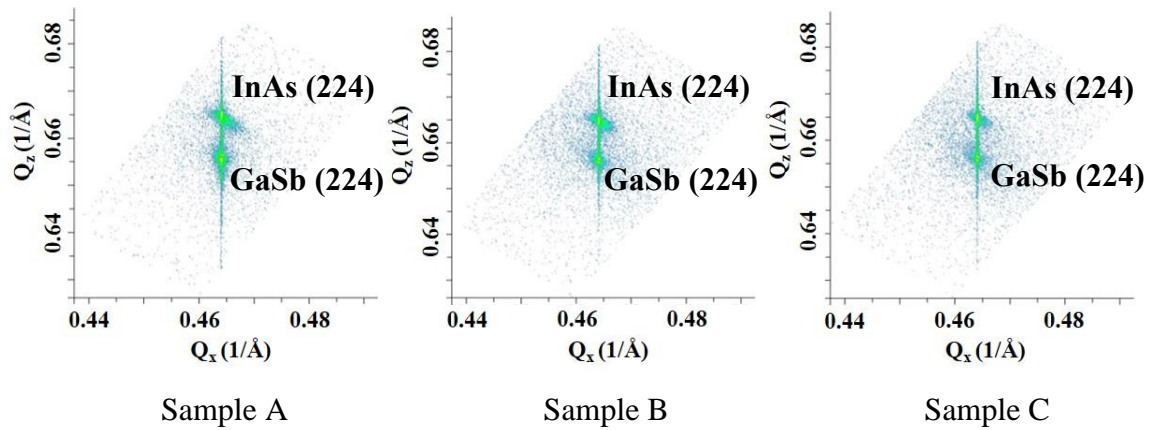


Figure 4-12 X-ray RSM images of one-step InAs on GaSb grown at constant temperature of 400 °C, 460 °C, and 520 °C (samples A, B, and C). The upper and lower peaks correspond to the (224) plane diffraction of the InAs layer and GaSb buffer and substrate, respectively. Q_x and Q_z denote the absolute values of in-plane and vertical reciprocal lattice vectors, respectively.

4.2.3 Pit suppression by the trace amount of Sb_2 irradiation

To suppress the pits formation discussed in the previous section, the Sb surfactant effect which are reported in other material systems [79-81] are examined. Trace amount of Sb_2 , BEP of 5.0×10^{-9} Torr, was irradiated during the growth of InAs at 400 °C, corresponding to sample D in Table 4-3. This growth produced ternary InAsSb with Sb composition of extremely small 0.35% confirmed by the X-ray diffraction measurement. Figure 4-13 shows the AFM images of sample D. Pits on the surface observed in sample A, B, and C were disappeared. As a result, a pit-free surface with relatively small RMS of 0.33 nm was obtained.

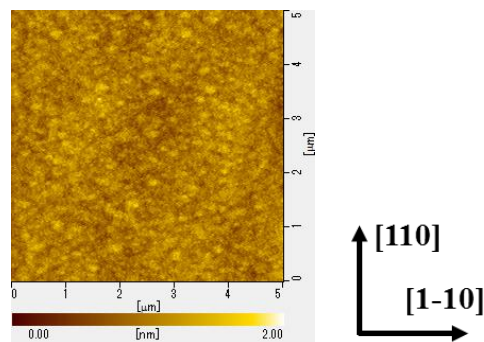


Figure 4-13 AFM image of InAsSb with Sb composition of 0.35% grown on GaSb with trace amount of Sb_2 irradiation during InAs growth (Sample D). The images are $5 \times 5 \mu m^2$. The color scales are 2 nm in height.

The cross-sectional TEM image of sample D observed from [1-10] direction is shown

in Fig. 4-14. There can be observed no pits or dislocations from cross-sectional evaluation same as AFM image. The X-ray RSM images of sample D is shown in Fig. 4-15. InAsSb layer seems to be pseudomorphically grown on GaSb same as the case of sample A, B, and C. From these results, the Sb acts as a surfactant on the InAs surface even in the case of trace amount of Sb_2 irradiation. It makes the preference of (001) plane growth larger at the low temperature growth to suppress the pit formation with high index planes. However, the (224) diffraction peak from the InAsSb in sample D is relatively broader than those from the InAs of samples A to C in Fig. 4-12. This means that the Sb content of the InAsSb layer was relatively inhomogeneous. This is because the BEP of Sb 5.0×10^{-9} Torr was too low to maintain the flux at a constant rate.

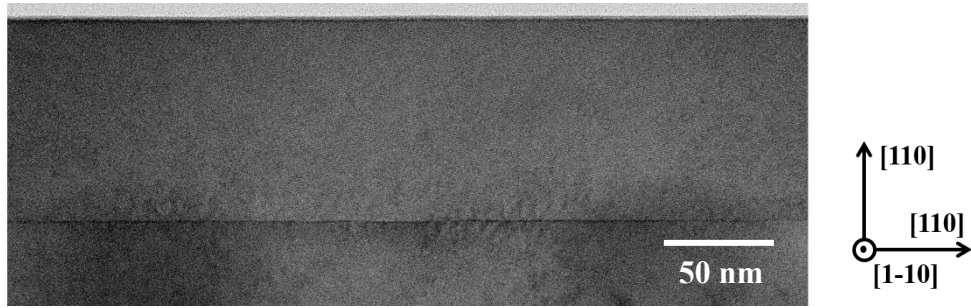


Figure 4-14 Cross-sectional TEM image of InAsSb layer with Sb composition of 0.35% on GaSb by trace amount of Sb_2 irradiation during InAsSb growth (Sample D). The observation was performed from the [1-10] direction.

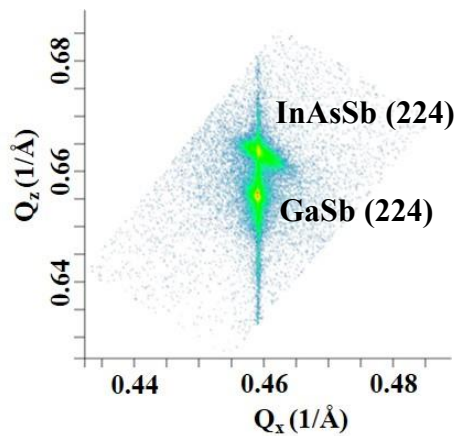


Figure 4-15 X-ray RSM image of InAsSb with Sb composition of 0.35% grown on GaSb (Sample D). The upper and lower peaks correspond to the (224) plane diffraction of the InAsSb layer and GaSb buffer and substrate, respectively. Q_x and Q_z denote the absolute values of in-plane and vertical reciprocal lattice vectors, respectively.

Moreover, since InAsSb tends to be easily oxidized to form such as Sb_2O_3 [82-84], they are concerned to trap photo-carriers. If the InAsSb layer is applied as a contact layer, there is a concern of deterioration in device characteristics such as responsivity of IR-PD. Thus, the growth method which suppresses the pits formation without the use of Sb irradiation is required. This will be discussed in the next section.

4.3 Effect of growth sequence on InAs hetero epitaxial growth on GaSb

4.3.1 Pit suppression by two-step InAs growth

In Section 4.2, it was found that a higher growth temperature is valid for forming smaller pits due to the preference of (001) growth preference. Regarding the interface between InAs and GaSb, however, a lower temperature growth seems to be effective for reducing intermixing or As/Sb exchange such as reported in [24]. Thus, two-step growth where initial InAs layer at the interface was grown at 400 °C and succeeding InAs layer at 520 °C was investigated. This corresponds to sample E in Table 4-3. Figures 4-16 and 4-17 show the AFM and TEM images of sample E, respectively. The pits were completely suppressed in the range of FOV of 20 μm without Sb irradiation during InAs growth. Moreover, the surface is extremely flat with the RMS of 0.20 nm where atomic steps are clearly confirmed as can be seen in Fig. 4-16 (a). From TEM image in Fig. 4-17, any dislocation could not be observed in InAs layer. This means that the two-step temperature sequence does not cause the lattice relaxation. This is also consistent with the result of X-ray RSM in Fig. 4-18, where pseudomorphic InAs layer is grown on GaSb.

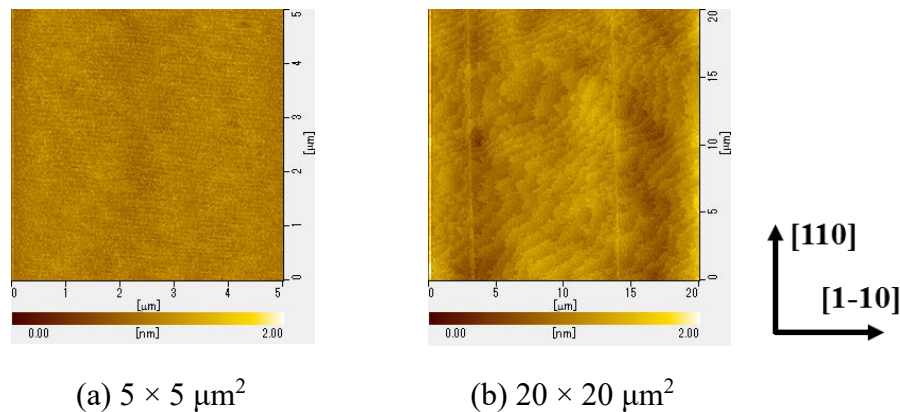


Figure 4-16 AFM images of InAs grown on GaSb by two-step low- and high- temperature sequence (Sample E). The images show (a) $5 \times 5 \mu\text{m}^2$ and (b) $20 \times 20 \mu\text{m}^2$, respectively. The color scales are 2 nm in height.

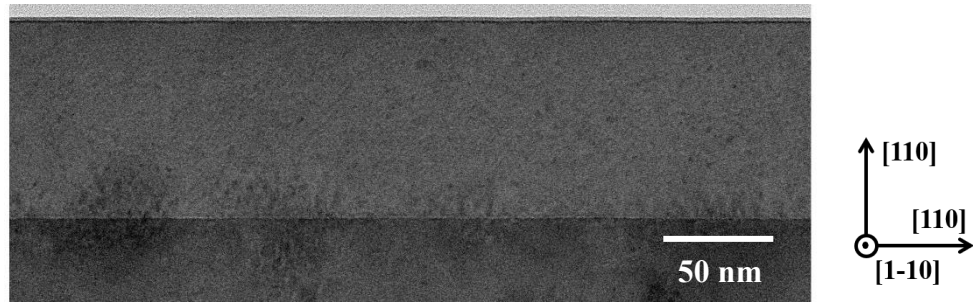


Figure 4-17 Cross-sectional TEM image of InAs grown on GaSb by two-step low- and high- temperature sequence (Sample E). The sample was observed from the [1-10] direction.

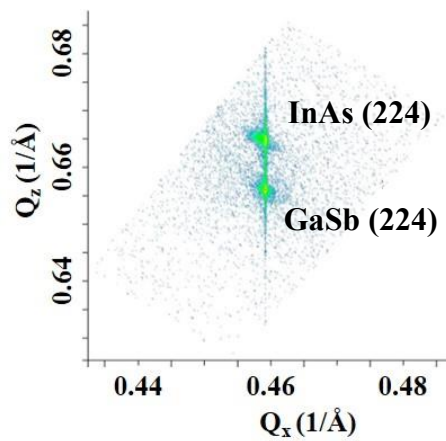


Figure 4-18 X-ray RSM image of InAs grown on GaSb by two-step low- and high temperature sequence (Sample E). The upper and lower peaks correspond to the (224) plane diffraction of the InAs layer and GaSb buffer and substrate, respectively. Q_x and Q_z denote the absolute values of in-plane and vertical reciprocal lattice vectors, respectively.

The case where the temperature is reversed was also considered. The two-step InAs growth where initial 5 nm-thick InAs and succeeding 80 nm-thick InAs were grown at 520 °C and 400 °C, respectively, corresponding to sample F. Figure 4-19 shows the AFM image of sample F. Interestingly, in contrast to sample E, the surface was quite rough with RMS of 7.68 nm. In addition, the density of the pits drastically increased. The same tendency can be seen in the TEM image in Fig. 4-20. The mechanism concerning these surface changes caused by different growth conditions will be discussed in the next section based on the growth mechanism.

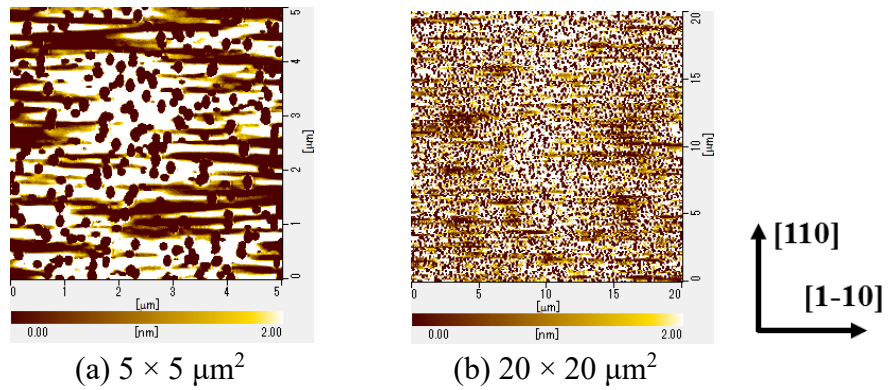


Figure 4-19 AFM images of InAs grown on GaSb by two-step high- and low- temperature sequence (Sample F). The images show (a) $5 \times 5 \mu\text{m}^2$ and (b) $20 \times 20 \mu\text{m}^2$, respectively. The color scales are 2 nm in height.

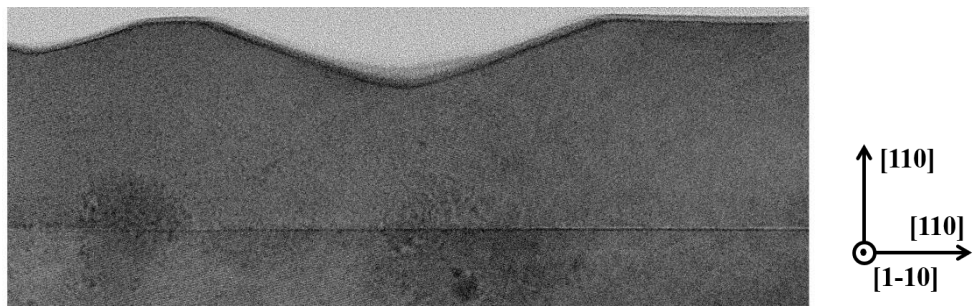


Figure 4-20 Cross-sectional TEM image of InAs grown on GaSb by two-step high- and low- temperature sequence (Sample F). The observation was performed from the $[1-10]$ direction.

4.3.2 Mechanism of pit suppression

Next, the experiments were performed to understand why two-step LT/HT growth can be effectively suppress the pits formation.

At first, since there is a suspect that Sb atoms diffusing from underlying GaSb layer act as a surfactant to suppress the pits formation, secondary ion mass spectroscopy (SIMS) measurement of InAs layer grown on GaSb was performed. Fig. 4-21 shows the SIMS profiles of Sb in InAs layer grown on GaSb in case of sample C and E.

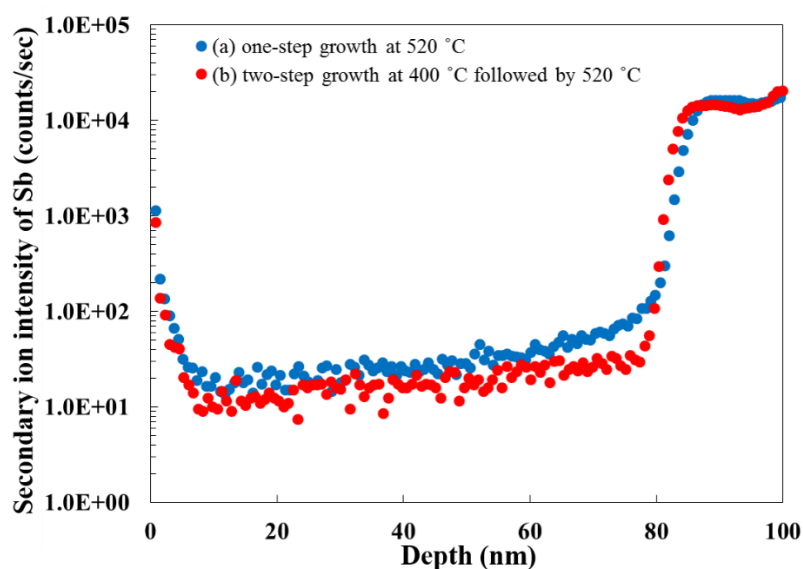


Figure 4-21 SIMS profiles of Sb in InAs layer grown on GaSb in the case of (a) one-step growth at 520 °C corresponding to sample C and (b) two-step growth at 400 °C and 520 °C corresponding to sample E. The piling up of Sb at the InAs surface is due to the influence of surface adsorbates.

The vertical axis indicates the secondary ion intensity of Sb. Sb carryover into InAs layer can be observed in both cases. However, that of sample E is lower than that of sample C in the entire InAs layer, especially at the interface between InAs and GaSb. This is because initial lower growth temperature of 400 °C makes Sb diffusion smaller than that of 520 °C. This also means that Sb surfactant effect do not play a role in the suppression of the pits in sample E.

As discussed in Section 4.2.2, citing Ref. [26], it is assumed that the surface morphology of the initial InAs heteroepitaxial growth on GaSb is critical to the subsequent InAs growth. Thus, the surface of initial 5-nm-thick InAs grown at 400 °C was observed. Figure 4-22 shows the AFM image. The surface appears very flat, with an

RMS of 0.12 nm, without pits in this range. This is due to the small amount of interdiffusion at the InAs/GaSb hetero interface at the relatively low growth temperature of 400 °C, as indicated by the SIMS measurement shown in Fig. 4-21.

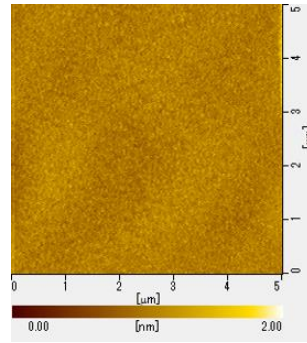


Figure 4-22 AFM image of 5-nm-thick InAs grown at 400 °C on GaSb. The image shows $5 \times 5 \mu\text{m}^2$. The color scales are 2 nm in height.

In addition, the subsequent growth at a higher temperature of 520 °C, essentially favors the (001) plane growth, as discussed in Section 4.2.2 related to Fig. 4-10 and 4-11. These two factors seem to help suppress the pits and make an extremely flat surface in sample E. On the other hand, in the case of sample F, the initial 5-nm-thick InAs grown at 520 °C should be rougher than the surface grown at 400 °C because of the larger interdiffusion at the InAs/GaSb hetero interface, as shown in the SIMS measurement in Fig. 4-21. Such roughness on the surface of the initial InAs layer will cause the appearance of pits in the succeeding InAs layer [26]. In addition, low-temperature 400°C growth of InAs also itself enlarges pits formation with high index planes, as can be seen in Fig. 4-10 and 4-11. The sequence of sample F, therefore, enhances pit formation.

4.3.3 Summary of Section 4.2 and 4.3

The effects of growth temperature, sequence, and Sb surfactant effects to InAs growth on GaSb were investigated. In the case of one-step InAs growth, the pits at the surface tend to be smaller with the increase in growth temperature, however, they remain even at the growth temperature of 520 °C. A trace amount of Sb irradiation during InAs growth could effectively suppress the pits formation even at a low temperature of 400 °C due to its surfactant effect. Moreover, the fabrication of InAs with pit-free and extremely flat surface was achieved by two-step initial low and succeeding high temperature growth without Sb irradiation. This might be caused by the high flatness at initial low temperature growth and preference of (001) plane at high temperature. The growth mechanisms on pits formation or suppression of InAs growths on GaSb in three cases are summarized

with the schematic diagrams below.

■ One-step HT growth



● Initial growth

✓ Surface roughness is large due to large As/Sb exchange.

● Subsequent bulk growth

✓ (001) plane growth preference is high but localized unstable areas due to initial roughness induce pits.

■ One-step LT growth



● Initial growth

✓ Surface roughness is small due to small As/Sb exchange.

● Subsequent bulk growth

✓ (001) plane growth preference is low and pits are easily formed.

■ Two-step LT/HT growth



● Initial growth

✓ Surface roughness is small due to small As/Sb exchange.

● Subsequent bulk growth

✓ Initial unstable areas are suppressed and (001) plane growth preference is maintained.

4.4 Summary of Chapter 4

To obtain high-quality thick InAs layer on GaSb applied to the contact layer, the effect of As₂ pressure, growth temperature, sequence, and Sb surfactant effect were investigated.

The transition layers with small lattice constants were formed at the interface due to As/Sb exchange by As₂ soaking before InAs growth. Their thickness decreased as the As₂ pressure decreased. At higher As₂ pressures, many misfit dislocations were formed at the transition layer. These lead to a large lattice relaxation of InAs layer. The misfit dislocation density decreased, whereas pits were formed as As₂ pressure decreased. Pits do not contribute to the lattice relaxation but to reduce the surface energy by forming the high index planes from strain analysis. By further lowering the As₂ pressure, accompanying the growth mode change, a pit-free, high-quality pseudomorphic InAs layer on GaSb was obtained.

Regarding the growth temperature of InAs, in the case of one-step InAs growth, the pits at the surface tend to be smaller with the increase in growth temperature, however, they remain even at the high growth temperature of 520 °C.

A trace amount of Sb irradiation during InAs growth could effectively suppress the pits formation even at a low temperature of 400 °C due to its surfactant effect.

Moreover, without Sb irradiation, the fabrication of InAs with pit-free and extremely flat surface was achieved by two-step initial low and succeeding high temperature growth. This might be caused by the high flatness at initial low temperature growth and preference of (001) plane at succeeding high temperature. It is expected that the InAs layer by this two-step growth method will be applied to the electrode contact layer of actual GaSb-based IR-PDs.

5 InAs/GaAs hetero epitaxial growth

Unlike the previous chapters of InAs/GaSb material system, different material InAs/GaAs hetero growth is studied. The aim of this chapter is to establish growth conditions for obtaining a high PL intensity at 1.28 μm . At first, to clarify the effect of the size and shape of the underlying quantum dots on the cover layer growth, the growth temperature dependence of InAs QDs was investigated. Secondary, for clarifying the cover layer growth condition, the effect of growth temperature and thickness of the cover layer was investigated. The GaAs growth on InAs dots can be regarded as growth under tensile strain, just like the growth of InAs on GaSb. Focusing on this similarities, the research was conducted using of the knowledge gained from InAs growth on GaSb research in Chapter 4.

5.1 Effects of the growth temperature of InAs QDs on their structural and optical properties

5.1.1 Experimental procedure

(1) Growth condition

- SS-MBE equipped with standard effusion cells was used.
- Valved cracker cell was used with As₄ (uncracked) mode.
- Figure 5-1 shows the schematic QD structure grown in this study.
- 8-stacked InAs QD structure sandwiched with AlGaAs cladding layer was grown on GaAs(001) substrate.
- InAs QD layer was covered by InGaAs SRL followed by GaAs middle layer Their total thickness is fixed at 40 nm.
- At the top of the surface, InAs QDs were formed with the same growth condition for monitoring InAs QD size, density, and shape.
- Growth temperature of InAs QD was mainly changed. Three samples A, B and C were grown with QD growth temperature of 490 °C, 500 °C, and 510 °C, respectively. The growth temperature was monitored by optical pyrometer.
- Then, InGaAs SRL were grown under the condition of suppressing the In out-diffusion from QDs as presented in Ref. [58]. After the growth of GaAs capping layer,

the growth temperature was elevated to 590 °C to form GaAs middle layer.

- The growth conditions in this experiment are summarized in Table 5-1.

(2) Sample evaluation

- AFM in the tapping mode was performed for InAs QDs observation at the top of the surface.
- Cross-sectional TEM was performed in the [-110] direction for structural observation.
- X-ray RSM were performed for strain analysis of 8-stacked QD structure.
- CW and TRPL were performed from 6 K to 300 K under the 780-nm laser light excitation.

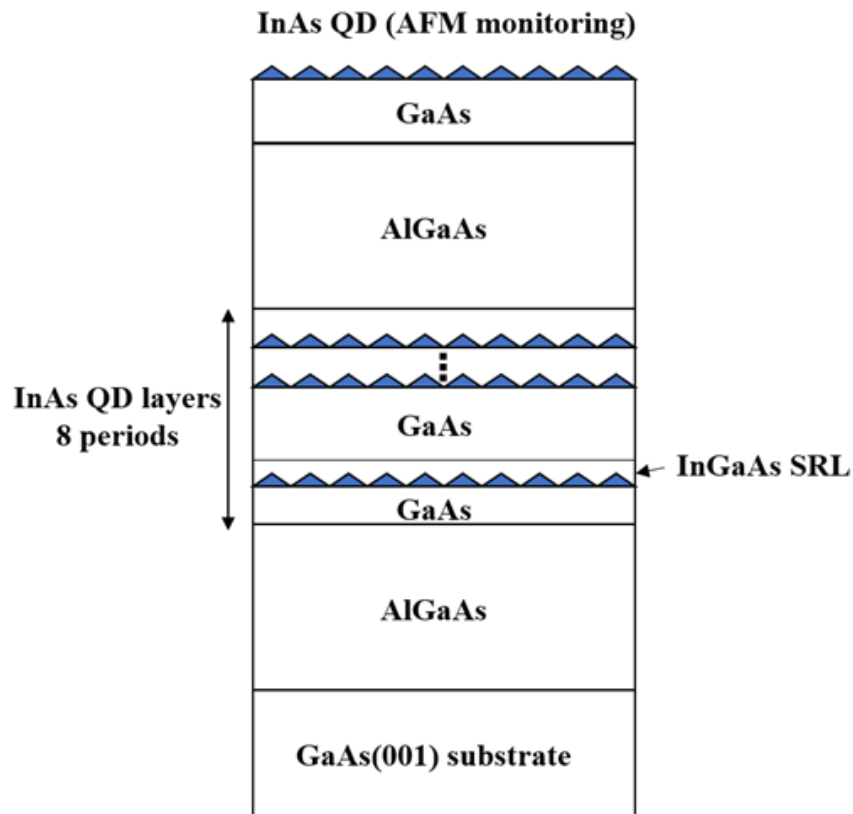


Figure 5-1 Schematic sample structure of 8-stacked InAs QD structure with InGaAs SRL and GaAs middle layer fabricated in this study. InAs QDs for AFM monitoring were formed on the top of the surface.

Table 5-1 Summary of the growth conditions of InAs QD structure in this study. T_s denotes the growth temperature.

Sample	T_s of InAs QD ($^{\circ}\text{C}$)	T_s of GaAs spacer layer ($^{\circ}\text{C}$)
Sample A	490	590
Sample B	500	
Sample C	510	

5.1.2 Structural characteristics of InAs/GaAs QD structures

AFM images of InAs QDs of samples A, B, and C, corresponding to their growth temperature of 490 $^{\circ}\text{C}$, 500 $^{\circ}\text{C}$, and 510 $^{\circ}\text{C}$, respectively, are shown in Fig. 5-2. The AFM images show $1 \times 1 \mu\text{m}^2$. Color scales are different and indicated in each image. The average heights and densities of the are 5.0 nm/ $1.0 \times 10^{11} \text{ cm}^{-2}$, 7.2 nm/ $4.7 \times 10^{10} \text{ cm}^{-2}$, 8.2 nm/ $2.7 \times 10^{10} \text{ cm}^{-2}$, for sample A, B, and C, respectively. As the growth temperature of InAs QDs increased from 490 $^{\circ}\text{C}$ to 510 $^{\circ}\text{C}$, the trend is that the density decreased, and the average height increased from 5.0 nm to 8.2 nm. This might be caused by the increase in In migration length with growth temperature increase. In case of sample A, In migration length at the surface is relatively shorter. This makes In atoms gather into a narrow area. Therefore, QDs with relatively smaller sizes are formed. As the growth temperature increases, the In migration length becomes longer, which makes In atoms gather at energetically stable positions to form larger size InAs QDs. Moreover, a number of giant QD, whose heights are over 10 nm, can be observed in sample A compared to samples B and C. The densities of giant QDs are $6.8 \times 10^8 \text{ cm}^{-2}$, $1.3 \times 10^7 \text{ cm}^{-2}$, and $1.3 \times 10^7 \text{ cm}^{-2}$, respectively. In sample A, distance between adjacent QDs is so short that QDs are easy to coalesce each other to form giant QDs as reported in Ref. [85]. At higher growth temperature, in the case of sample B and C, the density of coalesced dots is an order of magnitude lower compared to sample A. This is due to relatively larger distances between QDs.

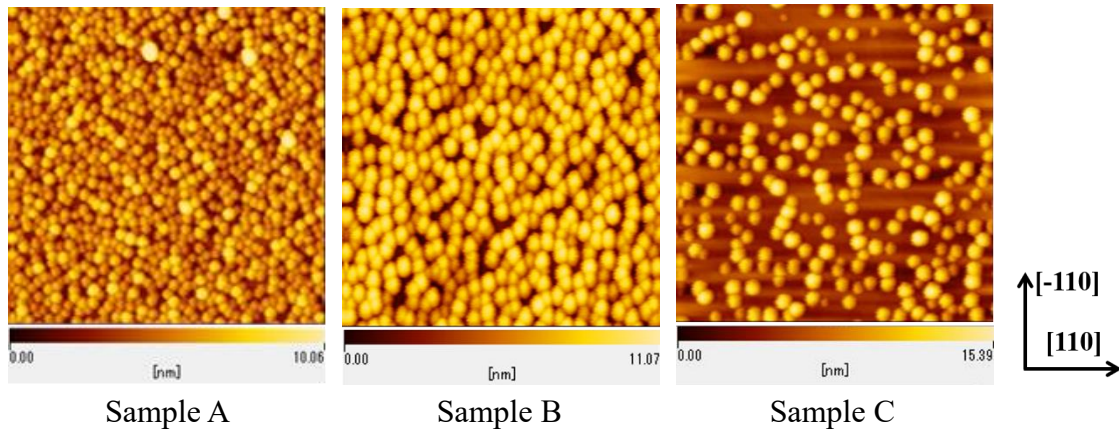
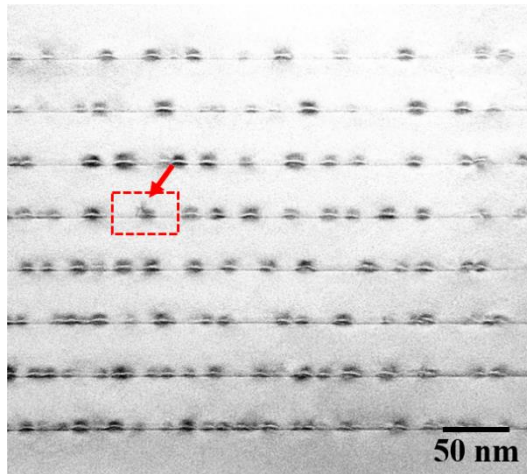
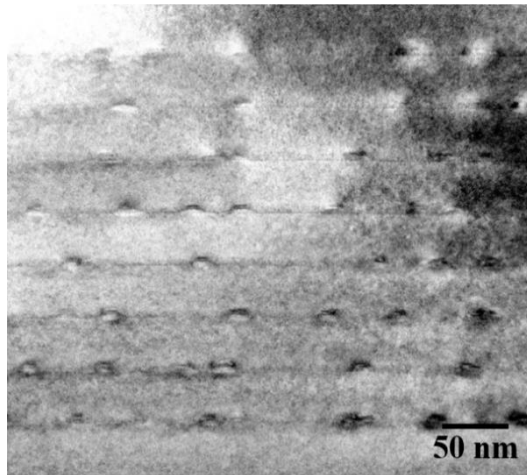
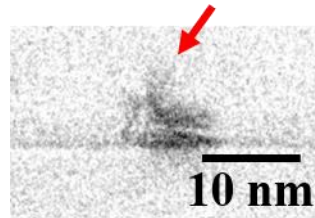


Figure 5-2 AFM images of the sample A, B, and C, corresponding to the InAs QD growth temperature of 490 °C, 500 °C, and 510 °C, respectively. Images show $1 \times 1 \mu\text{m}^2$. Color scales are indicated in each image.

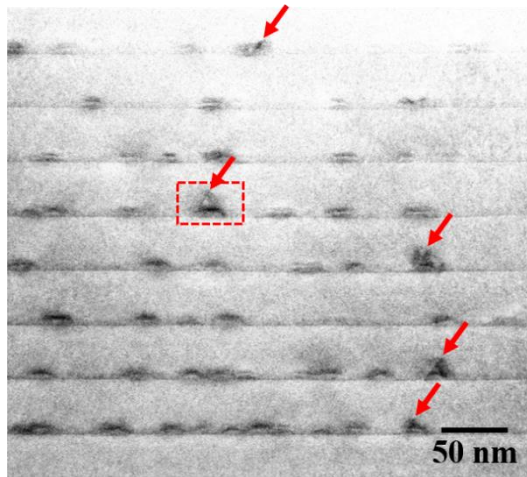
Figure 5-3 shows bright field cross-sectional TEM images of sample A, B, and C observed from $[-110]$ direction. In each sample, 8-stacked QDs layers are clearly seen. The dark contrasts mainly extending to the lateral direction could be observed in each sample. They are regarded to be derived from quantum dots. The top of QD in this study is relatively flat shape as can be seen in TEM image in Ref. [58]. Therefore, laterally extending dark contrasts in bright field TEM image in Fig. 5-3 are brought by the lattice strain between InAs and GaAs. On the other hand, the dark contrasts indicated by the red arrows could be regarded as the dislocations. This is because they are likely to occur in $[111]$ plane in zincblende lattice structure and originates from the compressively strained QD area. The densities of the dislocations estimated by the average of two field of view under the same sample thickness of 75 nm sliced by focused ion beam (FIB) are $1.39 \times 10^{14} \text{ cm}^{-3}$, $4.62 \times 10^{13} \text{ cm}^{-3}$, $4.16 \times 10^{14} \text{ cm}^{-3}$ for sample A, B, and C, respectively.



Sample A ($1.39 \times 10^{14} \text{ cm}^{-3}$)



Sample B ($4.62 \times 10^{13} \text{ cm}^{-3}$)



Sample C ($4.16 \times 10^{14} \text{ cm}^{-3}$)

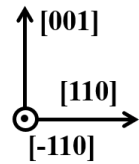
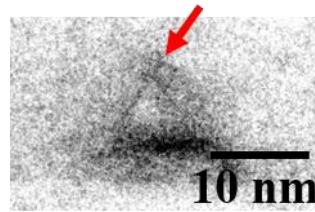
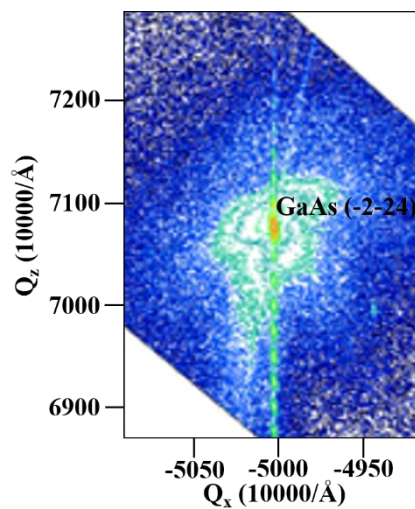


Figure 5-3 Bright field cross-sectional TEM images of the sample A, B, and C, corresponding to the InAs growth temperature of 490 °C, 500 °C, and 510 °C, respectively. The observation was performed from [-110] direction. Dislocations observed in each

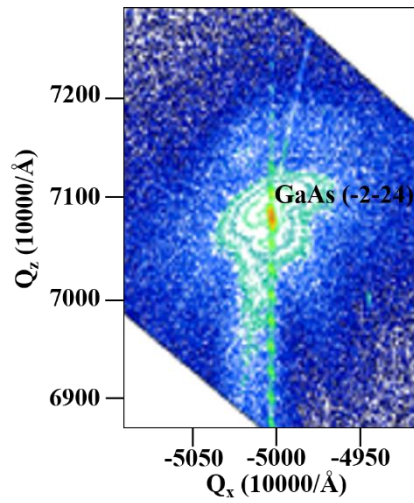
sample are indicated by red arrows. The magnified figures of dashed areas are also shown in sample A and C on the right. Dislocation density of each sample is also indicated in each TEM image.

Especially, dislocation density in QD structure is remarkably high in the case of sample C. As mentioned above, the relatively large heights of InAs QDs in sample C seems to contribute to the formation of the dislocations. This would cause the strain relaxation to form dislocations at InGaAs SRL and GaAs SL. The mechanism of the dislocation formation will be discussed in the letter section. Regarding Sample A, it has the second highest dislocation density. Although the average heights of InAs QDs is as small as 5.0 nm, there exists the highest density of giant QDs in sample A. These large size coalesced QDs will contribute to the formation of the dislocations same as sample C. Regarding sample B, the average height of InAs QDs is approximately 7 nm, and it is low enough to suppress the formation of dislocation. In addition, the density of coalesced QDs is as low as $1.3 \times 10^7 \text{ cm}^{-2}$, which also contribute to suppress the dislocation formation at InGaAs SRL and GaAs SL at a lower value in sample B.

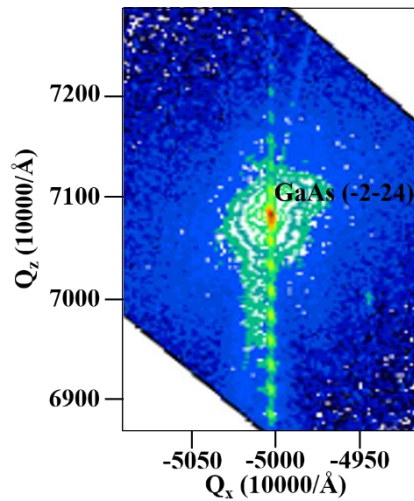
Since small dislocations were observed in the cross-sectional TEM images, it is interesting to observe the extent of lattice relaxation in each sample. To evaluate the strain relaxation macroscopically including dislocations, each sample was evaluated by the X-ray RSM. The X-ray RSM images of sample A, B, and C is shown in Fig. 5-4.



Sample A



Sample B



Sample C

Figure 5-4 X-ray RSM images of the sample A, B, and C. The largest peaks in each sample correspond to the (-2-24) plane diffraction of GaAs substrate. Q_x and Q_z denote the absolute values of reciprocal lattice vectors of in-plane [-1-10] and vertical [002] directions, respectively.

The diffraction peaks from GaAs(-2-24) are indicated in each figure. Satellite peaks from periodic QD layers of 40 nm were observed in each sample. In any sample, these satellite peaks are aligned in a straight line parallel to the Q_z direction. This means that the strain relaxation generated by the dislocation formation is so small that the X-ray RSM measurement could not identify it even in the case of sample C with the highest dislocation density among three samples.

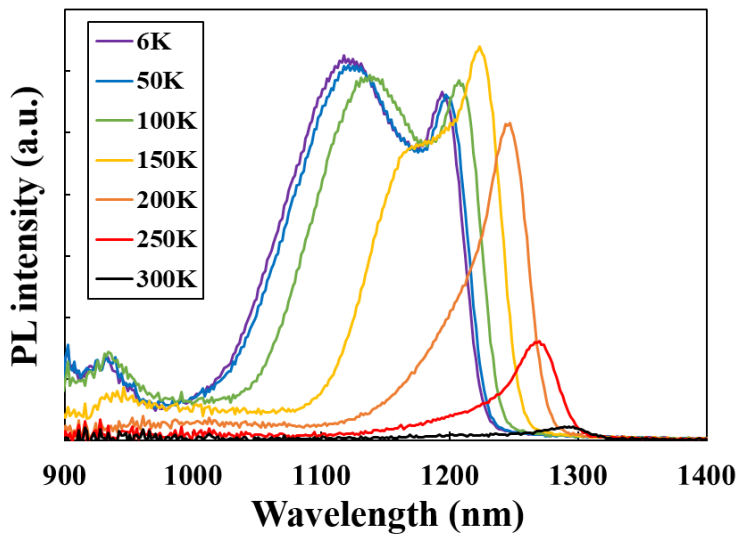
As explained in Section 4, X-ray RSM measurements were also performed in the case

of InAs hetero growth on GaSb shown in Fig. 4-8. Although the material system is not same as InAs/GaAs material system treated in this section, there is the case where lattice relaxation was not identified by X-ray RSM measurement even the dislocations were observed in TEM image shown in Fig. 4-5 (b) as an example. Thus, in this InAs/GaAs case, it is considered that very small strain relaxation in a limited local area was brought by the dislocations.

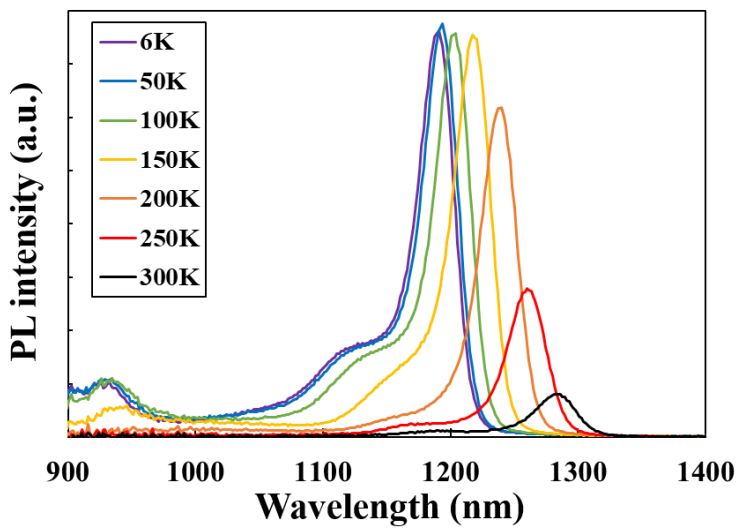
5.1.3 Optical characteristics of InAs/GaAs QD structures

As clear differences such as dislocation density were observed in structural properties of InAs QDs for their growth temperature, the relationship with their optical properties was interesting and investigated.

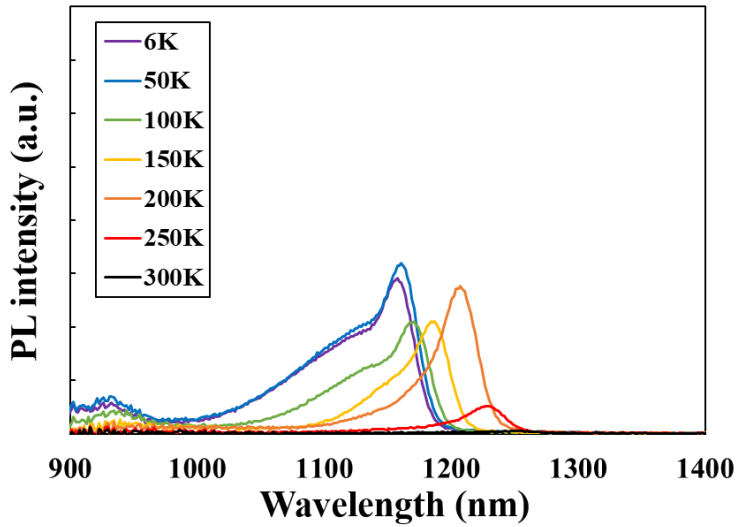
At first, Fig. 5-5 shows CW-PL spectra of sample A, B, and C at the measurement temperature from 6 K to 300 K. Relatively sharp peak at longer wavelength side observed in each sample is regarded as the emission from ground state of QDs. Emission shorter than ground state one is assumed to be from excited state of QDs or ground state of smaller size QDs. Although the average QD height of the sample C is the highest in three samples, the wavelength of ground state emission in sample C is approximately 40 nm shorter than the other two samples. Since the QDs growth temperature is the highest in sample C, the In interdiffusion between QDs and their surrounding layers is seemed to be the largest. This makes Ga composition of InGaAs QDs higher. This will blueshift the emission wavelength. Moreover, the emission peak around 950 nm observed at low temperature in each sample is thought to be the emission from InGaAs SRL.



Sample A (Ts 490 °C)



Sample B (Ts 500 °C)



Sample C (T_s 510 °C)

Figure 5-5 CW-PL spectra of the sample A, B, and C, corresponding to the InAs growth temperature of 490 °C, 500 °C, and 510 °C, respectively. The measurements were performed from 6 K to 300 K in 50 K increments. The scales of PL intensities are same among three samples.

The temperature dependence of PL integral intensity of sample A, B, and C was shown in Fig. 5-6. PL integral intensities tend to decrease monotonically with increasing temperature in sample A and B. Overall trend of sample C is same for sample A and B. On the other hand, some PL integral intensity fluctuations from 6 K to 200 K was observed in sample C. As similar phenomenon was reported in same InAs/GaAs QD system in Ref. [86], this is because carrier transition among QDs occurs due to small conduction band offset in sample C compared to sample A and B. Since the decrease of PL intensity to the temperature might relate to the activation of non-radiative center, the reduction rates of PL intensity had compared each other. As can be seen by the temperature dependence of PL intensity normalized by that of 6 K shown in Fig. 6 (b), reduction rates of PL intensity at 300 K to 6 K are approximately three times larger in the cases of sample A and C than that of sample B.

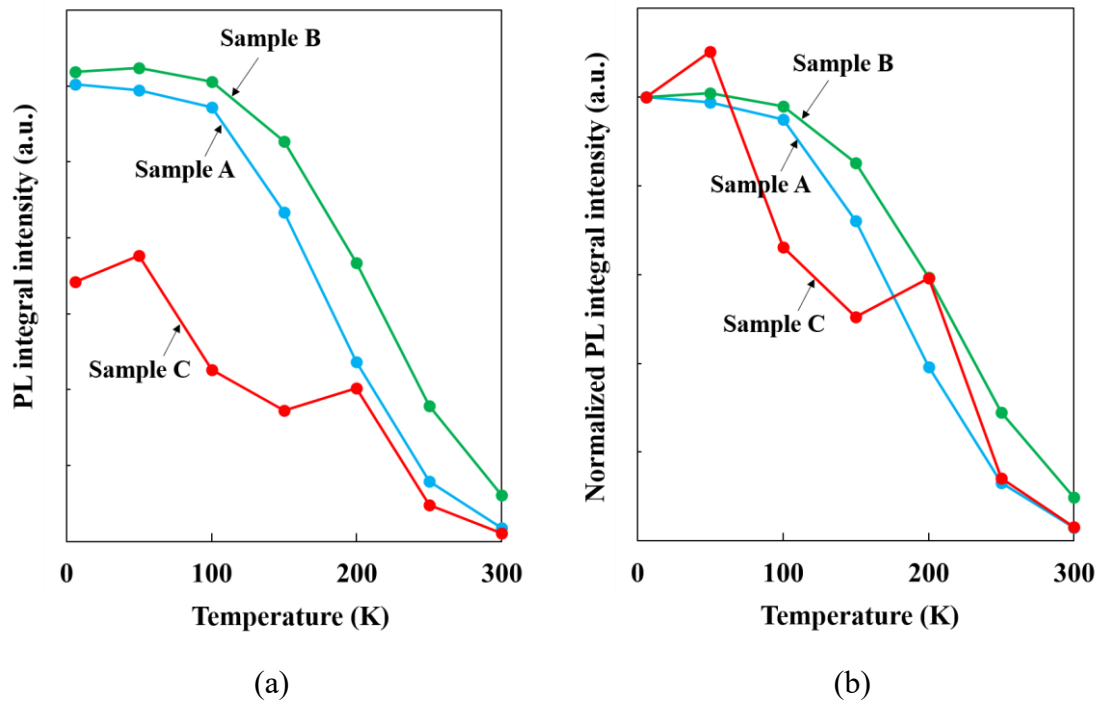


Figure 5-6 Temperature dependence of (a) PL integral intensity and (b) PL integral intensity normalized by that of 6 K in the case of the sample A, B, and C, corresponding to the InAs growth temperature of 490 °C, 500 °C, and 510 °C, respectively.

Since this PL intensity reduction might be related to the dislocation in QD structure, the TRPL of three samples were measured. The TRPL decays of three samples were measured at 6 K, 150 K, and 300 K, respectively, are shown in Fig. 5-7. In this study, the detection of TRPL was fixed at ground state emission peak of QDs for each sample. The PL lifetime of each sample was derived by monoexponential fitting of each TRPL decay. The fitting curve is indicated in each sample in Fig. 5-7.

At the measurement temperature of 6 K and 150 K, same tendency can be seen in the TRPL decays characteristics. On the other hand, at the measurement temperature of 300 K, a difference in the decay characteristics between the samples was observed. Thus, TRPL for each temperature was measured in more detail and the PL lifetime was derived.

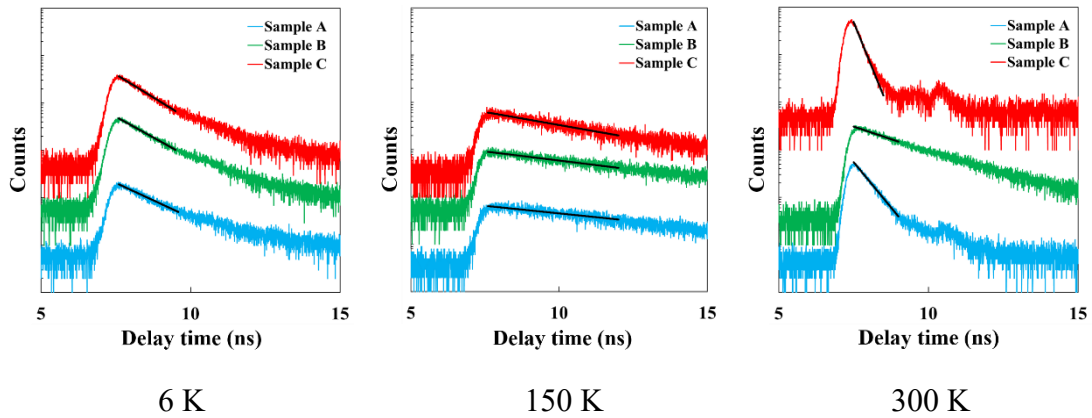


Figure 5-7 TRPL decays of the sample A, B, and C measured at 6 K, 150 K, and 300 K, respectively. The detection wavelength was fixed at the ground state of each sample at each temperature. The excitation wavelength was fixed at 780 nm. Monoexponential fitting curve of each TRPL result is also shown.

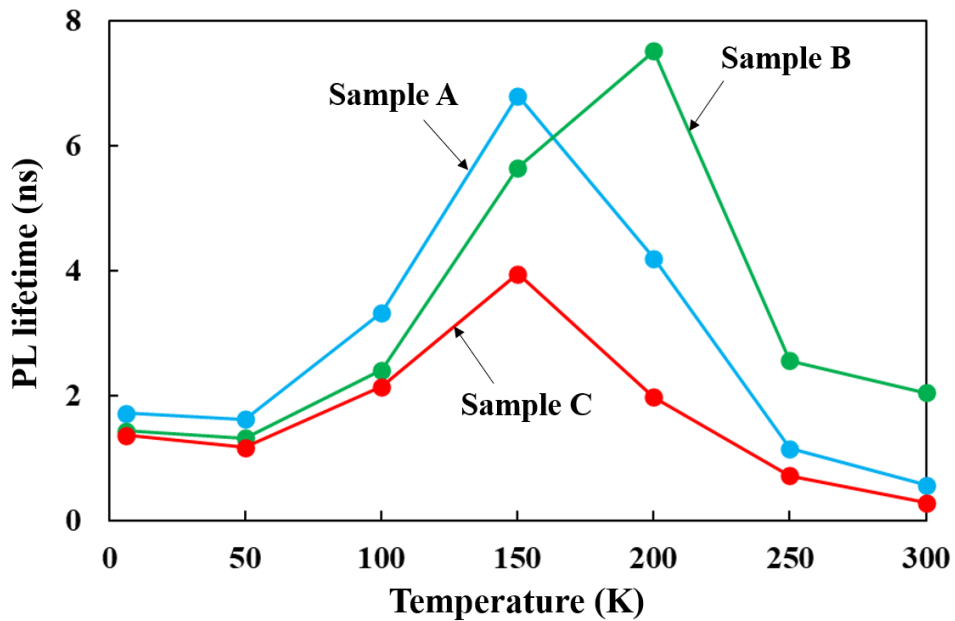


Figure 5-8 PL lifetime of the sample A, B, and C as a function of measured temperature. PL lifetime was derived by a monoexponential fitting to the ground state TRPL decay curve.

The temperature dependence of PL lifetime of three samples is shown in Fig. 5-8. At the measurement temperature of 6 K, the PL lifetime of each sample is almost same around 1.5 ns. On the other hand, PL lifetime of sample B is extremely longer than the other two samples at the measurement temperature of 300 K.

In the previous study of TRPL of QD structure, there were some reports that radiative recombination was dominant at a low temperature, whereas non-radiative recombination whose lifetime was relatively shorter made a large contribution in the temperature range close to room temperature due to the activation of non-radiative center [89-92].

If the dislocations in the QD structure discussed in the previous section act as a non-radiative recombination center, the longest PL lifetime of sample B could be attributed to its lowest dislocation density. Regarding to the PL lifetime increase near 150 K to 200 K, as previously reported in [89-92], the thermally induced carrier escape and transition among the QDs, this is so called “thermalization”, makes the carrier recombination time longer compared to that of below 50 K. Above 150 K or 200 K, the PL lifetime monotonically decreases with the increase in temperature in all three samples. This decrease was brought by the activation of dislocation related non-radiative recombination center around room temperature. As a result, dislocations are dominantly related to the optical quality of the QD structure. Thus, optimization of the growth temperature around 500 °C is important for the suppression of dislocation.

5.1.4 Summary of Section 5.1

Growth temperature dependence of InAs/GaAs QD structure was investigated by focusing on the relationship between structural and optical properties. Dislocations extending from QDs layers were prominently observed in the case of the highest growth temperature of 510 °C. Relatively larger size QDs grown at 510 °C seem to relate to the formation of dislocations. Temperature dependence of PL integral intensity indicated that the intensity reduction with increasing temperature was the lowest in the case of the sample with the lowest dislocation density grown at 500 °C. TRPL of 500 °C grown sample shows the longest lifetime at near room temperature. These tendencies indicate that the dislocations act as a non-radiative recombination center to deteriorate PL intensity at near room temperature. These results suggest that growth temperature around 500 °C suppresses the generation of larger size QDs which leads to the dislocation formation at InGaAs/GaAs covered layer. Thus, suppressing QD height by the control of its growth temperature is the key for fabricating high-quality multiple QDs structure.

In the next session, to explore the mechanism of dislocation formation and its suppression method, the thickness and growth temperature dependence of the low temperature InGaAs/GaAs cover layer were investigated under the InAs quantum dots growth temperature of 510 °C with high dislocation density.

5.2 Effects of low temperature cover layer growth of InAs QDs on their optical and structural properties

5.2.1 Experimental procedure

(1) Growth condition

- SS-MBE equipped with standard effusion cells.
- Valved cracker cell was used with As₄ (uncracked) mode.
- QD structure grown in this study is the same in Section 5.1 (Fig. 5-1).
- 8-stacked InAs QD structure sandwiched with AlGaAs cladding layer was grown on GaAs(001) substrate.
- Each InAs QD layer was covered by InGaAs SRL followed by GaAs layer, whose total thickness is fixed at 40 nm.
- At the top of the surface, InAs QDs were formed with the same growth condition for monitoring InAs QD size, density, and shape.
- The detailed structure around InAs QDs is shown in Fig. 5-9. The cover layer (CL) of InAs QDs consists of low temperature (LT) InGaAs/GaAs and high temperature (HT) GaAs.
- The growth temperature and thickness of low LT InGaAs/GaAs CL was changed under the fixed growth temperature of InAs QDs at 510 °C. The growth temperatures of LT InGaAs/GaAs CL were set at 510 °C (sample B), 480 °C (sample A), and 420 °C (sample C) under the thickness of 7.5 nm. In addition, the sample D of LT InGaAs/GaAs CL growth temperature of 480 °C with the thickness of 12.0 nm was also grown. The growth temperature of HT-GaAs was set at 590 °C in all samples. The sample discussed in Section 5.1 corresponds to the sample A in this experiment. The growth sequence of InAs QDs and the CL is shown in Fig. 5-10. The growth condition in this experiment is summarized in Table 5-2.

(2) Sample evaluation

- AFM in the tapping mode was performed for surface observation.
- Cross-sectional TEM was performed in the [-110] direction for structural observation.
- X-ray RSM were performed for strain analysis of 8-stacked QD structure.
- CWPL was performed at room temperature under the YAG laser light excitation at the wavelength of 1064 nm.

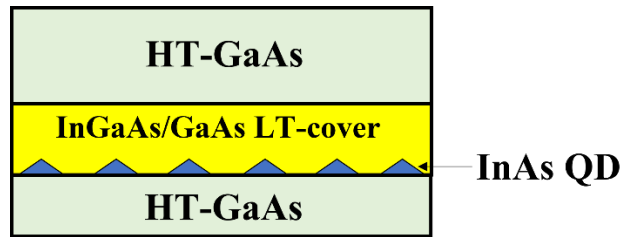


Figure 5-9 Detailed schematic sample structure around InAs QD.

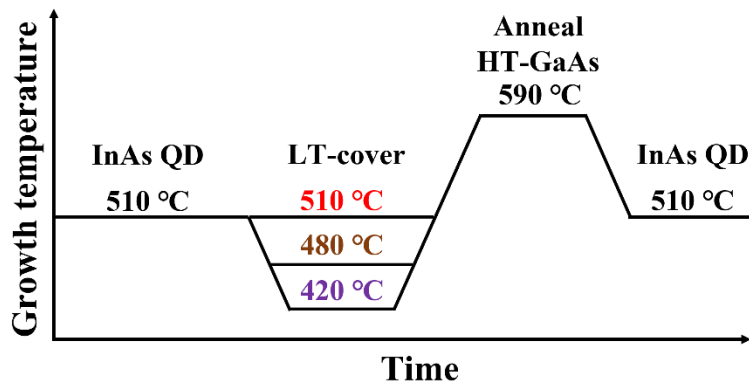


Figure 5-10 Growth sequence of InAs QDs structure adapted in this experiment. The growth temperatures of InAs QD and HT-GaAs were fixed at 510 °C and 590 °C, respectively.

Table 5-2 Summary of the growth conditions of InAs QDs and their surrounding layers in this experiment. T_s denotes the growth temperature.

Sample	T_s of InAs QD (°C)	T_s of HT GaAs layer (°C)	T_s of LT cover layer (°C)	Thickness of LT cover layer (nm)
Sample A	510	590	480	7.5
Sample B			510	
Sample C			420	
Sample D			480	

5.2.2 Relationship between optical and structural properties of InAs QD with various LT InGaAs/GaAs cover layer conditions

Figure 5-11 shows the PL spectra of 8-stacked InAs QD structures of sample A to D at room temperature. Although the PL intensity is low in sample A, an increase in PL intensity was observed under other growth conditions. In addition, the PL wavelengths of sample A, B, and C become longer than that of sample A. In terms of compatibility with the target wavelength of 1.28 μm , the condition of Sample D is the best in this experiment. Since the excitation wavelength is 1064 nm, photocarriers generation only occur within the InAs QDs considering the band lineup of the structure in Fig. 5-1. Thus, the differences in the PL intensity is assumed to be derived from the nonradiative center in InAs QD itself or its surrounding InGaAs/GaAs layer.

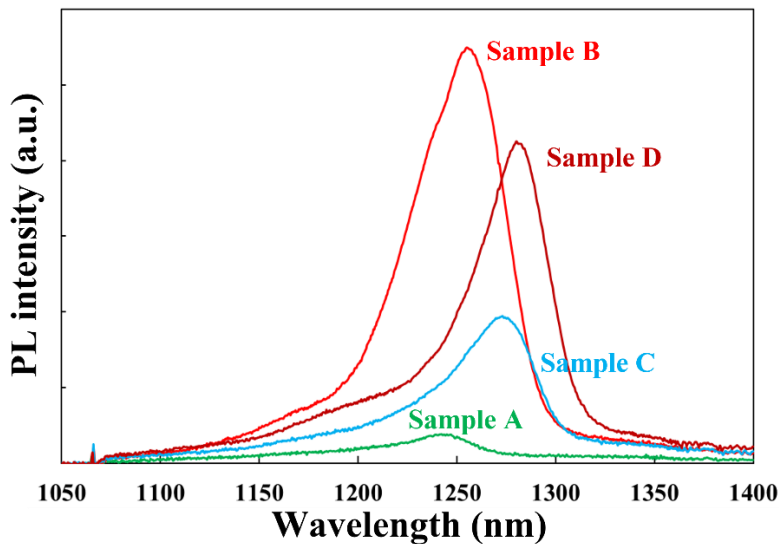
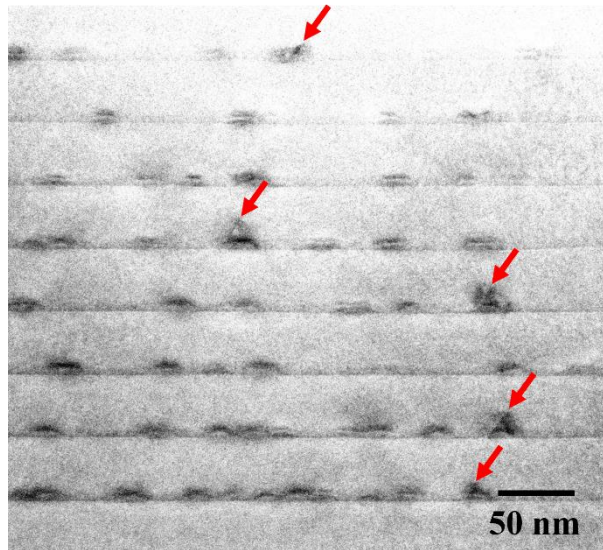


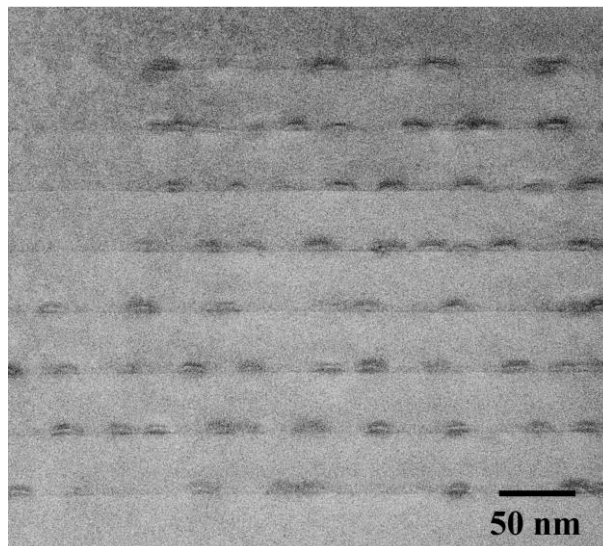
Figure 5-11 Room temperature PL spectra of 8-stacked InAs QD structures of sample A to D. 1064 nm YAG laser was used for excitation.

Same as discussed in Section 5.1, the dislocations in InAs QD structure also have a possibility to play a role in deteriorating the PL intensity. In order to compare the crystalline state with sample A, the cross-sectional TEM measurements were performed for sample B, C, and D. Figure 5-12 shows the bright field cross-sectional TEM image of 8-stacked InAs QDs structures of sample B, C, and D in addition to sample A (corresponding to the sample C in Fig. 5-3). Same as in sample A, the dislocations extending in the (111) direction starting from the InAs QDs were observed in sample B, C, and D as indicated by the red arrow. Dislocation density estimated from 75 nm thickness of FIB processed sample was also indicated in each image. The dislocation

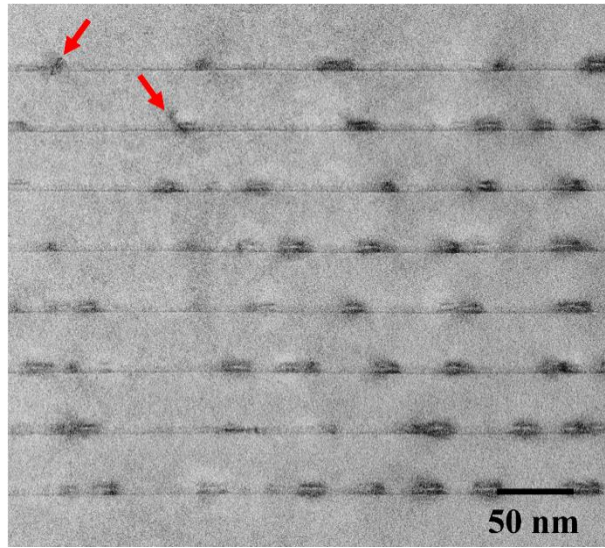
density of sample A, B, C, and D is $1.7 \times 10^9 \text{ cm}^{-2}$, $2.1 \times 10^8 \text{ cm}^{-2}$, $6.3 \times 10^8 \text{ cm}^{-2}$, and $4.2 \times 10^8 \text{ cm}^{-2}$, respectively. The dislocation density varies depending on the growth conditions. Figure 5-13 shows PL integral intensity as a function of dislocation density observed by TEM. As the dislocation density increases, PL integral intensity monotonically decreases. This suggests that the dislocations act as a nonradiative recombination center to deteriorate the PL characteristics same as discussed in Section 5.1.



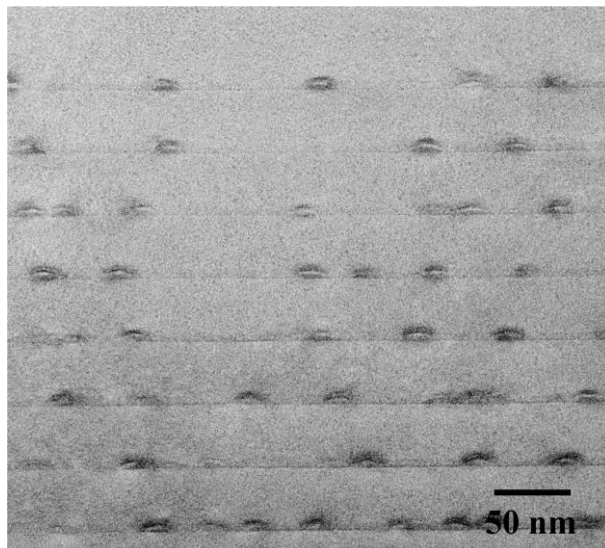
Sample A ($1.7 \times 10^9 \text{ cm}^{-2}$)



Sample B ($2.1 \times 10^8 \text{ cm}^{-2}$)



Sample C ($6.3 \times 10^8 \text{ cm}^{-2}$)



Sample D ($4.2 \times 10^8 \text{ cm}^{-2}$)

Figure 5-12 Bright field cross-sectional TEM image of 8-stacked InAs QDs structure of sample A, B, C, and D, respectively. The dislocation is indicated by the red arrow. The dislocation density is indicated in each image.

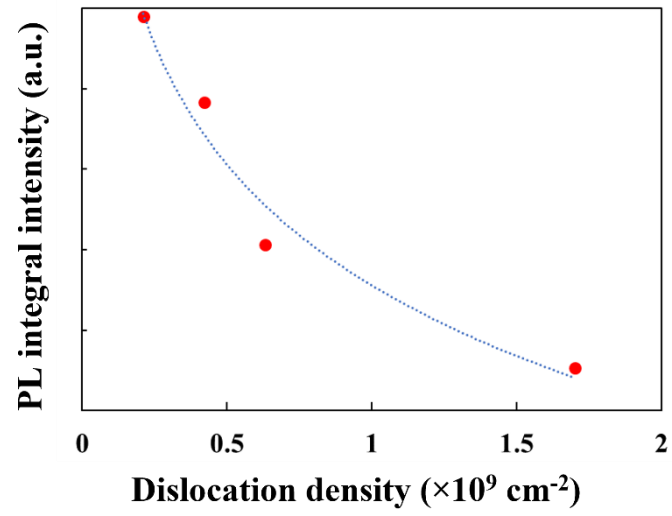


Figure 5-13 PL integral intensity of 8-stacked InAs QD structure as a function of dislocation density.

5.2.3 Surface observation of LT InGaAs/GaAs cover layer

In order to understand why dislocation density is different with LT InGaAs/GaAs cover layer growth condition, the surface after its growth was focused on and observed. Figure 5-14 shows the AFM images of the surface immediately after the growth of LT InGaAs/GaAs cover layer under the growth condition of sample A to D.

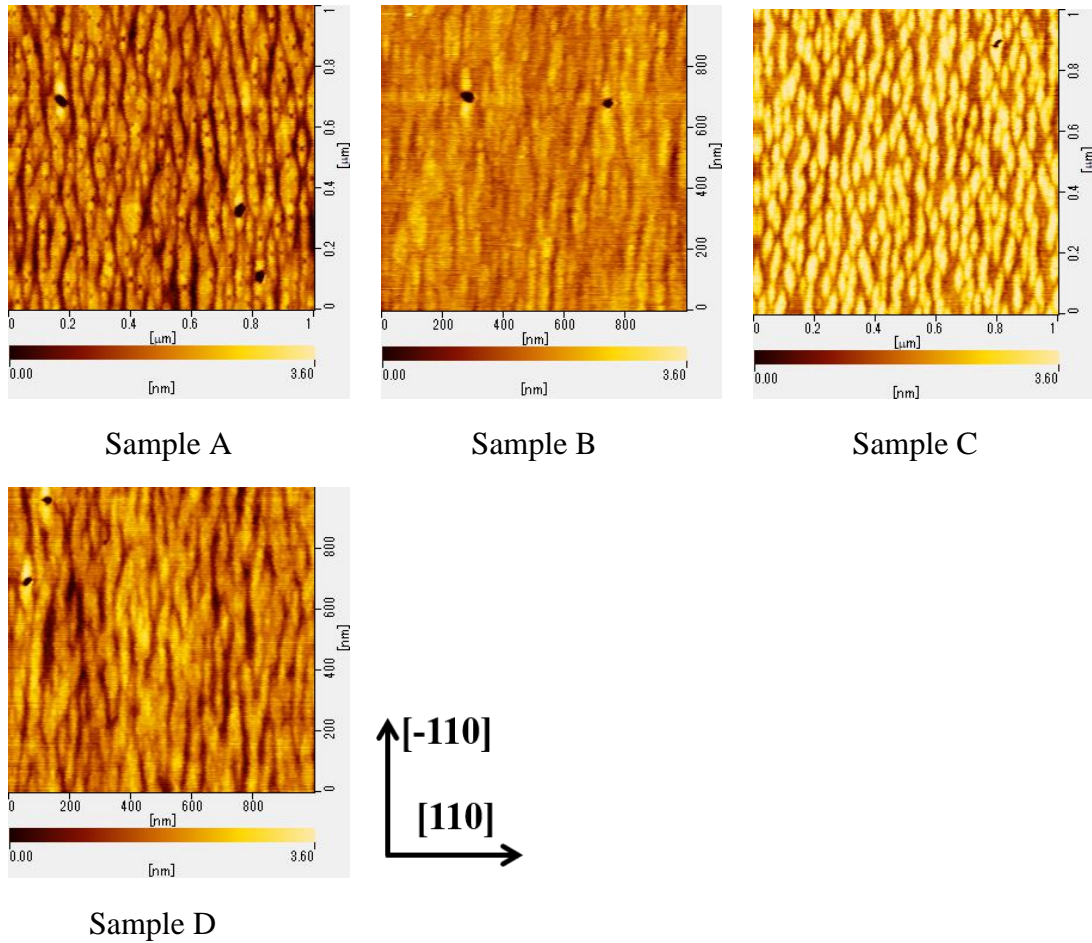


Figure 5-14 AFM image of the surface immediately after the growth of LT InGaAs/GaAs cover layer under the growth condition of sample A to D. Images show $1 \times 1 \mu\text{m}^2$. Color scale is 3.6 nm.

As can be seen from AFM images in Fig. 5-14, there exist pits on the surface. In the case of InGaAs/GaAs cover layer growth on InAs QDs, it has been reported that pits are formed directly above the InAs QDs due to the strain accumulation on the top of them [59]. The same phenomenon is considered to have occurred in this experiment.

Especially in sample A with $480^\circ\text{C}/7.5 \text{ nm}$ condition, extremely many pits, relatively small pits with large numbers and relatively large pits with small numbers were observed.

From the comparison with AFM image of InAs QDs grown at the same 510 °C shown in Fig. 5-2, the small pits were derived from standard size dots with their heights around 8 nm, and large pits were derived from large coalesced QDs with their heights of 10 nm or higher.

In the case of sample B with 510 °C/7.5 nm condition, the small pits observed in sample A were disappeared. The top of InAs QD is considered to be collapsed or intermixed during the LT cover layer growth at high temperature. This results in the reduction of the strain at the top of the QDs and suppression of pits formation with conformal coverage of LT cover layer. However, there still exist the giant QD-derived pits which could not be suppressed even with the above phenomena.

In the case of sample C with 420 °C/7.5 nm condition, the small pits were disappeared same as in the case of sample B. However, surface morphology is greatly different and InAs QDs are covered by the mountainous shape. This is because the surface migration length of Ga is so short due to low temperature growth that the GaAs layer is conformally formed on InAs QDs even the existence of strain. However, there still exists the pits which are derived from the giant QDs with larger strain same as sample B.

In the case of sample D with 480 °C/12.0 nm condition, the standard size QDs are fully covered by increasing the LT cover layer thickness higher than average QD height in spite of the strain of InAs QDs. However, even in this case, the pits caused by the giant dots remain on the surface.

Next, the effect of annealing on the surface of the low temperature cover layer was investigated. Figure 5-15 shows the AFM images of the surface of sample A to D after the low-temperature cover layer was grown and the temperature was raised to 590 °C (the surface just before the growth of the HT-GaAs layer).

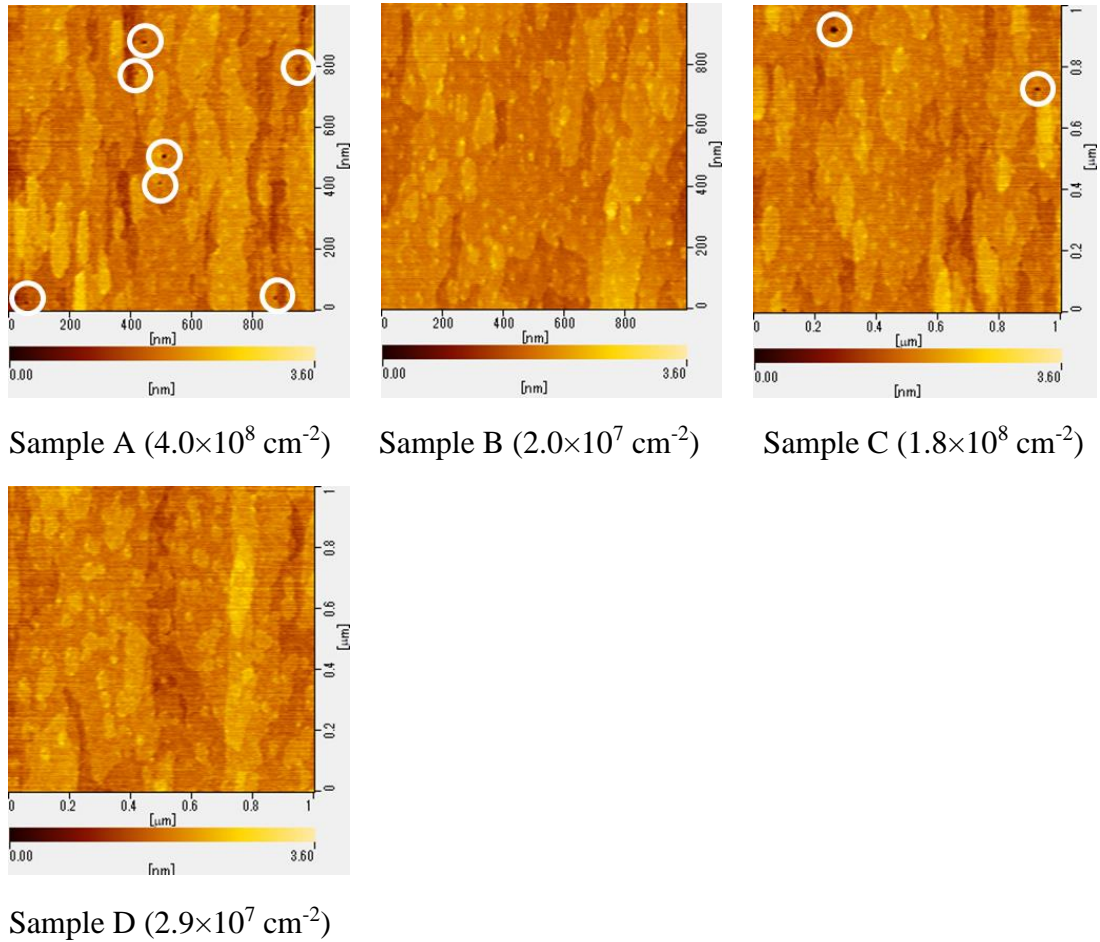


Figure 5-15 AFM image of the surface after the growth of LT InGaAs/GaAs cover layer was grown and the temperature was raised to 590 °C (the surface just before the growth of the HT-GaAs layer) under the growth condition of sample A to D. Images show $1 \times 1 \mu\text{m}^2$. Color scale is 3.6 nm.

From the comparison with the surface before annealing, the surface is flattened in any sample due to the surface migration of Ga atoms. However, although the pits on the surface become smaller, they still remain on the surface. Most of the remaining pits are thought to be caused by giant QDs, which were too deep to be flattened. Pit density averaged over four fields of view for each sample A, B, C, and D is $4.0 \times 10^8 \text{ cm}^{-2}$, $2.0 \times 10^7 \text{ cm}^{-2}$, $1.8 \times 10^8 \text{ cm}^{-2}$, and $2.9 \times 10^7 \text{ cm}^{-2}$, respectively. In terms of the relationship with dislocation density in Fig. 5-12, the dislocation density increases with the increase in pit density. Figure 5-16 shows the PL integral intensity as a function of pit density. Same as the case of the relationship with the dislocation density, the PL integral intensity monotonically decreases as the pit density increases.

Here, consider whether the dislocation originates from the pit or the other way around.

Let's focus on two samples with LT cover layer thicknesses of 7.5 nm and 12 nm under the growth temperatures of 480°C. If the pits are induced by the dislocations, the dislocations are already present on the surface at 7.5 nm growth. The pits are embedded and disappear after 12 nm growth of LT cover layer, but if dislocations exist, they should remain even after thicker growth. However, cross-sectional TEM clearly showed that the sample with 12 nm thick had fewer dislocations than the sample with 7.5 nm thick. Thus, from the viewpoint of comparing the densities of the dislocations and pits numerically, it is reasonable to assume that dislocations were not formed before the formation of the pits and that they were formed during HT-GaAs growth originating from the remaining pits after annealing. HT-GaAs prefers the (001) plane growth, however, if surface orientation other than the (001) plane exists, dislocations are likely to be formed from the boundary between the (001) plane and the other plane orientation. Thus, for the formation of quantum dot structures of good crystallinity with suppressed dislocations, it is important to ensure the surface flatness before HT-GaAs growth and after the growth of the low-temperature cover layer.

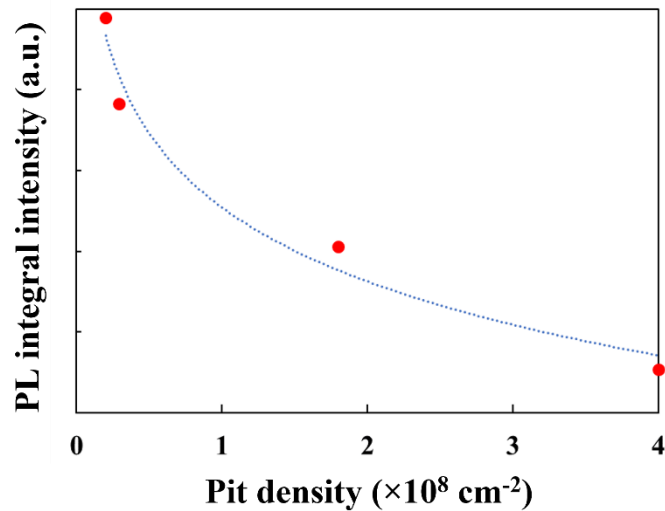
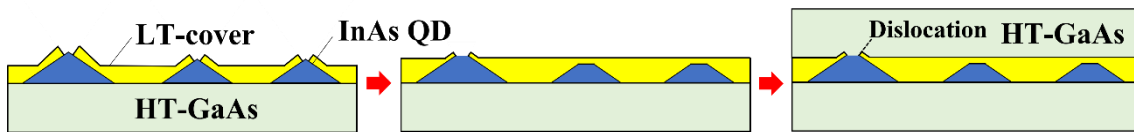


Figure 5-16 PL integral intensity of 8-stacked InAs QD structure as a function of pit density.

5.2.4 Mechanism of the dislocation formation in InAs QD structure

Based on the experimental results discussed in Section 5.2.2 and 5.2.3, growth mechanism concerning the dislocation formation during LT InGaAs/GaAs cover layer and HT GaAs layer is explained below using schematic figure with three steps; (1) Immediately after LT cover layer growth, (2) After annealing at 590 °C, and (3) After HT GaAs growth.

■ **Sample A (480 °C/7.5 nm)**



■ **Immediately after LT cover layer growth**

- ✓ Pits are formed directly above both small and large size InAs QDs.

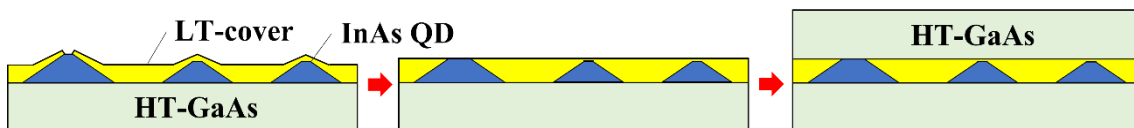
■ **After annealing at 590 °C**

- ✓ QDs heights are reduced by In-flashing and the surface is flattened.
- ✓ Pits remain directly above large QDs.

■ **After HT GaAs growth**

- ✓ Dislocations occur at the remaining pits.

■ **Sample B (510 °C/7.5 nm)**



■ **Immediately after LT cover layer growth**

- ✓ The top of the small dot is fully covered while collapsing.
- ✓ A small pit exists directly above the giant dot.

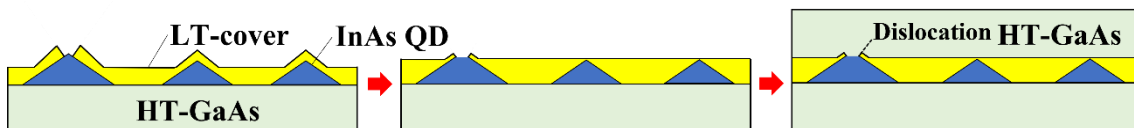
■ **After annealing at 590 °C**

- ✓ The pits directly above the large dots also disappear and are flattened.

■ **After HT GaAs growth**

- ✓ Growth proceeds on a flat surface without dislocation formation.

■ **Sample C (420 °C/7.5 nm)**



■ **Immediately after LT cover layer growth**

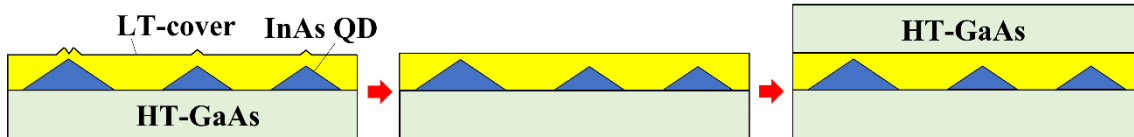
- ✓ Small QDs are conformally covered.
- ✓ Pits remain directly above large QDs.

■ **After annealing at 590 °C**

- ✓ The mountainous shape will be flattened.
- ✓ Some pits remain directly above the large QDs.

- **After HT GaAs growth**
 - ✓ Dislocations occur at the remaining pits.

- **Sample D (480 °C/12.0 nm)**



- **Immediately after LT cover layer growth**
 - ✓ Both small and large QDs are fully covered.
 - ✓ Pits remain directly above large QDs.
- **After annealing at 590 °C**
 - ✓ The pits directly above the large dots also disappear and are flattened.
- **After HT GaAs growth**
 - ✓ Growth proceeds on a flat surface without dislocation formation.

5.2.5 Summary of Section 5.2

The effects of LT InGaAs/GaAs cover layer growth of InAs QDs to their structural and optical properties were investigated by changing the growth temperature and thickness of the cover layer. PL intensity of InAs QD structure decreased as the dislocation density observed around InAs QD increased. Dislocations are formed during HT GaAs growth, originating from pits that remain on the surface after LT cover layer growth and subsequent annealing. In order to form the InAs quantum dot structure free from dislocations, it is important to have a highly flat surface with suppressed pits after LT cover layer growth and subsequent annealing.

5.3 Summary of Chapter 5

The relationship between structural optical properties of 8-stacked InAs QDs with InGaAs SRL was investigated from the two perspectives of InAs QDs growth and LT InGaAs/GaAs cover layer growth.

Regarding the InAs QDs growth, the growth temperatures of InAs QDs were changed at 490 °C, 500 °C, and 510 °C to observe the effect of InAs QD size to the cover layer growth. Dislocations extending from QDs layers were prominently observed in the case of the highest growth temperature of 510 °C where average QD height is the highest. Temperature dependence of PL integral intensity indicated that the PL intensity reduction with respect to the temperature was the lowest in the case of the sample with the lowest dislocation density grown at 500 °C. Moreover, TRPL of 500 °C grown sample shows the longest lifetime at near room temperature. These tendencies indicate that the dislocations act as a non-radiative recombination center to deteriorate PL intensity at near room temperature. These results suggest that growth temperature around 500 °C suppress the formation of a relatively large QDs which lead to the dislocation formation at the cover layer. Suppressing QD height in a uniform manner is therefore the key for fabricating high-quality multiple QDs structure.

Since the quality of the QDs grown at 510°C is likely to be high due to its high growth temperature, the optical properties are expected to be improved by exploring the mechanism of dislocation formation and establishing a method to suppress it.

Thus, the effect of LT InGaAs/GaAs cover layer growth on the optical properties of InAs QDs was investigated by changing the growth temperature and thickness of the LT cover layer under the fixed InAs QDs growth temperature of 510 °C. PL intensity of InAs QD structure decreased as the dislocation density observed around InAs QD increased, indicating that the dislocations mainly act as a nonradiative recombination center same as confirmed in the case of InAs QDs growth temperature dependence. It was revealed that dislocations are formed during HT GaAs growth, originating from pits that remain on the surface after LT cover layer growth and subsequent annealing. In order to form the InAs quantum dot structure free from dislocations, it is important to have a highly flat surface with suppressed pits after LT cover layer growth and subsequent annealing.

6 Conclusions

6.1 Overview of this research

In this study, tensile-strained hetero epitaxial growth with two different material system; (1) InAs hetero growth on GaSb and (2) InGaAs/GaAs hetero growth on InAs, were investigated using molecular beam epitaxy method for the purpose of obtaining good crystallinity with suppressed pits or dislocation, which leads to improved device characteristics.

(1) InAs hetero growth on GaSb

The effects of As₂ pressure and growth temperature were investigated. Regarding the As₂ pressure dependence, the transition layers with small lattice constants were formed at the interface by As₂ soaking before InAs growth, and their thickness decreased as the As₂ pressure decreased. At higher As₂ pressures, many misfit dislocations were formed originating from the transition layer. These lead to a large lattice relaxation of InAs layer. As the As₂ pressure decreased with the reduction of transition layer, the misfit dislocation density decreased, whereas pits were formed. From the comparison of strain analysis with the sample of lower As₂ pressure, it is assumed that the pit was not caused by lattice relaxation but was the formation of high-index planes as part of strain energy relaxation. By further lowering the As₂ pressure, a pit-free, high-quality pseudomorphic InAs layer on GaSb was obtained.

Secondary, the effects of growth temperature including growth sequence to InAs growth on GaSb were also investigated. In the case of one-step InAs growth, the pits at the surface tend to be smaller with the increase in growth temperature, however, they remain even at the growth temperature of 520 °C. A trace amount of Sb irradiation during InAs growth could effectively suppress the pits formation due to its surfactant effect with sacrificing the mosaicity of InAs layer. Without Sb irradiation, we have succeeded in the fabrication of InAs with pit-free and extremely flat surface by two-step initial low and succeeding high temperature growth. This should be caused by the high flatness at initial low temperature growth and preference of (001) plane at high temperature.

(2) InGaAs/GaAs hetero growth on InAs

The effect of the underlying InAs QDs growth and LT InGaAs/GaAs cover layer growth on the structural and optical properties of 8-stacked InAs QDs structures were investigated.

Regarding the underlying InAs QDs growth, their growth temperatures were changed

at 490 °C, 500 °C, and 510 °C. As the growth temperature of InAs QDs increases, the average QDs height becomes higher due to the enlargement of In migration length. Dislocations extending from QDs layers were prominently observed in the case of the highest growth temperature of 510 °C. QDs height seems to be related to the formation of dislocation. Temperature dependence of PL integral intensity and TRPL results indicate that the dislocations act as a non-radiative recombination center to deteriorate PL intensity. Optimizing the growth temperature around 500 °C suppresses the generation of larger size QDs which lead to the dislocation formation at the cover layer. Therefore, suppressing QD height in a uniform manner is the key for fabricating high-quality multiple QDs structure.

From another perspective, since the quality of the QDs grown at 510°C is likely to be high due to its high growth temperature, the optical properties are expected to be improved by exploring the mechanism of dislocation formation and establishing a method to suppress it.

Thus, under the fixed InAs QDs growth temperature of 510 °C, the effect of LT InGaAs/GaAs cover layer growth on the optical properties of InAs QDs was investigated by changing the growth temperature and thickness of the LT cover layer. The PL characteristics showed significant differences depending on the growth conditions of the LT cover layer. PL intensity decreased as the dislocation density observed around InAs QD increased, indicating that the dislocations mainly act as a nonradiative recombination center same as confirmed in the case of InAs QDs growth temperature dependence. It was revealed that dislocations are formed during HT GaAs growth, originating from pits that remain on the surface after LT cover layer growth and subsequent annealing. In order to form the InAs quantum dot structure free from dislocations, it is important to have a highly flat surface with suppressed pits after LT cover layer growth and subsequent annealing.

6.2 Conclusions

The following table summarizes the contrast between the two types of hetero epitaxial growth.

Growth type	LT growth	HT growth	LT/HT growth
InAs on GaSb	<p>(001) plane preference is low, and pits are formed by strain energy relaxation in thick layer growth.</p> <p>The initial layer has high flatness due to small As/Sb exchange.</p>	<p>(001) plane preference is high.</p> <p>The initial layer is unstable due to large As/Sb exchange.</p>	<p>Pits are suppressed by the insertion of an initial LT layer that preserves flatness.</p>
GaAs on InAs	<p>A pit is formed directly above the dot.</p> <p>Pit formation is highly dependent on the growth temperature.</p> <p>As the thickness increases, small pits are embedded, but large pits tend to remain.</p>	<p>(001) plane preference is high.</p> <p>Growth is affected by the unevenness of the underlying layer.</p>	<p>Dislocations are formed from the remaining pits.</p> <p>Dislocation density can be reduced by decreasing pit density with high flatness by increasing the LT layer thickness.</p>

As a conclusion of this study, in the tensile strained III-V compound semiconductor epitaxial growth, ensuring the surface flatness of the initial LT growth before subsequent HT growth is the important for preparing a high-quality crystal with suppressed pits and dislocations.

To ensure the flat surface at initial hetero epitaxial layer stage, (1) growth temperature and (2) thickness should be controlled properly as described below.

(1) Growth temperature should be low enough to suppress the interdiffusion with the underlying layer during initial layer growth. Too high growth temperature causes the roughness or collapse of the underlying QDs during the initial layer growth. On the other hand, too low growth temperature results in the mountainous shape due to relatively short surface migration length of group-III atoms, causing the surface roughness even after HT annealing.

(2) Regarding the thickness of the initial layer, too thick LT layer causes the pit formation or roughness due to low (001) plane preference growth. On the other hand, too thin LT layer results in the remaining pits on the surface even after HT annealing. Therefore, it is important to suppress the solid-state interdiffusion and embed the pits at the initial stage of LT growth if the QD is underlying layer. If the initial underlying surface is flat in the case of GaSb, 1 ML is assumed to be sufficient for initial layer thickness. Then, at HT annealing, surface migration of group-III atoms is caused to flatten while the solid-state interdiffusion between the initial LT layer and the underlying layer is suppressed to keep the crystal quality.

Appendix

In Section 4.2, binary Sb_2 was used for the GaSb homo epitaxial growth. Although Sb chemical bonding state is different in the case of Sb_4 discussed in Chapter 3 and Section 4.1, the flat with pits free GaSb surface was obtained. AFM image of GaSb homo epitaxial layer grown by two-step $560\text{ }^\circ\text{C}/520\text{ }^\circ\text{C}$ growth is shown in Fig. A-1. Images show $1 \times 1\ \mu\text{m}^2$. Color scale is 0.96 nm.

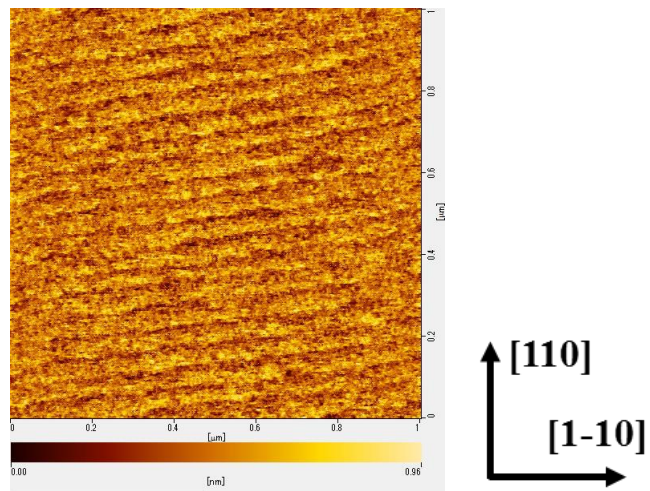


Figure A-1 AFM image of two-step GaSb homo epitaxial layer where the first/second layers were grown at $560\text{ }^\circ\text{C}/520\text{ }^\circ\text{C}$. Images show $1 \times 1\ \mu\text{m}^2$. Color scale is 0.96 nm.

References

- [1] A. Rogalski, P. Martyniuk, and M. Kopytko, *Appl. Phys. Rev.* **4**, 031304 (2017).
- [2] A. Haddadi, R. Chevallier, A. Dehzangi, and M. Razeghi, *Appl. Phys. Lett.* **110**, 101104 (2017).
- [3] G. R. Savich, D. E. Sidor, X. Du, G. W. Wicks, M. C. Debnath, T. D. Mishima, M. B. Santos, T. D. Golding, M. Jain, A. P. Craig, and A. R. J. Marshall, *J. Vac. Sci. Technol. B* **35**, 02B105 (2017).
- [4] M. D. Goldflam, E. A. Kadlec, B. V. Olson, J. F. Klem, S. D. Hawkins, S. Parameswaran, W. T. Coon, G. A. Keeler, T. R. Fortune, A. Tauke-Pedretti, J. R. Wendt, E. A. Shaner, P. S. Davids, J. K. Kim, and D. W. Peters, *Appl. Phys. Lett.* **109**, 251103 (2016).
- [5] A. Haddadi, S. Adhikary, A. Dehzangi, and M. Razeghi, *Appl. Phys. Lett.* **109**, 021107 (2016).
- [6] D. Jiang, W. Xiang, F. Guo, H. Hao, X. Han, X. Li, G. Wang, Y. Xu, Q. Yu, and Z. Niu, *Appl. Phys. Lett.* **108**, 121110 (2016).
- [7] A. Haddadi, R. Chevallier, G. Chen, A. M. Hoang, and M. Razeghi, *Appl. Phys. Lett.* **106**, 011104 (2015).
- [8] E. Giard, I. Ribet-Mohamed, J. Jaeck, T. Viale, R. Haïdar, R. Taalat, M. Delmas, J.-B. Rodriguez, E. Steveler, N. Bardou, F. Boulard, and P. Christol, *J. Appl. Phys.* **116**, 043101 (2014).
- [9] F. Callewaert, A. M. Hoang, and M. Razeghi, *Appl. Phys. Lett.* **104**, 053508 (2014).
- [10] Y.-F. Lao, P. K. D. D. P. Pitigala, A. G. Unil Perera, E. Plis, S. S. Krishna, and P. S. Wijewarnasuriya, *Appl. Phys. Lett.* **103**, 181110 (2013).
- [11] D. Zuo, P. Qiao, D. Wasserman, and S. L. Chuang, *Appl. Phys. Lett.* **102**, 141107 (2013).

- [12] S. A. Pour, E. K. Huang, G. Chen, A. Haddadi, B.-M. Nguyen, and M. Razeghia, *Appl. Phys. Lett.* **98**, 143501 (2011).
- [13] K. Hackiewicz and P. Martyniuk, *Proc. SPIE* **10433**, 104330X (2017).
- [14] L.-P. Yang, J. Deng, Y.-L. Shi, Y.-Y. Chen, and B. Wu, *Proc. SPIE* **8907**, 890741 (2013).
- [15] M. Razeghi, A. Haddadi, A.M. Hoang, E.K. Huang, G. Chen, S. Bogdanov, S.R. Darvish, F. Callewaert and R. McClintock, *Infrared Physics & Technology* **59** (2013) 41.
- [16] G. Ariyawansa, E. Steenbergen, L. J. Bissell, J. M. Duran, J. E. Scheihing, and M. T. Eismann, *Proceedings of SPIE*, **9070** (2014) 90701J.
- [17] H. Kroemer, *Physica E* **20** (2004) 196
- [18] G. C. Dente and M. L. Tilton, *Physical Review B* **66** (16), (2002) 165307.
- [19] L. W. Wang, S. H. Wei, T. Mattila, A. Zunger, I. Vurgaftman, and J. R. Meyer, *Physical Review B* **60** (8), (1999) 5590.
- [20] F. Szmulowicz, H. Haugan, and G. J. Brown, *Physical Review B* **69** (15), (2004) 155321.
- [21] Becky Martinez, J. Patrick Flint, G. Dallas, B. Smith, M. Tyberg, Shanmugam Aravazhi and Mark J. Furlong, *Proceedings of SPIE*, **10177** (2014) 101772L.
- [22] S. McDonnell, B. Brennan, E. Bursa, R.M. Wallace, K. Winkler, P. Baumann, *J. Vac. Sci. Technol. B* **32** (2014) 041201.
- [23] B.Z. Nosho, B.R. Bennett, E.H. Aifer and M. Goldenberg, *Journal of Crystal Growth* **236** (2002) 155.
- [24] Q. Xie, J. E. Van Nostrand, J. L. Brown, and C. E. Stutz, *J. Appl. Phys.* **86**, 329 (1999).

- [25] M. Losurdo, P. Capezzuto, G. Bruno, A. S. Brown, T. Brown, and G. May, *J. Appl. Phys.* **100**, 013531 (2006).
- [26] H. Ye, L. Li, R. T. Hinkey, R. Q. Yang, T. D. Mishima, J. C. Keay, M. B. Santos, and M. B. Johnson, *J. Vac. Sci. Technol. B* **31**, 03C135 (2013).
- [27] J. B. Babua and K. Yoh, *Appl. Phys. Lett.* **97**, 072102 (2010).
- [28] X. Q. Shen and T. Nishinaga, *Journal of Crystal Growth* **146** (1995) 374.
- [29] M. Hata, T. Isu, A. Watanabe, and Y. Katayama, *Appl. Phys. Lett.* **56**, 2542 (1990).
- [30] J. H. G. Owen, W. Barvosa-Carter, and J. J. Zinck, *Appl. Phys. Lett.* **76**, 3070 (2000).
- [31] Y. Arakawa and H. Sakaki, *Appl. Phys. Lett.* **40**, 939 (1982).
- [32] H. Y. Liu and M. Hopkinson, *Appl. Phys. Lett.* **82**, 3644 (2003).
- [33] V.M. Ustinov, N.A. Maleev, A. E. Zhukov, A.R. Kovsh, A.Yu. Egorov, A.V. Lunev, B.V. Volovik, I.L. Krestnikov, Yu.G. Musikhin, N.A. Bert, P.S. Kop'ev, Zh. I. Alferov, N.N. Ledentsov, and D. Bimberg, *Appl. Phys. Lett.* **74**, 2815 (1999).
- [34] H.Y. Liu, M. Hopkinson, C.N. Harrison, M.J. Steer, R. Frith, I.R. Sellers, D.J. Mowbray, and M. S. Skolnick, *J. App. Phys.* **93**, 2931 (2003).
- [35] J. Bloch, J. Shah, W. S. Hobson, J. Lopata, and S.N.G. Chu, *Appl. Phys. Lett.* **75**, 2199 (1999).
- [36] J. Bloch, J. Shah, L. N. Pfeiffer, K.W. West, and S.N.G. Chu, *Appl. Phys. Lett.* **77**, 2545 (2000).
- [37] H. Y. Liu, X. D. Wang, J. Wu, B. Xu, Y. Q. Wei, W. H. Jiang, D. Ding, X. L. Ye, F. Lin, J. F. Zhang, J. B. Liang, and Z. G. Wang, *J. App. Phys.* **88**, 3392 (2000).
- [38] T. Yang, J. Tatebayashi, S. Tsukamoto, M. Nishioka, and Y. Arakawa, *Appl. Phys.*

Lett. **84**, 2817 (2004).

[39] A. Passaseo, R. Rinaldi, M. Longo, S. Antonaci, A. L. Convertino, R. Cingolani, A. Taurino, and M. Catalano, *J. Appl. Phys.* **89**, 4341 (2001).

[40] N. Weir, R. Yao, C-S. Lee, and W. Guo, *J. Cryst. Growth*, **451**, 79 (2016).

[41] K. Watanabe, T. Akiyama, Y. Yokoyama, K. Takemasa, K. Nishi, Y. Tanaka, M. Sugawara, and Y. Arakawa, *J. Cryst. Growth*, **378**, 627 (2013).

[42] S. Adhikary, N. Halder, S. Chakrabarti, S. Majumdar, S. K. Ray, M. Herrera, M. Bonds, and N. D. Browning, *J. Cryst. Growth*, **312**, 724 (2010).

[43] A. Hospodkova', J. Pangra', J. Oswald, P. Hazdra, K. Kuldova', J. Vyskoc'cil, and E. Hulcius, *J. Cryst. Growth*, **315**, 110(2011).

[44] T. Yang, M. Nishioka, and Y. Arakawa, *J. Cryst. Growth*, **310**, 5469 (2008).

[45] V. Celibert, E. Tranvouez, G. Guillot, C. Bru-Chevallier, L. Grenouillet, P. Duvaut, P. Gilet, P. Ballet, and A. Million, *J. Cryst. Growth*, **275**, e2313 (2005).

[46] S. Saravanan and H. Shimizu, *J. Cryst. Growth*, **289**, 14 (2006).

[47] A.R. Kovsh, N.A. Maleev, A.E. Zhukov, S.S. Mikhrin, A.P. Vasil'ev, E.A. Semenova, Yu.M. Shernyakov, M.V. Maximov, D.A. Livshits, V.M. Ustinov, N.N. Ledentsov, D. Bimberg, and Zh.I. Alferov, *J. Cryst. Growth* **251**, 729 (2003).

[48] V.M. Ustinov, A.E. Zhukov, N.A. Maleev, A.R. Kovsh, S.S. Mikhrin, B.V. Volovik, Yu.G. Musikhin, Yu.M. Shernyakov, M.V. Maximov, A.F. Tsatsul'nikov, N.N. Ledentsov, Zh.I. Alferov, J.A. Lott, and D. Bimberg, *J. Cryst. Growth*, **227**, 1155 (2001).

[49] F. Ferdos, M. Sadeghi, Q.X. Zhao, S.M. Wang, and A. Larsson, *J. Cryst. Growth*, **227**, 1140 (2001).

[50] J. C. Norman, R. P. Mirin, and J. E. Bowers, *J. Vac. Sci. Technol. A* **39**, 020802 (2021).

- [51] T. Kageyama, K. Nishi, M. Yamaguchi, R. Mochida, Y. Maeda, K. Takemasa, Y. Tanaka, T. Yamamoto, M. Sugawara, and Y. Arakawa, CLEO/Europe and EQEC 2011 Conference Digest, OSA Technical Digest (CD) (Optical Society of America, 2011), paper PDA_1.
- [52] W. W. Chow, and F. Jahnke, Progress in Quantum Electronics, **37**, 109 (2013).
- [53] A. Capua, L. Rozenfeld, V. Mikhelashvili, G. Eisenstein, M. Kuntz, M. Laemmlin, and D. Bimberg, Opt. Express **15**, 5388 (2007).
- [54] Y. Tanaka, M. Ishida, K. Takada, T. Yamamoto, H. Song, Y. Nakata, M. Yamaguchi, K. Nishi, M. Sugawara, and Y. Arakawa, Conference on Lasers and Electro-Optics 2010, OSA Technical Digest (CD) (Optical Society of America, 2010), paper CTuZ1.
- [55] URL of QD laser, Inc. <https://www.qdlaser.com/>
- [56] K. Nishi, H. Saito, S. Sugou, and J-S, Lee, Appl. Phys. Lett. **74**, 1111 (1999).
- [57] X. D. Wang, Z.C. Niu, S.L. Feng, Z.H. Miao, J. Cryst. Growth **223**, 363 (2001).
- [58] K. Nishi, T. Kageyama, M. Yamaguchi, Y. Maeda, K. Takemasa, T. Yamamoto, M. Sugawara, and Y. Arakawa, J. Cryst. Growth **378**, 459 (2013).
- [59] W-S. Liu, H. Chang, Y-S. Liu, and J-I. Chyi, J. Appl. Phys., **99**, 114514 (2006).
- [60] A. J. Ptak, Handbook of Crystal Growth, Principles of Molecular Beam Epitaxy (Chapter 4) (2015).
- [61] B. L. VanMil, A. J. Ptak, N. C. Giles, T. H. Myers, P. J. Treado, M. P. Nelson, J. Elec. Mat., **30**, 785 (2001).
- [62] H. H. Farrell, J.L. deMiguel, M. C. Tamargo, J. Appl. Phys. **65**, 4084 (1989).
- [63] Y. S. Wu, C.R. Becker, A. Waag, R.N. Bicknell-Tassius, G. Landwehr, J. Appl. Phys., **69**, 268 (1991).

- [64] P. Frigeri, L. Seravalli, G. Trevisi, S. Franchi, 3.12: Molecular Beam Epitaxy: An Overview. In: P. Bhattacharya, R. Fornari, H. Kamimura, editors. *Comprehensive Semiconductor Science and Technology*, 3. Amsterdam: Elsevier; 2011.
- [65] J. J. Harris, B.A. Joyce, P. J. Dobson. *Surf. Sci.*, **103** L90 (1981).
- [66] C. E. C. Wood. *Surf. Sci.*, **108** L441 (1981).
- [67] J.J. Harris, B.A. Joyce, P.J. Dobson, *Surf. Sci.*, **108**, L444 (1981).
- [68] J. H. Neave, B.A. Joyce, P.J. Dobson, N. Norton, *Appl. Phys. A*, **31** 1 (1983).
- [69] J. M. Van Hove, C.S. Lent, P.R. Pukite, P.I. Cohen, *J. Vac. Sci. Technol. B* **1** 741 (1983).
- [70] J. R. Arthur. Molecular beam epitaxy. *Surf. Sci.*, **500** 189 (2002).
- [71] G. Pletikapić, and N. I. DeNardis, *Nat. Hazards Earth Syst. Sci.*, **17**, 31 (2017).
- [72] P.D. Brewer, D.H. Chow and R.H. Miles, *Journal of Vacuum Science & Technology B* **14** (1996) 2335.
- [73] M. Lee, D.J. Nicholas, K.E. Singer, and B. Hamilton, *Journal of Applied Physics* **59** (1986) 2895.
- [74] A.S. Bracker, M.J. Yang, B.R. Bennett, J.C. Culbertson and W.J. Moore, *Journal of Crystal Growth* **220** (2000) 384.
- [75] N. Bertru, M. Nouaoura, J. Bonnet, L. Lassabatere, *Journal of Crystal Growth* **160** (1996) 1.
- [76] R. W. Schwoebel and E. J. Shipsey, *Journal of Applied Physics* **37** 3682 (1966).
- [77] G. Ehrlich and F. G. Hudda, *Journal of Chemical Physics* **44** 1039 (1966).

- [78] L. M. Murray, A. Yildirim, S. R. Provenca, D. T. Norton, T. F. Boggess, and J. P. Prineas, *Journal of Vacuum Science and Technology B* **31**, 03C108 (2013).
- [79] C. M. Fetzer, R. T. Lee, J. K. Shurtleff, G. B. Stringfellow, S. M. Lee, and T. Y. Seong, *Appl. Phys. Lett.* **76**, 1440 (2000).
- [80] J. K. Shurtleff, S. W. Jun, and G. B. Stringfellow, *Appl. Phys. Lett.* **78**, 3038 (2001).
- [81] J. C. Harmand, L. H. Li, G. Patriarche, and L. Travers, *Appl. Phys. Lett.* **84**, 3981 (2004).
- [82] P. S. Dutta, H. L. Bhat, and V. Kumar, *J. Appl. Phys.* **81**, 5821 (1997).
- [83] V. M. Bermudez, *J. Appl. Phys.* **114**, 024903 (2013).
- [84] S. McDonnell, B. Brennan, E. Bursa, R. M. Wallace, K. Winkler, and P. Baumann, *J. Vac. Sci. Technol. B*, **32**, 041201-1 (2014).
- [85] T. Kaizu and K. Yamaguchi, *Jpn. J. Appl. Phys.* **42**, 4166 (2003).
- [86] L. M. Kong, Z. C. Feng, Z. Y. Wu, and W. Lu, *Semicond. Sci. Technol.* **23** 075044 (2008).
- [87] A. Fiore, P. Borri, W. Langbein, J. M. Hvam, U. Oesterle, R. Houdré, R. P. Stanley, and M. Illegems, *Appl. Phys. Lett.* **76**, 3430 (2000).
- [88] F. Pulizzi, A. J. Kent, A. Patané, L. Eaves, and M. Henini, *Appl. Phys. Lett.* **84**, 3046 (2004).
- [89] L. Kong, Z. C. Feng, Z. Wu, and W. Lu, *J. Appl. Phys.* **106**, 013512 (2009).
- [90] C. Cheng, S-D. Lin, C-H. Pan, C-H. Lin, Y-J. Fu, *Phys. Lett. A* **376**, 1495 (2012).
- [91] G. Wang, B. Liang, B-C. Juang, A. Das, M. C. Debnath, D.L. Huffaker, Y. I. Mazur, M. E. Ware, and G. J. Salamo, *Nanotechnology* **27**, 465701 (2016).

[92] O. Nasr, N. Chauvin, M. H. H. Alouane, H. Maaref, C. Bru-Chevallier, L. Sfaxi, and B. Ilahi, *J. Opt.* **19**, 025401 (2017).

Publication list

Regular paper

[1] S. Okumura, S. Tomabechei, R. Suzuki, Y. Matsukura, K. Tsunoda, J. Kon, and H. Nishino, “Improvement in surface morphology of GaSb buffer layer by two-step high and low temperature growth” *Journal of Crystal Growth*, 477 (2017) 243-248.

[2] S. Okumura, S. Tomabechei, R. Suzuki, K. Tsunoda, J. Kon, and H. Nishino, “Effects of As₂ pressure on InAs heteroepitaxial growth on vicinal GaSb(001) substrate by molecular beam epitaxy”, *Japanese Journal of Applied Physics*, 57 (2018) 115502.

[3] S. Okumura, R. Suzuki, K. Tsunoda, H. Nishino, and M. Sugiyama, “Suppression of three-dimensional pit formation of InAs on GaSb(0 0 1) by Sb-free two-step molecular beam epitaxy”, *Journal of Crystal Growth*, 528 (2019) 125269.

[4] S. Okumura, K. Fujisawa, M. Yamaguchi, T. Naruke, K. Nishi, K. Takemasa, M. Sugawara, and M. Sugiyama, “Impact of dislocations in InAs quantum dot with InGaAs strain-reducing layer structures on their optical properties”, *Japanese Journal of Applied Physics*, 60 (2021) 035507.

[5] S. Okumura, K. Fujisawa, T. Naruke, K. Nishi, Y. Onishi, K. Takemasa, M. Sugawara, and M. Sugiyama, “Impact of low temperature cover layer growth of InAs/GaAs quantum dots on their optical properties”, to be submitted in a Journal.

International conference

[1] S. Okumura, S. Tomabechei, R. Suzuki, Y. Matsukura, K. Tsunoda, J. Kon, and H. Nishino, “Improvement in surface morphology of GaSb buffer layer by 2-step high and low temperature growth”, 19th International Conference on Molecular Beam Epitaxy (IC-MBE 2016), Tu-P-64.

[2] S. Okumura, S. Tomabechei, R. Suzuki, K. Tsunoda, J. Kon, and H. Nishino, “The effect of As₂ pressure on InAs quality on GaSb (001) substrate”, The 33rd North American Conference on Molecular Beam Epitaxy (NAMBE 2017), TU-12.

[3] S. Okumura, R. Suzuki, K. Tsunoda, H. Nishino, and M. Sugiyama, “Suppression of

three-dimensional pit formation of InAs on GaSb(001) by two-step MBE”, Compound Semiconductor Week (CSW 2019), MoP-A-9.

Domestic conference

[1] 奥村滋一, 苫米地秀一, 鈴木僚, 松倉祐輔, 角田浩司, 今純一, 西野弘師, “高温/低温2段成長によるGaSbバッファ層表面モフォロジーの向上”, 第77回応用物理学会秋季学術講演会, 2016, 16a-B9-5.

[2] 奥村滋一, 苫米地秀一, 鈴木僚, 角田浩司, 今純一, 西野弘師, “微傾斜GaSb(001)基板上InAs成長のAs₂圧依存性”, 第64回応用物理学会春季学術講演会, 2017, 17a-B5-11.

[3] 奥村滋一, 鈴木僚, 角田浩司, 西野弘師, 杉山正和, “2ステップMBE成長によるGaSb(001)上InAsのピット形成の抑制”, 第80回応用物理学会秋季学術講演会, 2019, 18p-B31-10.

[4] 奥村滋一, 藤澤和輝, 山口正臣, 成毛環美, 西研一, 武政敬三, 菅原充, 杉山正和, “InAs/GaAs量子ドット構造中の転位の発光特性への影響”, 第81回応用物理学会秋季学術講演会, 2020, 9p-Z01-12.

[5] 奥村滋一, 藤澤和輝, 成毛環美, 西研一, 大西裕, 武政敬三, 菅原充, 杉山正和, “InAs/GaAs量子ドット構造における低温カバー層成長の光学特性への影響”, 第82回応用物理学会秋季学術講演会, 2021, 12a-N406-3.(発表予定)

Acknowledgements

I would like to thank all the people who were involved in carrying out this research.

This research was conducted by the University of Tokyo, Fujitsu Laboratories, and QD Laser.

First of all, I would like to thank Professor Masakazu Sugiyama for his precise guidance in conducting this research. It was difficult to tie the two different topics together, but I appreciate the constructive advice and encouragement.

I would like to thank Dr. Kentaroh Watanabe and Mr. Meita Asami of Sugiyama Laboratory for their support and guidance on XRM and TRPL measurements of InAs QD samples.

Regarding the InAs/GaSb related research, I would like to thank to the members of Fujitsu Laboratories, Mr. Hironori Nishino, Mr. Junichi Kon, Dr. Koji Tsunoda, Mr. Ryo Suzuki, late Mr. Yusuke Matsukura, and Dr. Shuichi Tomabechi for conducting the research and their encouragements. Also, I express my gratitude to Mr. Masayuki Kawabata for his technical support of the AFM measurement and Dr. Kenichi Kawaguchi for his constructive advice on InAs/GaSb hetero epitaxial growth.

Regarding the InAs/GaAs related research, I would like to thank to the members of QD laser, Inc., Dr. Mitsuru Sugawara, Mr. Keizo Takemasa, Dr. Yutaka Onishi, Dr. Kenichi Nishi, Mr. Masaomi Yamaguchi, Ms. Tamami Naruke, and Mr. Kazuki Fujisawa for conducting the research and their encouragements.

I would like to specially thank Dr. Keiji Watanabe and Dr. Norikazu Nakamura of Fujitsu Laboratories for giving me the chance to study in the doctoral program of the University of Tokyo as a businessperson, as well as the personnel department of Fujitsu Laboratories and QD laser.

Finally, I would like to thank to my partner Noriko and my children Kaname for giving me encouragement and mental peace.

Shigekazu Okumura

奥村滋一